Geoscience BC

Geoscience BC Report 2018-04

Summary of Activities 2017:

Energy

GEOSCIENCE BC SUMMARY OF ACTIVITIES 2017: ENERGY

Geoscience BC Report 2018-4

This publication is also available, free of charge, as colour digital files in Adobe Acrobat® PDF format from the Geoscience BC website: http://www.geosciencebc.com/s/SummaryofActivities.asp.

Every reasonable effort is made to ensure the accuracy of the information contained in this report, but Geoscience BC does not assume any liability for errors that may occur. Source references are included in the report and the user should verify critical information.

When using information from this publication in other publications or presentations, due acknowledgment should be given to Geoscience BC. The recommended reference is included on the title page of each paper. The complete volume should be referenced as follows:

Geoscience BC (2018): Geoscience BC Summary of Activities 2017: Energy; Geoscience BC, Report 2018-4, 96 p.

Summary of Activities: Energy (Geoscience BC)
Annual publication

ISSN 2561-4606 (Print)
ISSN 2561-4614 (Online)

Geoscience BC
1101–750 West Pender Street
Vancouver, British Columbia V6C 2T7
Canada

Cover photos and credits (clockwise from top left): 1) Peace project sonic drilling program, northeastern BC (A. Cahill, 2017); **2)** GHGmap project launch event, Vancouver, BC (Vision Photography, 2017); **3)** GHGmap small unmanned aerial vehicle (sUAV), Vancouver, BC (Vision Photography, 2017); **4)** Installing piezometers near Coles Lake, northeastern BC (S. Abadzadesahraei, 2016); **5)** Installed seismograph near Fort Nelson, BC (Nanometrics, 2013); **6)** Fugitive-gas field research site near Hudson's Hope, BC (A. Cahill, 2017); **7)** Sample collection at Kiwigana River, BC (Kerr Wood Leidal, 2014); **8)** Peace airborne EM survey (SkyTEM Surveys ApS, 2015).

Foreword

Geoscience BC is pleased to once again present results from our ongoing projects in our annual *Summary of Activities* publication. For the past 10 years, we have published the results from our energy and minerals projects in one volume. This year we have decided to publish the 'Energy' and 'Minerals and Mining' papers in two separate volumes. This volume, *Summary of Activities 2017: Energy*, contains 10 papers from Geoscience BC–funded projects and 2017 scholarship winners. A second volume, *Summary of Activities 2017: Minerals and Mining*, contains 11 papers on projects throughout British Columbia (BC). Both volumes are also available for download from our website.

Summary of Activities 2017: Energy

Whiticar et al. present an exciting new project aimed at measuring and mapping real-time greenhouse gas emissions using an optical microsensor mounted on a small quadcopter drone. Initial project activities included flights over natural gas compression and distribution sites, as well as municipal landfill and sewage sites. Evans and Hayes present an update on the British Columbia Natural Gas Atlas project, which is focused on geochemically 'fingerprinting' natural gas in northeastern BC and compiling the results into a database.

Three projects examine seismicity induced by hydraulic fracturing in northeastern BC. Babaie Mahani and Kao provide an update on induced seismicity research funded through the BC Seismic Research Consortium (BC Oil and Gas Commission, Geoscience BC, BC Oil and Gas Research and Innovation Society, Canadian Association of Petroleum Producers and Yukon Geological Survey). Bustin and Longobardi focus on collecting ground-motion data for the mitigation and prevention of induced seismicity; and Monahan et al. look at mapping ground-motion amplification hazard in an area of induced seismicity in northeastern BC.

Two papers examine petroleum systems in northeastern BC. Silva and Bustin report on the preliminary liquid hydrocarbon potential assessment of the Doig Formation, and Wilson and Bustin focus on Devonian shales in the Horn River and Liard basins, and the Cordova Embayment.

Water continues to be a major focus of Geoscience BC projects. Cahill et al. introduce an exciting new multidisciplinary study on fugitive gas, which will help to inform surface gas flux and groundwater monitoring approaches. Quinton et al. highlight ongoing work on permafrost in northern BC and the Northwest Territories, which will be wrapping up in late 2018. Finally, Simons et al. present a numerical modelling study examining disposal of saline wastewater into the Paddy and Cadotte members.

Geoscience BC Energy Publications 2017

In addition to the two *Summary of Activities* volumes, Geoscience BC releases interim and final products from our projects as Geoscience BC reports. All Geoscience BC data and reports can be accessed through our website. Geoscience BC released the following energy reports in 2017:

- 14 technical papers in the *Geoscience BC Summary of Activities 2016* volume (the volume also includes minerals papers)
- **Direct Use Geothermal Resources in British Columbia: Follow-Up Project**, by Tuya Terra Geo Corp. (Geoscience BC Report 2017-07)
- **North-East BC Sonic Drilling Project Physical Log Descriptions and Interpretations**, by V. Levson and M. Best (Geoscience BC Report 2017-16)
- **Summary Report on Proposed Water Well Locations for Halfway River First Nation Area**, by V. Levson and M. Best (Geoscience BC Report 2017-17)
- **Petrophysical Interpretation on Six Shallow Wells in the Peace Region of BC**, by Y. Mykula (Geoscience BC Report 2017-18)

All releases of Geoscience BC reports and data are announced through our website and e-mail list. If you are interested in receiving information regarding these reports and other Geoscience BC news, please contact info@geosciencebc.com. Most final reports and data can be viewed through our Earth Science Viewer at http://www.geosciencebc.com/s/WebMaps.asp.

Acknowledgments

Geoscience BC would like to thank all authors and reviewers of the *Summary of Activities: Energy* papers for their contributions to this volume. RnD Technical is also acknowledged for their work in editing and assembling the volume. As well, Geoscience BC would like to thank the Province of British Columbia and our project funding partners for their ongoing support of public geoscience and express appreciation for the leaders and volunteers in British Columbia's mineral exploration, mining and energy sectors who support our organization through their guidance, use and recognition of the information that we collect and distribute.

Christa Pellett
Project Co-ordinator
Geoscience BC
www.geosciencebc.com

Contents

GHGMap: Novel Approach for Aerial Measurements of Greenhouse Gas Emissions, British Columbia

M.J. Whiticar, University of Victoria and Geochemical Analytic Services Corporation, Victoria, BC, whiticar@uvic.ca

L.E. Christensen, NASA Jet Propulsion Laboratory, California Institute of Technology, Pasadena, US

C.J. Salas, Geoscience BC, Vancouver, BC

P. Reece, InDro Robotics, Salt Spring Island, BC

Whiticar, M.J., Christensen, L.E., Salas, C.J. and Reece, P. (2018): GHGMap: novel approach for aerial measurements of greenhouse gas emissions, British Columbia; *in* Geoscience BC Summary of Activities 2017: Energy, Geoscience BC, Report 2018-4, p. 1–10.

Introduction

Based on Intergovernmental Panel on Climate Change (IPCC) estimates, the annual global emissions of non–carbon dioxide greenhouse gases (GHG) are roughly 10 000 million metric tons (megatonnes, Mt) of carbon dioxide equivalents (CO_2e) or more than 23% of global GHG annual emissions (Stocker et al., 2013). This compares with global carbon dioxide (CO_2) emissions of approximately 32 000 Mt (de la Chesnaye et al., 2006). Over the last 250 years, the concentration of methane (CH_4) in the atmosphere has increased by 162%, as cited in the Global Carbon Budget 2016 (Le Quéré et al., 2016) and by the Intergovernmental Panel on Climate Change (Stocker et al., 2013). Present-day CH_4 emissions to the troposphere are ~550 Tg/yr. (550 Mt CH_4/yr.) of which 50–65% are from anthropogenic sources (Ciais et al., 2013). This equates to anthropogenic CH_4 emissions of ~6800 Mt CO_2e in 2006, which is expected to rise to ~8000 Mt CO_2e by 2020 (United States Environmental Protection Agency, 2006).

In 2014, British Columbia's (BC) total industrial GHG emissions were estimated by the BC Climate Action Secretariat to be 20.3 Mt CO_2e (BC Ministry of Environment, 2016b). This figure excludes electricity import operations and any BC operations annually emitting less than 10 kt of CO_2e/yr. This 20.3 Mt CO_2e represents about 32% of the BC total emissions of 64.5 Mt CO_2e in 2014. The BC Ministry of Environment (BCMoE) reports the total BC GHG emissions in 2014 to be 62.7 Mt CO_2e, rather than 64.5 Mt CO_2e, if 1.8 Mt CO_2e in offsets from forest management projects are subtracted (BC Ministry of Environment, 2016b). The BC 2014 GHG emission level of 64.5 Mt CO_2e is a drop from the high of >70 Mt CO_2e around 2004 (Figure 1). Energy-related activities are, by a wide margin, the highest sector of GHG emissions (~50.1 Mt CO_2e), more than waste (~5.6 Mt CO_2e), industrial processes (~3.5 Mt CO_2e), deforestation (~3.0 Mt CO_2e) and agriculture activities (~2.3 Mt CO_2e; Figure 2; BC Ministry of Environment, 2016b). A detailed

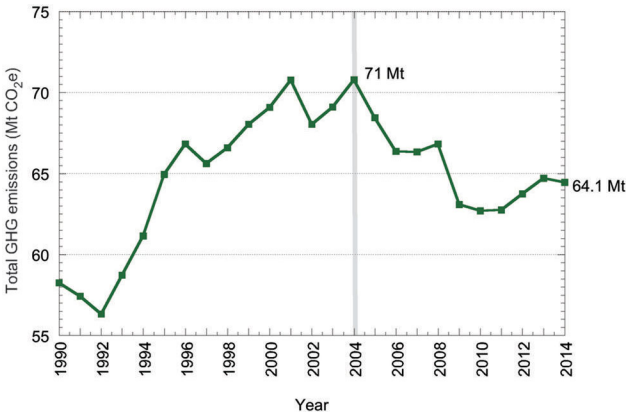

Figure 1. Estimated total greenhouse gas (GHG) emissions from 1990 to 2014 in British Columbia (from BC Ministry of Environment, 2016c). Abbreviations: CO_2e, carbon dioxide equivalents; Mt, megatonnes.

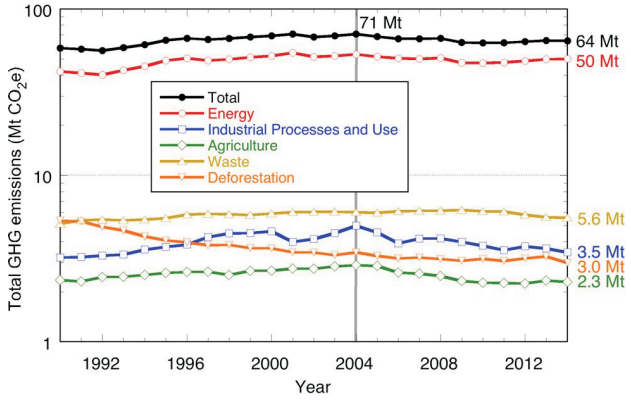

Figure 2. Estimated greenhouse gas (GHG) emissions in British Columbia from 1990 to 2014, reported by major emission sectors (from BC Ministry of Environment, 2016b). Numbers on the right side are 2014 values in megatonnes (Mt) of carbon dioxide equivalents (CO_2e).

This publication is also available, free of charge, as colour digital files in Adobe Acrobat® PDF format from the Geoscience BC website: http://www.geosciencebc.com/s/SummaryofActivities.asp.

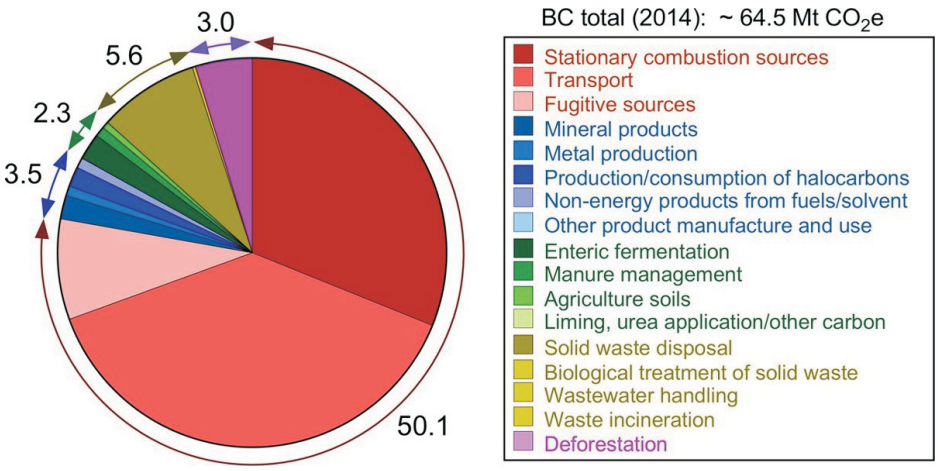

Figure 3. Detailed breakdown by subsector of estimated greenhouse gas (GHG) emissions in British Columbia for 2014. Numbers outside the wedges are 2014 emission sector values in megatonnes (Mt) of carbon dioxide equivalents (CO_2e; from BC Ministry of Environment, 2016c).

breakdown and relative proportions of the major BC GHG emissions sources within the different sectors is illustrated in Figure 3.

Within the industrial reporting sector, the major CH_4 emitters are oil and gas (50%), mining and smelting (14%) and cement/lime production (9%). In 2014, CH_4 accounted for a total of 10 Mt CO_2e, province-wide, with 3.6 Mt CO_2e attributed to the energy sector. Of this, it is estimated that over 2.8 Mt CO_2e (78%) were fugitive CH_4 emissions, whereas stationary combustion sources made up most of the remaining energy sector CH_4 emissions (0.64 Mt CO_2e; BC Ministry of Environment, 2016b).

It must be recognized that these reported CO_2e values are only best estimates and are not based on actual, routine, direct GHG measurements in BC. Rather the emission estimates rely on modelled values using the Canada's National Inventory Report (NIR), as prepared by the Environment and Climate Change Canada (ECCC) audit (Environment and Climate Change Canada, 2017). These modelled values are based on emission factors as outlined in schedules, such as the 2006 IPCC Guidelines for National Greenhouse Gas Inventories (Eggleston et al., 2006) or listed in the ECCC NIR on Greenhouse Gases and Sinks in Canada (Environment and Climate Change Canada, 2017). Fugitive emission estimates are based on

1) Canadian Association of Petroleum Producers (CAPP) average emission factors generated by Clearstone Engineering Ltd. (2005, 2014); and
2) augmented by data from oil and gas companies conducting formal leak management programs.

The limitations of modelling emissions are well stated in BCMoE reports as "Uncertainty in inventory estimates is inherent and the inventory should only be viewed as an approximation of total emissions." (BC Ministry of Environment, 2012, 2016a).

For clarification, the BC reporting of GHG emissions uses the CO_2e strategies that incorporate recent science based on the IPCC Guidelines for National Greenhouse Gas Inventories (Eggleston et al., 2006). Thus, the amounts of the different GHG species, such as CH_4 and nitrous oxide (N_2O), are not reported using their specific masses (e.g., Mt CH_4). Rather the amounts are converted to the amount of CO_2 that would result in the equivalent change in atmospheric radiative forcing by CO_2, that is, CO_2e. The rationale for using CO_2e is to permit a more simplified relation between different GHGs to a uniform Global Warming Potential (GWP) CO_2 basis. The emission values used by BC are given in Table 1.

Unfortunately, this IPCC CO_2e convention is somewhat arbitrary because the GWP is calculated on the basis of a presumed 100-year lifetime of CO_2. Referring to the IPCC Second Assessment Report (Houghton et al., 1996), the stated GWP of CH_4 is 21 times that of CO_2. This value was revised in the IPCC Fourth and Fifth Assessment Reports (Solomon et al., 2007; Myhre et al., 2013) to 25 times, that is, over 100 years, 1 molecule of CH_4 contributes to the GWP the equivalent of 25 molecules of CO_2. An important consideration of this CO_2e relation is that the actual lifetime of tropospheric CH_4 is approximately 10 years (not the ~100 years of CO_2). Using a 10-year average lifetime of CH_4 in the troposphere, the actual radiative forcing of CH_4 is about 104 times that of CO_2 (CO_2e^{10}), that is, 1 molecule of CH_4 is equivalent to 104 molecules of CO_2 on a decadal time scale. It should also be noted that the GWP of CH_4 is actually greater if the indirect GWP contributions from CH_4 photochemical oxidation products are considered. A further complication in calculating the GWP arises if the CH_4 were combusted to CO_2, for example, as an energy source or mitigation strategy. Due to the mass difference of 2.74 between CO_2 and CH_4 (molar mass CO_2 = 44.01 g/mol versus CH_4 = 16.04 g/mol), the actual GWP reduction by the combustion conversion would only be 38 times, not 104.

The importance of reducing fugitive CH_4 emissions can be emphasized by the following calculation using a CH_4 GWP factor of 104 CO_2e^{10} (10-year average lifetime of CH_4). The BC and Alberta provincial governments have both declared their objectives to reduce energy-related CH_4 emissions by

Table 1. Global Warming Potentials (GWPs) of important greenhouse gases (GHGs) relative to CO_2 (CO_2e) from the 1996 Intergovernmental Panel on Climate Change's Second Assessment Report (Houghton et al., 1996) and the 2007 Intergovernmental Panel on Climate Change's Fourth Assessment Report (Solomon et al., 2007). The BC Ministry of Environment's GHG inventory in 2012 (BC Ministry of Environment, 2012) used the 1996 GWP CO_2e values, whereas later reports used the 2007 GWP CO_2e values (e.g., BC Ministry of Environment, 2016b).

Greenhouse gas	100-year GWP values in 1996[1]	100-year GWP values in 2007[2]
Carbon dioxide (CO_2)	1	1
Methane (CH_4)	21	25
Nitrous oxide (N_2O)	310	298
Nitrogen trifluoride (NF_3)		17 200
Sulphur hexafluoride (SF_6)	23 900	22 800
Hydrofluorocarbon - 23 (CHF_3)	11 700	14 800
Hydrofluorocarbon - 32 (CH_2F_2)	650	675
Perfluorocarbons - 116 (C_2F_6)	9200	12 200

[1]Houghton et al. (1996)
[2]Solomon et al. (2007)

45% by 2025. The annual reduction in these CH_4 emissions for BC would be 64 kt CH_4 or 6.7 Mt CO_2e[10]. This is the equivalent of a ~33% reduction in BC's total industrial GHG emissions or a ~13% reduction of the total 50.3 Mt CO_2 emissions in the province. As mentioned above, the calculated reduction in radiative forcing would be 2.74 times less if the CH_4 emissions were combusted to CO_2 and not just eliminated.

The primary sources of these energy-related fugitive CH_4 emissions are

- *conventional crude oil extraction and processing: releases from wells, flow lines and batteries; venting of casing and solution gas; and evaporative losses from storage facilities;*
- *natural gas extraction and processing: releases from wells, gathering systems, field facilities and gas batteries; seal leaks; line cleaning operations; formation CO_2 removal and pneumatic devices; and*
- *natural gas transmission: equipment leaks, compressor start-up venting and purging of lines during maintenance* (e.g., plant turnaround; BC Ministry of Environment, 2012).

As these stationary and fugitive emissions represent major sources of GHGs, especially CH_4 in the western provinces, this GHGMap research and development project focuses on developing and testing new instrumentation and approaches to monitoring and verifying energy sector emissions. Any real reductions in GHG emissions, including the stationary and fugitive energy emissions of CH_4 in BC, require robust and consistent verification. This is particularly important for the consistent and correct application of carbon tax credits. Conventional methods to monitor energy sector emissions require onsite and/or ground-based measurements, that is, by people travelling to the locations and making point-source measurements by hand or collecting samples for analysis in an offsite laboratory. Fixed-wing aircraft and satellite-based surveys have attempted to make these measurements using remote methodologies but they are best suited for only very large emission sources (e.g., Johnson et al., 2017; Kshtriya, 2017). These measurement approaches are costly, time consuming, uncertain and sometimes difficult to conduct (e.g., outside parties require training and supervision, extensive logistics, etc.). The goal of GHGMap is to develop and replace these point-source and fixed-wing methodologies with fast and cost-effective, remote observational approaches.

GHGMap Project Objectives

The three-year GHGMap project is jointly funded by Geoscience BC and Western Economic Diversification Canada. The project's aim is to measure and map, in real-time and at high spatial resolution, the concentration distributions of primary GHG emissions (e.g., CH_4, CO_2, C_2H_6 [ethane]) using an optical microsensor mounted on a small unmanned aerial vehicle (sUAV). The primary component of GHGMap is the deployment of a unique 400 g optical spectrometer (open-path laser spectrometer [OPLS] developed by NASA Jet Propulsion Laboratory) on a specialized drone (InDro Robotics Inc.'s quadcopter) for the detection, location, quantification and flux calculation of GHGs over natural and fugitive GHG emitters. The GHGMap project will provide data from detailed, unmanned site-specific surveys (e.g., well and pipeline integrity, landfills, feedlots, etc.) in the western provinces of Canada (BC, Alberta, Saskatchewan). Initial testing was undertaken over a landfill site, sewage screening plant and natural gas processing, compression and distribution plants and well pad sites in BC.

The OPLS/sUAV system can detect parts per billion (ppb) levels of atmospheric GHGs at a measurement rate of 10 hertz (Hz) and fly for periods of up to 45 min. The data collected is stored on the OPLS, and simultaneously sent in real-time to the receiver station in the drone control system. The high precision navigation on the drone allows repeatable positioning of the sUAV within 50 cm; the real-time geographic position of the sUAV can be determined continuously and with high accuracy using the on-board Global Positioning System (GPS) and inertial flight navigation (IFN) instrumentation. It also has extremely reduced flying altitude (1–10 m) compared with helicopter or fixed-wing aircraft surveys (>150 m; e.g., Karion et al., 2013). These high precision, proximal measurements by OPLS/sUAV combined with the low flight velocities (1–3 m/s) permit in-

creased and precise detection capabilities. These are unparalleled by other methods, such as handheld monitors, land-vehicle–mounted mobile sensors, manned aircraft or satellites.

The NASA JPL OPLS mid-infrared methane/ethane/carbon dioxide sensor was developed and first flown on a quadcopter in early 2016 (NASA, 2016). Since then, the NASA JPL team has been working with California and U.S. federal agencies, upstream and downstream natural gas producers/distributors, and energy industry consortiums to understand how best this tool can be used.

GHGMap Methodology

The OPLS used in the GHGMap project detects trace gases utilizing an open-path analysis region (e.g., open-path optical cell; Figure 4; Christensen, 2014). Its mid-infrared (MIR) laser produces light radiation that passes through a small volume of atmospheric gas to detect trace amounts of GHG. As the MIR radiation passes through the gas in the OPLS path, some of its energy is absorbed by the gas (light attenuation) at certain wavelengths. The range of wavelengths at which a trace gas exhibits characteristic absorption depends on the molecular properties of the trace gas (Figure 5). For example, CH_4 has strong absorbance bands at wavelengths of between 3.2 and ~3.5 µm. The MIR lasers operate in the spectral region where molecular transitions of the GHGs are up to 100 times stronger than those for near-infrared telecom lasers. The degree of absorption at the specific wavelengths is used to determine the concentration of the trace GHG according to the Beer-Lambert Law (equation 1):

$$A = a(\lambda) \cdot b \cdot c \qquad 1$$

where A is the measured light absorbance, a(λ) is the wavelength-dependent absorptivity coefficient, b is the optical path length in the OPLS, and c is the specific GHG concentration.

The highly novel innovations in the OPLS, enable this small, light, yet very sensitive instrument to be deployed on a small drone to measure GHG concentrations (CH_4, C_2H_6, CO_2). The result is extremely rapid, real-time measurements at 10 Hz (10 measurements per second), at atmospheric ppm to ppb concentration levels (i.e., at tropospheric mixing ratios). A critical feature of the OPLS, and one that demonstrably differentiates it from any other measurement instruments, including other optical spectrometers, is that the OPLS is so compact and requires such low power that it can be mounted and operated remotely on a sUAV.

Initial Activities

In BC, the OPLS (Figure 6) was mounted and flown on a sUAV (Figure 7) for several test missions over

1) municipal landfill site (Hartland Landfill, Saanich; Figure 8),
2) municipal sewage screening site (Macaulay Point Sewage Outfall, Esquimalt Land District),
3) natural gas distribution facility (Victoria region; Figure 9),
4) natural gas processing, compression, and water treatment sites (Fort St. John region; Figures 10–12), and
5) completed producing and abandoned natural gas well pad sites (Fort St. John region).

Figure 13 shows an example of the time series of CH_4 concentrations measured by OPLS and the corresponding GPS

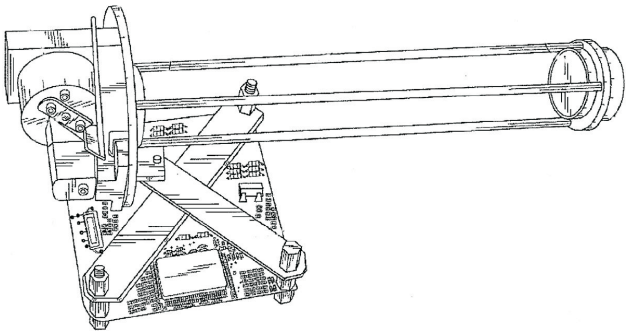

Figure 4. Patented open-path laser spectrometer (OPLS) for the measurement of greenhouse gases (modified from Christensen, 2014). The OPLS includes an electronic system, laser with thermoelectric cooler, analysis region with first and second mirrors, and detector.

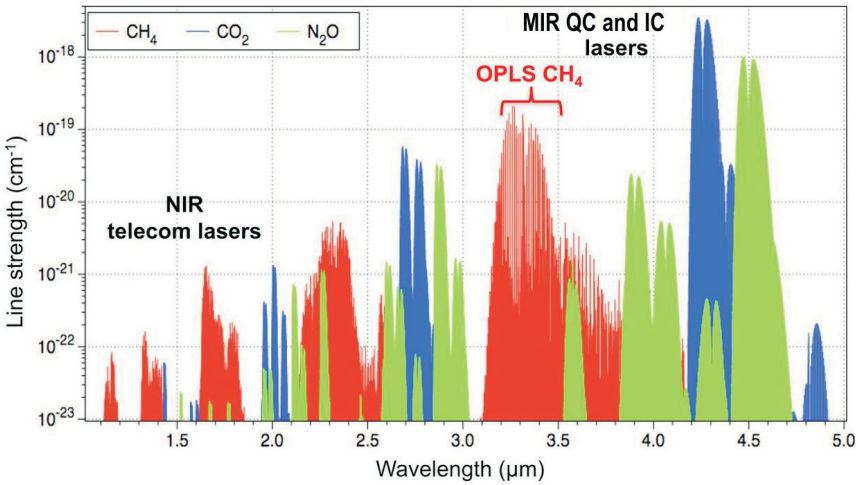

Figure 5. Infrared spectra for major greenhouse gases. The methane open-path laser spectrometer (OPLS) uses new mid-infrared (MIR) quantum cascade (QC) and interband cascade (IC) lasers. These QC and IC lasers can access molecular transitions for methane that are 100x stronger than conventional near-infrared (NIR) telecom laser spectral regions.

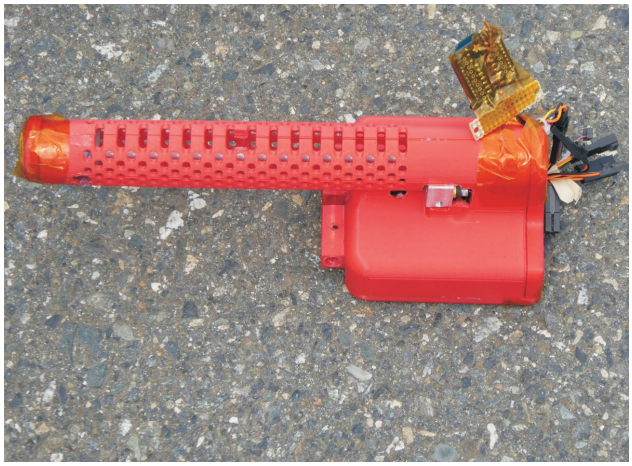

Figure 6. NASA Jet Propulsion Laboratory's open-path laser spectrometer (OPLS) detector probe head.

Figure 7. Deployment of NASA Jet Propulsion Laboratory's open-path laser spectrometer mounted on InDro Robotics Inc.'s small unmanned aerial vehicle.

Figure 8. Open-path laser spectrometer on small unmanned aerial vehicle at Hartland Landfill near Victoria, British Columbia.

Figure 9. Open-path laser spectrometer on small unmanned aerial vehicle at gas distribution plant in Victoria region, British Columbia.

Figure 10. Open-path laser spectrometer on small unmanned aerial vehicle at gas processing plant in Fort St. John region, British Columbia.

Figure 11. Open-path laser spectrometer on small unmanned aerial vehicle at gas processing plant in Fort St. John region, British Columbia.

altitude/position obtained from the sUAV (flown at a natural gas processing plant near Fort St. John, northeastern BC). The example in Figure 13 illustrates the dramatic variations in CH_4 concentrations at different locations on the survey site. Several locations have anomalous CH_4 levels over 10 ppm (~5 times the background CH_4 value of ~1.8 ppm). A single location recorded CH_4 levels over 25 ppm. The survey was also conducted with planned step changes in altitude, from ground level to over 40 m, to resolve the vertical magnitude and distribution of the anomalous CH_4 emissions. The vertical CH_4 survey pattern shows the vertical dissipation, and thus lowering, of CH_4 concentrations with elevation from the ground. This survey technique allows a 3-D definition of the geometry/pattern of the CH_4 emission anomalies at this site. This permits the generation of maps of CH_4 plumes at survey sites.

Figure 14 is a real-time Google Earth™ map view of a natural gas processing plant near Fort St. John during a flight mission. The figure shows a vector plot of the CH_4 concentration levels as colours and the wind direction and speed as the vector length. The cool colours are sites of low CH_4 concentration and the warm to hot colours show increasing levels of anomalous CH_4 concentration.

Figure 15 is an example of post-survey processing and display of the GHG data collected by OPLS/sUAV. The GHG plume is represented as a vertical flux plane of CH_4 concentrations that were measured downwind of a natural gas processing facility. Coupled with microscale meteorology data (boundary layer meteorology) obtained by 3-D–anemometer at the site or directly by instruments on the sUAV, the concentration distributions can be used for eddy covariance flux calculations (also termed eddy correlation) to measure and calculate vertical turbulent fluxes (Aubinet et al., 2012) and thus enable mass flow and quantitative emission mass estimates. The 2-D vertical plane in Figure 15 illustrates a cross-section of the CH_4 concentration downwind of the site. The CH_4 concentrations are scaled as colours with cooler to hotter colours mapped to increasing CH_4 levels.

Ongoing Activities

The current 2017–2018 research and development focus of GHGMap is on

1) optimal integration of OPLS with a sUAV, including GPS navigation, light detecting and ranging (LiDAR) instrument altitude, high definition (HD) video hyperspectral imaging and real-time GHG measurement and drone operation;
2) development of quantitative GHG flux measurement capability using ground-based sonic 3-D–anemometry and a micro, sonic, 3-D–anemometer mounted directly on the sUAV, permitting quantitative determinations of the mass of GHG released (e.g., kg CH_4/yr.), rather than just a GHG distribution map for a survey region; this development will provide information on active localization versus passive back-trajectory modelling;
3) development of real-time and post-survey data processing, reporting and visualization tools; and
4) experimental deployment of OPLS/sUAV over major natural and human-made GHG emission sources (e.g., oil and gas operations, landfills, thermokarst lakes, feedlots, etc.).

Figure 12. Open-path laser spectrometer on small unmanned aerial vehicle at water clarification pond in Fort St. John region, British Columbia.

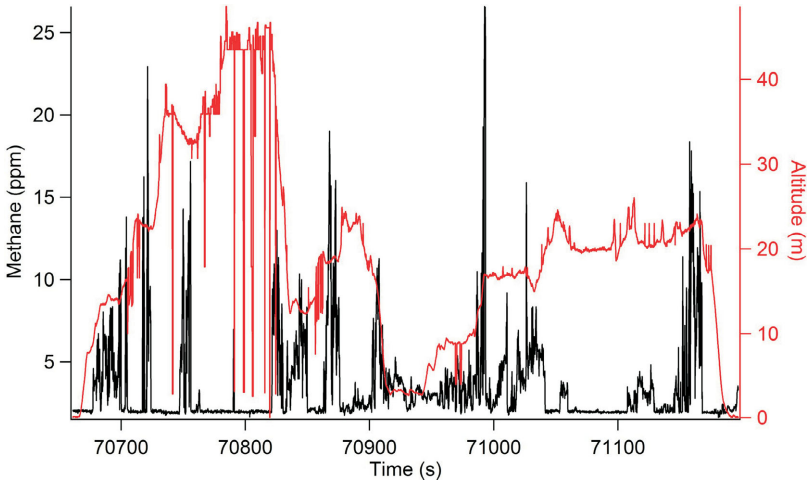

Figure 13. Example of real-time survey results at a gas plant near Fort St. John, British Columbia, using an open-path laser spectrometer (OPLS) on a small unmanned aerial vehicle (sUAV) system. The relationship between OPLS-measured methane concentration anomalies in the atmosphere (black line) and the GPS altitude of the sUAV (red line) is shown.

Figure 14. Example of a vector plot of methane emission data collected by an open-path laser spectrometer (OPLS) on a small unmanned aerial vehicle (sUAV) system at a natural gas well pad, near Fort St. John, British Columbia. Methane concentrations are scaled as cooler to hotter colours indicating increasing levels of anomalous methane concentration. The vector lengths indicate the wind direction and speed. The black line is the flight track. Map data: Google, DigitalGlobe.

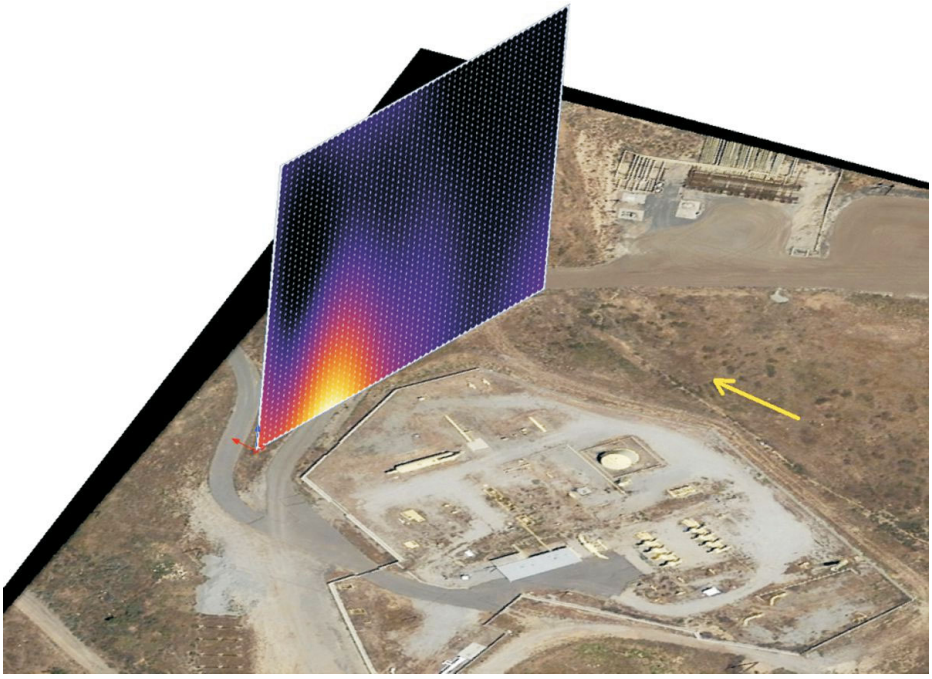

Figure 15. Example of post-survey processing and display of methane emission data collected using an open-path laser spectrometer on a small unmanned aerial vehicle system at a natural gas processing facility. The 2-D vertical plane shows the cross-section of methane concentrations scaled as colours, with cooler (blue) to hotter (red to yellow to white) colours mapped to increasing methane levels. The yellow arrow indicates the predominant wind direction.

Conclusions

The effects and consequences of climate change, brought on significantly through increased anthropogenic emissions of GHGs, pose serious global social, environmental and economic challenges. Today, established emission models with minimal actual measurements are generally relied upon to characterize the GHGs emission inventories. Although these models may represent a consensus approach for estimating and reporting of GHGs, and provide a convenient methodology to establish GHG assessments, they are seriously flawed. Part of the problem with implementing wide-scale GHG measurements is, in fact, the scale. Traditionally, GHG measurements are made using stationary, point-source instrumentation. However, the coverage (measurement density) is limited in space and time, and suffers from data underrepresentation. Any reduction in GHG emissions requires robust and verifiable GHG information and budgets based on quantitative measurements.

Recently, mobile measurements by land vehicles have offered some improvement, but these are costly and limited to accessible locations. Satellites have the potential to provide global coverage but, unfortunately, the satellites (e.g., SCIAMACHY, GOSAT, TES, GHGSat, AIRS on Aqua, IASI on Metop, SathyabamaSat and even the recently launched TROPOMI) have either insufficient spatial resolution and/or sensitivity to detect small- and medium-sized GHG emissions, such as from a compressor plant, and thus are of limited use for facilities with footprints of less than a kilometre. Studies that include aircraft-based measurements, using fixed-wing aircraft, provide good coverage and detail (e.g., CalNex, INTEX-A, HIAPER, HIPPO). Their limitations lie in a) the minimal flight elevations, which limit the size of emission that can be identified; and b) the operational costs of surveys.

The GHGMap OPLS/sUAV system offers a novel, mobile, technological approach that can efficiently bridge the spatial gap between point-source/ground and fixed-wing aircraft/satellite measurement scales. The OPLS/sUAV system is a fast, precise and cost-effective method to conduct site-specific and regional surveys, including conventional (landfills, gas plants, feedlots, etc.) and challenging locations and facilities (pipelines, dams, thermokarst lakes, etc.). Extensive deployments of the OPLS/sUAV system represent an emerging opportunity for various GHG stakeholders, including governments, First Nations, industry and the public.

This new monitoring method permits verifiable control and quantification of emission provenances, budgets and mitigation operations. The initial GHGMap program is focusing primarily on waste, agriculture and energy GHG emissions in western Canada, but the work will expand in scope to other major GHG emitters nationally and potentially internationally.

Acknowledgments

The authors would like to thank C. Evans, University of Victoria, for his review of the manuscript. Funding for GHGMap is generously provided by grants from Geoscience BC and Western Economic Diversification Canada.

References

Aubinet, M., Vesala, T. and Papale, D., editors (2012): Eddy Covariance, A Practical Guide to Measurement and Data Analysis; Springer, Germany, 438 p.

BC Ministry of Environment (2012): British Columbia greenhouse gas inventory report 2012; BC Ministry of Environment, 78 p., URL <https://www2.gov.bc.ca/assets/gov/environment/climate-change/data/provincial-inventory/2012/pir-2012-full-report.pdf> [October 2017].

BC Ministry of Environment (2016a): Methodology document for the British Columbia provincial greenhouse gas inventory; BC Ministry of Environment, Climate Action Secretariat, 30 p., URL <https://www2.gov.bc.ca/assets/gov/environment/climate-change/data/provincial-inventory/2014/303525_provincial_inventory-2014-methodology.pdf> [October 2017].

BC Ministry of Environment (2016b): Provincial inventory tables, 1990-2014; BC Ministry of Environment, Climate Action Secretariat, URL <https://www2.gov.bc.ca/assets/gov/environment/climate-change/data/provincial-inventory/2014/pir-2014-workbook.xlsx> [November 2017].

BC Ministry of Environment (2016c): Trends in greenhouse gas emissions in B.C. (1990-2014); BC Ministry of Environment, Environmental Reporting BC, URL <http://www.env.gov.bc.ca/soe/indicators/sustainability/ghg-emissions.html> [November 2017].

Christensen, L.E. (2014): Miniature tunable laser spectrometer for detection of a trace gas; United States Patent and Trademark Office, patent number US 20140204382 A1, URL <https://www.uspto.gov> [November 2017].

Ciais, P., Sabine, C., Bala, G., Bopp, L., Brovkin, V., Canadell, J., Chhabra, A., DeFries, R., Galloway, J., Heimann, M., Jones, C., Le Quéré, C., Myneni, R., Piao, S. and Thornton, P. (2013): Carbon and other biogeochemical cycles; *in* Climate Change 2013: The Physical Science Basis, Working Group I Contribution to the Fifth Assessment Report of the Intergovernmental Panel on Climate Change, T.F. Stocker, D. Qin, G.-K. Plattner, M. Tignor, S.K. Allen, J. Boschung, A. Nauels, Y. Xia, V. Bex and P.M. Midgley (ed.), Cambridge University Press, Cambridge, United Kingdom and New York, New York, p. 465–570, URL <http://www.ipcc.ch/pdf/assessment-report/ar5/wg1/WG1AR5_Chapter06_FINAL.pdf> [November 2017].

Clearstone Engineering Ltd. (2005): A national inventory of greenhouse gas (GHG), criteria air contaminant (CAC) and hydrogen sulphide (H_2S) emissions by the upstream oil and gas industry; prepared for Canadian Association of Petroleum Producers, v. 1–5, 794 p.

Clearstone Engineering Ltd. (2014): Update of fugitive equipment leak emission factors; report prepared for Canadian Association of Petroleum Producers, 47 p.,

URL <http://www.capp.ca/publications-and-statistics/publications/238773> [November 2017].

de la Chesnaye, F.C., Delhotal, C., DeAngelo, B., Ottinger-Schaefer, D.O. and Godwin, D. (2006): Past, present, and future of non-CO_2 gas mitigation analysis; *in* Human-Induced Climate Change: An Interdisciplinary Assessment, M. Schlesinger, H. Keshgi, J. Smith, F.C. de la Chesnaye, J.M. Reilly, T. Wilson and C. Kolstad (ed.), Cambridge University Press, Cambridge, United Kingdom, p. 266–281.

Eggleston, H.S., Buendia, L., Miwa, K., Ngara, T. and Tanabe, K., editors (2006): 2006 IPCC Guidelines for National Greenhouse Gas Inventories; prepared by the National Greenhouse Gas Inventories Programme, Institute for Global Environmental Strategies, Hayama, Japan, 5 volumes.

Environment and Climate Change Canada (2017): National inventory report 1990-2015: greenhouse gas sources and sinks in Canada; Environment and Climate Change Canada, Parts 1–3, 654 p., URL <http://unfccc.int/national_reports/annex_i_ghg_inventories/national_inventories_ submissions/items/9492.php> [October 2017].

Houghton, J.T., Meira Filho, L.G., Callander, B.A., Harris, N., Kattenberg, A. and Maskell, K. (1996): Climate Change 1995, The Science of Climate Change, Contribution of Working Group I to the Second Assessment Report of the Intergovernmental Panel on Climate Change; Cambridge University Press, Cambridge, United Kingdom and New York, New York, 572 p.

Johnson, M.R., Tyner, D.R., Conley, S., Schwietzke, S. and Zavala-Araiza, D. (2017): Comparisons of airborne measurements and inventory estimates of methane emissions in the Alberta upstream oil and gas sector; Environmental Science & Technology, v. 51, issue 21, p. 13008–13017, doi:10.1021/acs.est.7b03525

Karion, A., Sweeney, C., Pétron, G., Frost, G., Hardesty, R., Kofler, J., Miller, B., Newberger, T., Wolter, S., Banta, R., Brewer, A., Dlugokencky, E., Lang, P., Montzka, S., Schnell, R., Tans, P., Trainer, M., Zamora, R. and Conley, S. (2013): Methane emissions estimate from airborne measurements over a western United States natural gas field; Geophysical Research Letters, v. 40, p. 4393–4397, doi:10.1002/grl.50811

Kshtriya, J. (2017): Autonomous ground target tracking, testing, commissioning and operations for greenhouse gas satellite demonstrator (GHGSat-D); Ph.D. thesis, University of Toronto, ProQuest, Dissertation 10254589, 112 p.

Le Quéré, C., Andrew, R.M., Canadell, J.G., Sitch, S., Korsbakken, J.I., Peters, G.P., Manning, A.C., Boden, T.A., Tans, P.P., Houghton, R.A., Keeling, R.F., Alin, S., Andrews, O.D., Anthoni, P., Barbero, L., Bopp, L., Chevallier, F., Chini, L.P., Ciais, P., Currie, K., Delire, C., Doney, S.C., Friedlingstein, P., Gkritzalis, T., Harris, I., Hauck, J., Haverd, V., Hoppema, M., Klein Goldewijk, K., Jain, A.K., Kato, E., Körtzinger, A., Landschützer, P., Lefèvre, N., Lenton, A., Lienert, S., Lombardozzi, D., Melton, J.R., Metzl, N., Millero, F., Monteiro, P.M.S., Munro, D.R., Nabel, J.E.M.S., Nakaoka, S., O'Brien, K., Olsen, A., Omar, A.M., Ono, T., Pierrot, D., Poulter, B., Rödenbeck, C., Salisbury, J., Schuster, U., Schwinger, J., Séférian, R., Skjelvan, I., Stocker, B.D., Sutton, A.J., Takahashi, T., Tian, H., Tilbrook, B., van der Laan-Luijkx, I.T., van der Werf, G.R., Viovy, N., Walker, A.P., Wiltshire, A.J. and Zaehle, S. (2016): Global carbon budget 2016; Earth System Science Data, v. 8, p. 605–649, URL <http://www.earth-syst-sci-data.net/8/605/2016/.pdf> [December 2017].

Myhre, G., Shindell, D., Bréon, F.-M., Collins, W., Fuglestvedt, J., Huang, J., Koch, D., Lamarque, J.-F., Lee, D., Mendoza, B., Nakajima, T., Robock, A., Stephens, G., Takemura, T. and Zhang, H. (2013): Anthropogenic and natural radiative forcing; Chapter 8 *in* Climate Change 2013: The Physical Science Basis, Working Group I Contribution to the Fifth Assessment Report of the Intergovernmental Panel on Climate Change, T.F. Stocker, D. Qin, G.-K. Plattner, M. Tignor, S.K. Allen, J. Boschung, A. Nauels, Y. Xia, V. Bex and P.M. Midgley (ed.), Cambridge University Press, Cambridge, United Kingdom and New York, New York, p. 659–740.

NASA (2016): Mini NASA methane sensor makes successful flight test; NASA Jet Propulsion Laboratory, news release, March 28, 2016, URL <http://www.jpl.nasa.gov/news/news.php?feature=6192> [October 2017].

Solomon, S., Qin, D., Manning, M., Chen, Z., Marquis, M., Averyt, K.B., Tignor, M. and Miller, H.L., editors (2007): Climate Change 2007: The Physical Science Basis, Contribution of Working Group I to the Fourth Assessment Report of the Intergovernmental Panel on Climate Change; Cambridge University Press, Cambridge, United Kingdom and New York, New York, 996 p.

Stocker, T.F., Qin, D., Plattner, G.-K., Tignor, M., Allen, S.K., Boschung, J., Nauels, A., Xia, Y., Bex, V. and Midgley, P.M., editors (2013): Climate Change 2013: The Physical Science Basis, Working Group I Contribution to the Fifth Assessment Report of the Intergovernmental Panel on Climate Change; Cambridge University Press, Cambridge, United Kingdom and New York, New York, 1535 p.

United States Environmental Protection Agency (2006): Global anthropogenic non-CO2 greenhouse gas emissions: 1990-2020; United States Environmental Protection Agency, Climate Change Division, Office of Atmospheric Programs, Report EPA-430-R-06-003, 274 p.

British Columbia Natural Gas Atlas Update 2017: Recorrelation Changes the Picture

C. Evans, School of Earth and Ocean Sciences, University of Victoria, Victoria, BC, c2evans@uvic.ca

B.J. Hayes, Petrel Robertson Consulting Limited, Calgary, AB

Evans, C. and Hayes, B.J. (2018): British Columbia Natural Gas Atlas update 2017: recorrelation changes the picture; *in* Geoscience BC Summary of Activities 2017: Energy, Geoscience BC, Report 2018-4, p. 11–14.

Introduction

After the publication of Evans and Whiticar (2017), the British Columbia Natural Gas Atlas (BCNGA; http://bc-NGA.ca/BC-NGA_Home.html) moved in a new direction in 2017. The project currently relies on gas composition and isotopic data submitted by industry to the BC Oil and Gas Commission (BCOGC). It was identified that these submissions had incomplete stratigraphy in the data and some could not be mapped. As a result, a correlation review was undertaken on the entire dataset intended for use in the northeastern British Columbia (NEBC; Figure 1) portion (more than 9000 entries of gas composition and approximately 200 entries of isotopic data) of the BC NGA under a separate contract funded by Geoscience BC. The recorrelation will have impacts on the future mapping because the identification of similar stratigraphic horizons is key to the geochemistry.

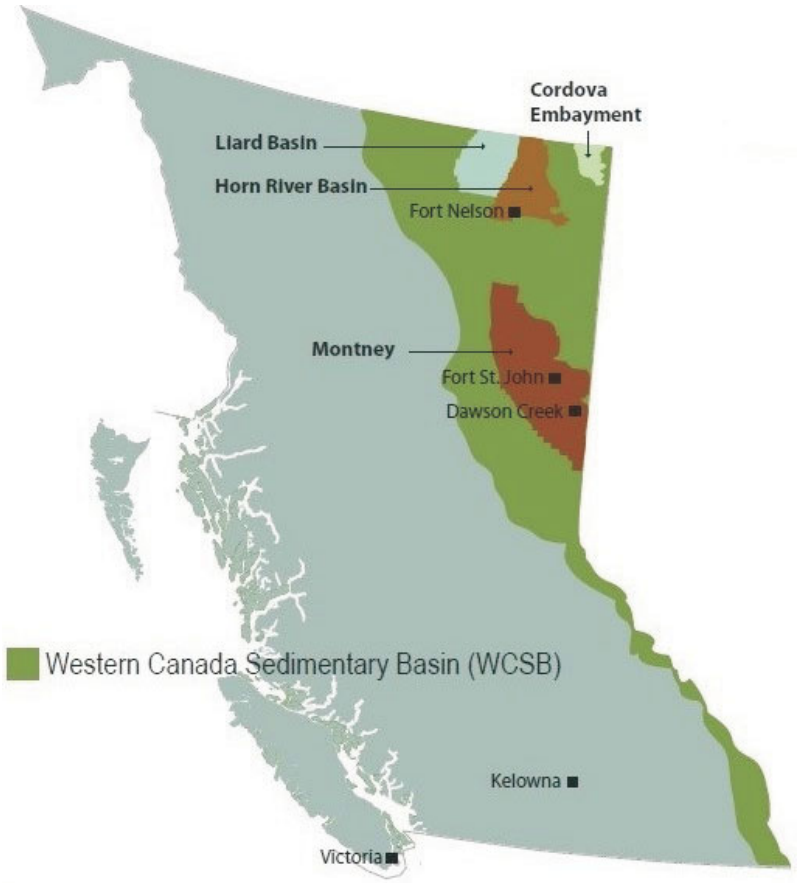

Figure 1. Location of the northeastern British Columbia portion of the Western Canada Sedimentary Basin (in green). The four sub-basins shown are current targets of natural gas exploration and development by industry (Evans and Whiticar, 2017)

Background

Raw gas molecular composition data were previously downloaded from the BCOGC and filtered to a representative dataset for regional mapping. Filtering data was based on geographical distribution, well type, declustering well pads, making a representative point for horizontal wells and grouping strata (Evans and Whiticar, 2017). Some stratigraphic intervals retained almost all data points, whereas other intervals underwent strong filtering, particularly recent production intervals dominated by horizontal wells. Gas isotopic data are more recent and sparsely distributed across a few geological formations, but there was no correlation coding associated with these data and new codes were required for correlation. Almost all isotopic data that can be reasonably traced to original lab reports have been used.

Methods

Wells and test intervals with molecular composition or isotopic data were compared against the geophysical logs publicly available from the BCOGC and new stratigraphic intervals were assigned where warranted. The original BCOGC formation codes have been retained for reference.

This publication is also available, free of charge, as colour digital files in Adobe Acrobat® PDF format from the Geoscience BC website: http://www.geosciencebc.com/s/SummaryofActivities.asp.

Results

The recorrelation exercise is creating two types of results. Samples that originally had no formation code (generally on reports of shallow molecular composition tests and all reports of isotopic tests) were correlated and a small percentage of samples that were identified as incorrectly correlated were recorrelated. Continuing through the whole collection is resulting in new or changed formation (Fm) codes in addition to the original BCOGC formation codes.

The following are examples of the changes made, stratigraphically from the top. The BCOGC Fm codes are listed in parentheses after the formation name.

The Spirit River (2350) Fm in the BCOGC data currently has one sample location, but its members have significantly more: the Notikewin (2400) Member has more than 500 locations and the Falher (2500) Member and sub-members have more than 100 locations. The similar geochemistry of the Falher submembers have already been combined to member level for mapping purposes. The Notikewin and Falher can be readily identified from each other only to the south of a paleo-shoreline. To the north of that limit, the new correlation will assign all reservoir sands in the strata to the Spirit River Fm. Further mapping will be done to determine whether the Spirit River Fm should be mapped as one formation or split into the members.

The coarsening-upward marine shoreline sandstones and conglomerates of the Bluesky (2600) Fm have a large dataset (approximately 750 locations) and the fluvial and/or floodplain Gething (2700) Fm has a distinct set of more than 600 locations; however, where the formations are combined and previously thought to be undifferentiated, now are correlated as predominantly Bluesky Fm only. There are a significant number of Gething Fm tests where the fluvial and/or floodplain regime can be correlated with confidence. The Gething Fm does include the only coalbed methane tests in NEBC and needs to be mapped separately from the marine influenced strata.

The Chinkeh (2805) Fm, located only in the Liard Basin, is stratigraphically distinct from the Cadomin (2800) Fm, but they will be mapped together as an apparent contiguous dataset with a clear boundary between the areas. This may change if there is a large change in geochemistry between the formations.

The Dunlevy (2900) Fm is an obsolete stratigraphic term based on outcrop descriptions that were never reliably correlated to the subsurface. Detailed correlation and mapping has reassigned Dunlevy to the Buick Creek Sandstone (2890), which is laterally equivalent to the Nikanassin (2850) Fm, and in rarer cases the Dunlevy is now assigned to the younger Cadomin or Gething formations.

One of the largest datasets with more than 800 locations is the Baldonnel (4100) Fm, but sampling complexity occurs in three situations where

a) the Baldonnel (4100) Fm is merged with the Charlie Lake (4500) Fm near the subcrop edge of the Charlie Lake Fm as the Baldonnel unconformably lies on top of the Charlie Lake. Tests here have been assigned to be Baldonnel only.

b) near the northern subcrop edge of the Nordegg (3200) Member, some reservoirs have been assigned erroneously to the 'Nordegg-Baldonnel' or 'Nordegg'. These are actually basal Cretaceous deposits, formed by reworking of older Baldonnel and Nordegg strata into highly variable mixtures of radioactive shale, carbonate and sand that can easily be mistaken for the actual Nordegg or Baldonnel on geophysical logs. The combination Nordegg-Baldonnel is in an isolated area with very few samples. It was not recorrelated because it is not planned to be part of the overall mapping exercise—this may change in the future if analysis shows compatibility with any other formation.

c) within the Rocky Mountain Foothills area, the Baldonnel gets structurally complicated with the Pardonet (4050) Fm. Tests here have been assigned to be Baldonnel only.

Other subcrop issues arise where the Lower Cretaceous Bluesky (2600) Fm and Gething (2700) Fm, by way of the sub-Cretaceous unconformity, erode down to the underlying formations of Charlie Lake (4500) Fm and Montney (5000) Fm. Where separate zones are distinct, the previously merged formation codes were subdivided to allow some separate mapping. In some locations, where further correlation work is required, the zones had to remain merged and will be the subject of a focused mapping exercise.

The Halfway (4800) Fm has the largest dataset with more than 1400 locations, but there is often an accompanying test in an interval called the lower Halfway (4805) Fm. It was determined that this interval was more like the Doig (4900) Fm and thus was recorrelated to Doig. Mapping will confirm that the geochemistry data are compatible.

The Montney (5000) Fm is the other large dataset with just less than 1400 locations after declustering horizontal well data. These data points are spread throughout a thickness that ranges up to 300 m. There is strong interest in production categories and reservoir characterization of the many different stratigraphic intervals within the Montney, but that formal subdivision and correlations have not yet been published. The correlations have been found to only be robust when based on geological ages at a very fine level that is often beyond the resolution of downhole geophysical logs. Further work will be required on this dataset.

The Kiskatinaw (7250) Fm is a well-defined clastic unit of Pennsylvanian age at the base of the Stoddart Group. Production is not always distinguished from the sour-gas–prone, overlying Permian Belloy (6200) Fm, but the testing in the Kiskatinaw is limited to approximately 50 locations and apparently the geochemistry maps very well with the underlying Debolt (7400) Fm. This will be confirmed in the future and may provide further information on the intervening Golata Formation shale. Any combination tests as Kiskatinaw plus Belloy were assigned to the Belloy Fm only.

The Rundle Group is not as well subdivided in NEBC as it is farther south. In NEBC, the hydrocarbon occurrences are concentrated near the top of the group in the Debolt (7400) Fm. All tests from the Rundle Group formations (Elkton [7450], Shunda [7500] and Pekisko [7600]) are now classified as being sourced from the Debolt Fm.

The Slave Point (8400) Fm, Keg River (8450) Fm, Sulphur Point (8500) Fm and Pine Point (8600) Fm have counts of sample locations as 390, 003, 001 and 043 respectively. These formations are stacked Devonian reefal carbonates bordering the Horn River Basin, Liard Basin and smaller embayments. Where good well control exists and the formations are fully developed, they can be subdivided with confidence. In many places, however, there are relatively few complete penetrations and diagenetic overprints can make it difficult to accurately distinguish stacked carbonate units. Currently, all are assigned to the Slave Point, but that will be confirmed in future work.

A stratigraphic chart showing these complexities is being generated for a later report.

Future Work

Ongoing mapping is illustrating clear trends in some horizons that match some already published material (Wood and Sanei, 2016). More work is required to ensure an accurate picture of the 'gas fingerprint' (Evans and Whiticar, 2017) is presented in the public data and manual confirmation of recorrelations is underway. Further stratigraphic work is required on the appropriateness of

- mapping grouped datasets (e.g., Kiskatinaw with Debolt);
- merging datasets that are too small or peripheral (e.g., the Nordegg-Baldonnel); and
- deciding if there is a need to split large datasets into finer correlations (e.g., the Montney).

Future publications will include a stratigraphic chart showing detailed correlation issues that will affect mapping and the interpretations for splitting versus grouping versus discarding some datasets.

Conclusions

The work on the BCNGA continues in the direction previously identified (Evans and Whiticar, 2017) with an expected completion of the NEBC portion in November 2018. Alignment of the project with stratigraphy will continue for the coming year.

Acknowledgments

The authors thank Geoscience BC, the BC Oil and Gas Research and Innovation Society and the Province of British Columbia for the opportunity to undertake this project. Support for the BCNGA project has been sustained from the BCOGC; the staff has been very helpful in supplying data, explaining data analysis and providing updates to the source database. Discussions with staff at Geoscience BC have influenced the direction of studies and Geoscience BC will be supporting future releases of map products. Further support has been provided by the members of the Project Advisory Committee, who are still proactive in a challenging time for the energy industry. Also, the active operators have been very open with discussions and have provided support for the interim results. The authors thank M. Dawson for his review of this paper.

References

Evans, C. and Whiticar, M.J. (2017): British Columbia Natural Gas Atlas project: 2016 project update; *in* Geoscience BC Summary of Activities 2016, Geoscience BC, Report 2017-1, p. 75–78, URL <http://www.geosciencebc.com/i/pdf/SummaryofActivities2016/SoA2016_Evans.pdf> [December 2017].

Wood, J.M. and Sanei, H. (2016): Secondary migration and leakage of methane from a major tight-gas system; Nature Communications, v. 7, art. 13614. doi:10.1038/ncomms13614

Attenuation of Ground-Motion Amplitudes from Small-Magnitude Earthquakes in the Montney Play, Northeastern British Columbia

A. Babaie Mahani, Geoscience BC, Vancouver, BC, ali.mahani@mahangeo.com

H. Kao, Natural Resources Canada, Geological Survey of Canada-Pacific, Sidney, BC

Babaie Mahani, A. and Kao, H. (2018): Attenuation of ground-motion amplitudes from small-magnitude earthquakes in the Montney play, northeastern British Columbia; *in* Geoscience BC Summary of Activities 2017: Energy, Geoscience BC, Report 2018-4, p. 15–22.

Introduction

Analysis of local ground-motion data recorded by seismographic stations is essential in understanding the potential seismic hazard in a region. Ground-motion prediction equations (GMPE) are key elements in every seismic hazard assessment, especially at distances close to the source of shallow induced earthquakes, which have the potential of causing damage to structures close to injection sites (Novakovic and Atkinson, 2015). Near-source evaluation of ground-motion amplitudes is now possible in areas such as western Alberta and northeastern British Columbia (BC) with the recent increase in seismograph stations for the purpose of monitoring the induced seismicity from hydraulic fracturing and wastewater injection (Schultz et al., 2015; Babaie Mahani et al., 2016). The aim of this project is to analyze a rich database of ground-motion amplitudes from small-magnitude, potentially induced earthquakes in the Montney play of northeastern BC recorded at short hypocentral distance. The majority of data used in this study are from waveforms recorded by the private seismograph stations near hydraulic fracturing and wastewater injection operations. Of particular interest is understanding the characteristics of the observed ground-motion amplitudes from events with amplitudes large enough for the onset of damage. This paper details the datasets used in this study, followed by the analysis of attenuation of ground-motion amplitudes in the Montney play. Understanding the local ground-motion parameters in the study area is important for the assessment of the potential seismic hazard from induced events to infrastructure, such as the BC Hydro Site C dam on the Peace River near Fort St. John.

Database

Waveforms from local and regional broadband seismographic stations in the study area were used to analyze ground-motion amplitudes from small induced earthquakes. Most of the waveforms are from two networks of five stations operated by Canadian Natural Resources Limited (CNRL) in the Graham and Septimus areas (Figure 1) to monitor the disposal of wastewater. Waveforms from three other private networks were also used: ARC Resources Ltd. (ARC) and Encana Corporation (Encana) for monitoring of hydraulic fracturing and Canbriam Energy Inc. (Canbriam) for monitoring of hydraulic fracturing and wastewater disposal.

Besides the data from private seismograph stations, waveforms from three Canadian National Seismograph Network (CNSN) stations in the region were also included to complement the database used in this study (Figure 1). Station number 1, in the Graham area, was originally a CNRL station but converted to a CNSN station in 2016.

Waveforms from 219 local events were used in this study, of which 129 events are in the Graham area and 90 events are in the Septimus area. For the Graham area, the CNRL network recorded 123 events for the period between March 21, 2014 and August 28, 2015 while the Canbriam network recorded two events on May 1 and June 11, 2016. There are also data from four events at CNSN station 1 on December 30, 2016, April 19 and 21, 2017 and June 8, 2017. For the Septimus area, the CNRL network recorded 81 events for the period between April 16 and October 12, 2014. The ARC network recorded four events on January 14 and 16, 2017 and June 10, 2017 while the Encana seismograph station recorded five events for the period between July 15 and 29, 2017. Data from ARC also includes the waveforms from the two CNSN stations in the Septimus area (Figure 1).

A database of ground-motion amplitudes was compiled after correcting each waveform for instrument response and filtering with a high-pass, second-order Butterworth filter at a corner frequency of 0.1 hertz (Hz). Ground-motion amplitudes for peak ground acceleration (PGA), peak ground velocity (PGV) and response spectral acceleration (PSA) at frequencies of 1, 2, 3.3, 5 and 10 Hz were compiled for the vertical component and the geometric mean of the horizontal components. The available dataset contains ground-motion amplitudes from events with local magnitude (M_L) from 1.5 to 3.8 and hypocentral distance between 1.6 and 42 km (M_L 1.5–3.8 and distance between 2.3 and 19 km in

This publication is also available, free of charge, as colour digital files in Adobe Acrobat® PDF format from the Geoscience BC website: http://www.geosciencebc.com/s/SummaryofActivities.asp.

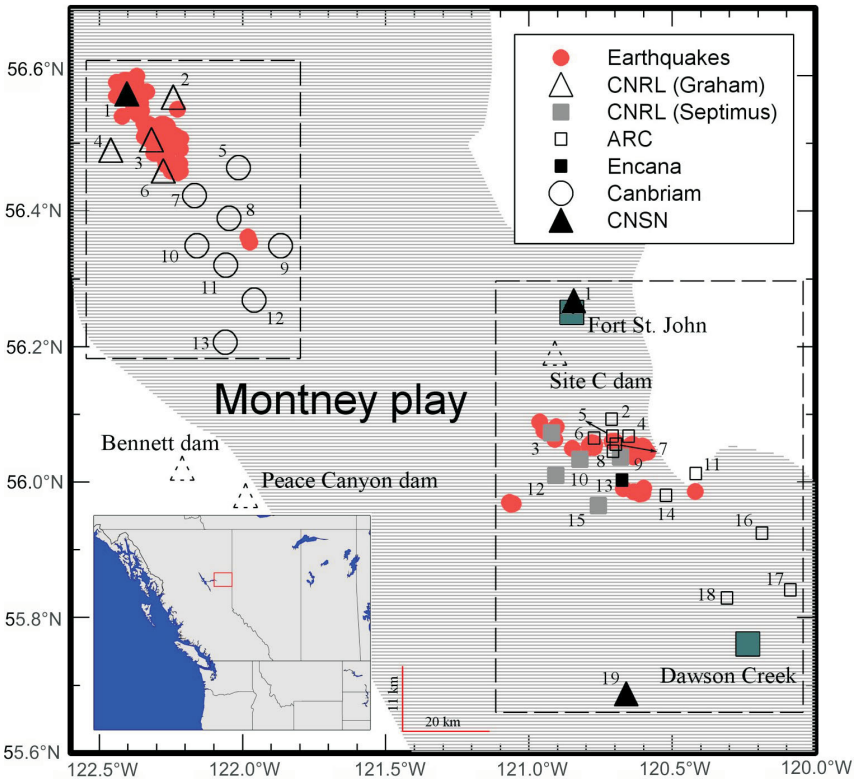

Figure 1. Map of part of the Montney play of northeastern British Columbia and distribution of the earthquakes and stations used in this study. Boxes show the Graham (northwest) and Septimus (southeast) areas with stations numbered in each area. Triangles with stations numbered in each area. Triangles with dashed outlines mark the approximate locations of BC Hydro dams. The inset shows the location of the study area in British Columbia. Abbreviations: ARC, ARC Resources Ltd.; Canbriam, Canbriam Energy Inc.; CNRL, Canadian Natural Resources Limited; CNSN, Canadian National Seismograph Network; Encana, Encana Corporation.

the Graham area and M_L 1.5–3.0 and distance between 1.6 and 42 km in the Septimus area). Most of the ground-motion amplitudes used in this study are from events with magnitude <2 and focal depth between 3 and 4 km. No event in this dataset is deeper than 8 km (for events with unknown depths, a value of 2 km was assigned).

Due to the shallow depth of induced events, damage can still be expected from small earthquakes at short hypocentral distance. Worden et al. (2012) analyzed the relationship between ground-motion amplitudes (PGA and PGV) versus modified Mercalli intensity (MMI) in California. Based on their results, the onset of damage (MMI at level VI; Wald et al., 1999) corresponds to PGA between 50 and 300 cm/s^2 and PGV between 3.8 and 24 cm/s. For the dataset used in this study, all PGA values are below the lower bound for the onset of damage (<50 cm/s^2). At the hypocentral distance of ~2.6 km, however, a relatively large ground acceleration was recorded at one of the ARC seismographic stations (station 8, Figure 1) with a maximum PGA value of ~115 cm/s^2 on the east-west component from an M_L 3 event. In Figure 2, the three-component waveforms from the three events recorded at stations 8 and 5 (closer to the source) are shown. Since events are very close in space, the hypocentral distance to station 5 is ~2.2 km whereas it is ~2.6 km for station 8. It is clear in Figure 2 that PGA is higher at station 8 for all three events and components despite the larger hypocentral distance. Local site condition or radiation pattern might be the reason for the larger observed ground motion at this station.

Attenuation of Ground-Motion Amplitudes

One of the key parameters in seismic hazard assessment is the GMPE, which describes the amplitudes of motions and their attenuation for given magnitude, distance and site condition. Understanding the expected level of ground motion from local seismic events at infrastructure such as the BC Hydro Site C dam (Figure 1) helps with the mitigation of seismic hazard from events caused by fluid injection. This information can also be used for implementation of exclusion zones around critical infrastructures. For this study area, a GMPE has been developed for the geometric mean of the horizontal components of motion, using the ground-motion amplitudes described in the 'Database' section above. These amplitudes have been corrected to the reference site condition with an average shear-wave velocity in the top 30 m (Vs_{30}) of 760 m/s, using the linear component of correction factors provided by Boore et al. (2014) and the estimated Vs_{30} values of Babaie Mahani and Kao (in press) for each seismograph station in the study area. For the purpose of this study, the datasets from the Graham and Septimus areas have been combined. In order to understand the differences in ground motion between the two areas, the ratio of ground-motion amplitudes (Graham to Septimus) were calculated for magnitude and distance bins using the geometric mean of the horizontal components of motion corrected to the reference site condition (Vs_{30} = 760 m/s) in each region. Overall, ground motions are comparable between the two areas with the exception of some frequencies at magnitude bin 2.5–3.0.

The Atkinson (2015) ground-motion model was used for the development of local GMPE as

$$\log Y = c_0 + c_1 M + c_2 M^2 + c_3 \log R \qquad 1$$

where Y is the observed geometric mean of the horizontal components of ground-motion amplitude (e.g., PGA) corrected to the reference site condition (Vs_{30} = 760 m/s). M is

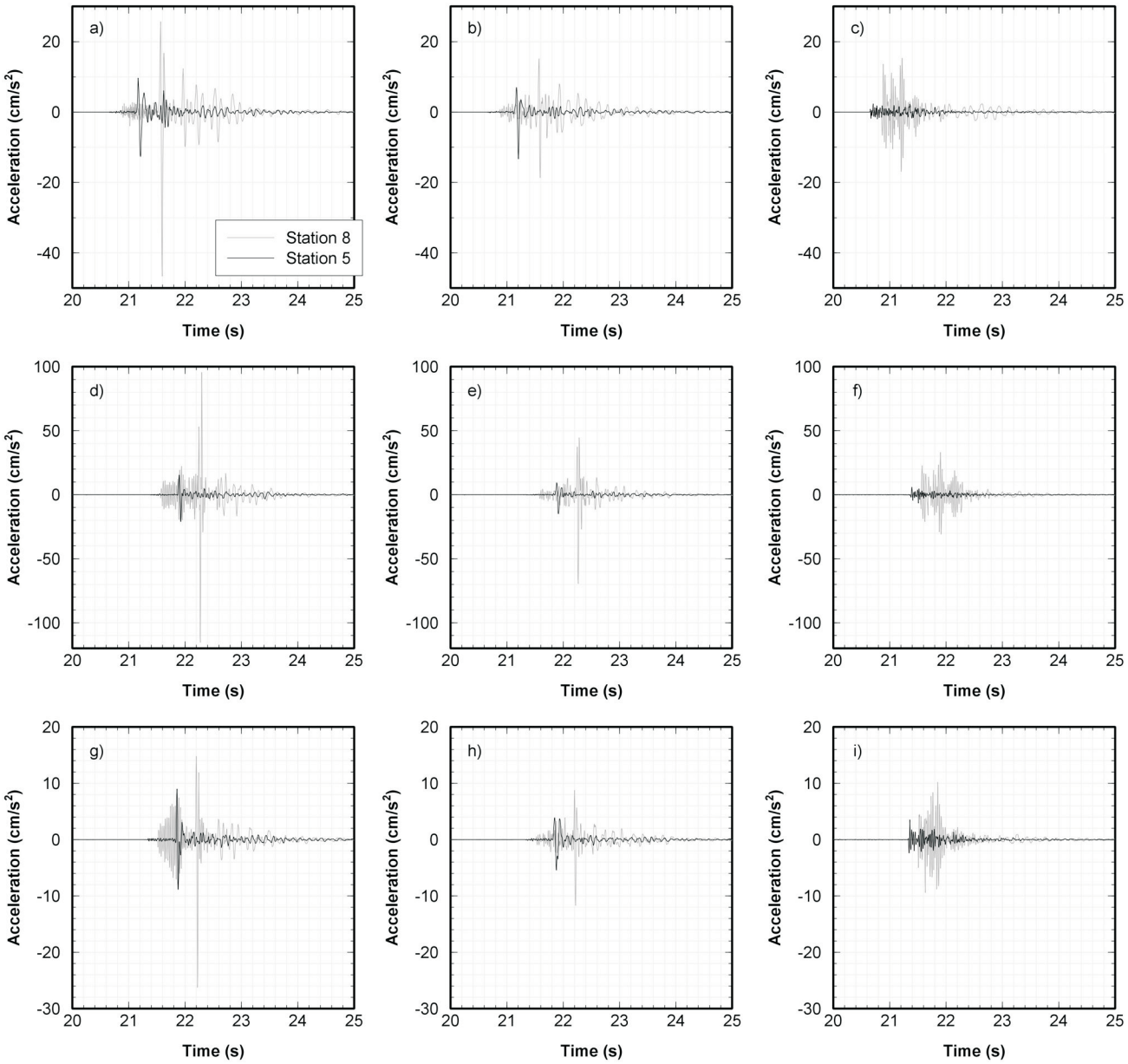

Figure 2. Waveforms of the three events recorded by stations 5 and 8 of the ARC Resources Ltd. seismograph network (northeastern British Columbia; Figure 1). Panels **a)**, **d)** and **g)** are the east-west component, **b)**, **e)** and **h)** are the north-south component, and **c)**, **f)** and **i)** are the vertical component. Top and middle rows are from events with local magnitude 3 and the bottom row is from an event with local magnitude 2.5.

magnitude and R is the effective distance that includes near-source distance-saturation effects using an effective depth parameter, h,

$$R = \sqrt{R_{hypo}^2 + h^2} \qquad 2$$

In equation (2), R_{hypo} is hypocentral distance and h is set as

$$h = \max(1, 10^{(-1.72 + 0.43M)}) \qquad 3$$

The parameters of equation (1) were determined in two steps. In the first step, the distance dependence is determined through calculation of the geometrical spreading coefficient (c_3) along with a source term for each earthquake. In the second step, the magnitude dependency is analyzed by obtaining the coefficients c_0, c_1 and c_2 through the regression between the source terms and event magnitudes using the first three terms in equation (1). Table 1 presents these coefficients determined for the combined dataset used in this study. In Table 1, σ_{intra} and σ_{inter} are the intra-event and inter-event components of standard deviation of the residuals (difference, in log unit, between the observed and predicted values). The total standard deviation was obtained as

$$\sigma_{total} = \sqrt{\sigma_{intra}^2 + \sigma_{inter}^2} \qquad 4$$

Table 1. Coefficients of the regression model (equation 1) for the geometric mean of the horizontal components (corrected for reference site condition with an average shear-wave velocity in the top 30 m [Vs_{30}] of 760 m/s) of peak ground acceleration (PGA), peak ground velocity (PGV) and response spectra acceleration (PSA) at frequencies 1, 2, 3.3, 5 and 10 hertz (Hz) using the combined dataset from the Graham and Septimus areas, northeastern British Columbia.

	c_0	c_1	c_2	c_3	σ_{intra}	σ_{inter}	σ_{total}
PGA	–0.11	0.52	0.07	–2.35	0.33	0.19	0.38
PGV	–2.08	0.55	0.08	–2.29	0.32	0.17	0.36
PSA 10 Hz	–0.11	0.71	0.03	–2.15	0.32	0.17	0.36
PSA 5 Hz	–0.75	0.85	0.02	–2.11	0.31	0.16	0.35
PSA 3.3 Hz	–1.18	0.79	0.04	–1.98	0.26	0.14	0.29
PSA 2 Hz	–1.59	0.73	0.06	–2.07	0.23	0.16	0.29
PSA 1 Hz	–2.49	0.77	0.06	–1.98	0.23	0.16	0.28

Figure 3 shows the residuals from equation (1) for PGA and PGV versus hypocentral distance and magnitude. Overall, there are no trends in the residuals and their mean values are close to zero for the distance and magnitude ranges considered in this study when sufficient number of data are available (hypocentral distance 3–20 km and magnitude 1.5–3.5).

Figure 4 shows the attenuation models for different magnitudes along with the observed ground-motion amplitudes

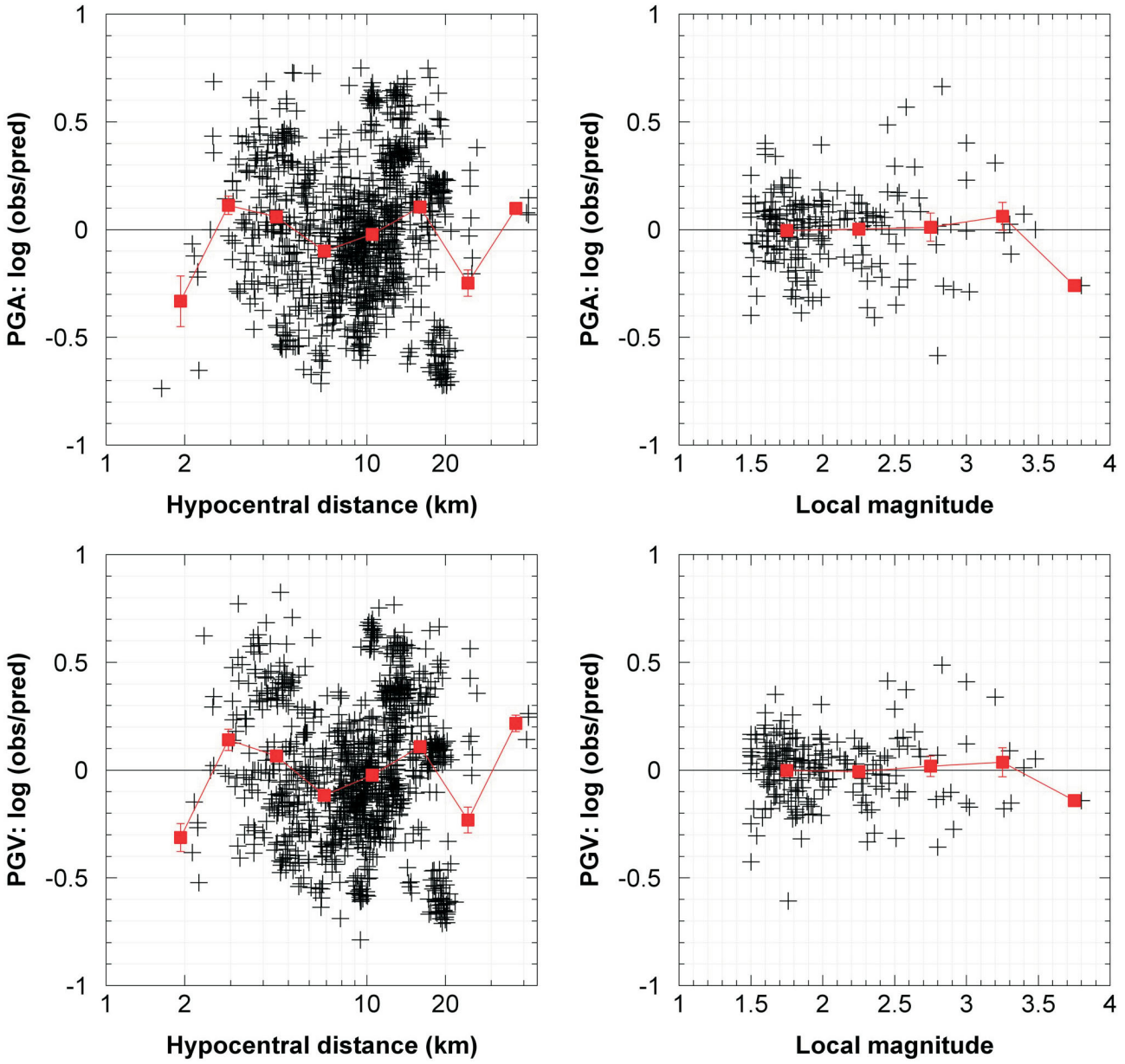

Figure 3. Residuals, defined as the difference (in log unit) between the observed (obs) and predicted (pred) values of peak ground acceleration (PGA) and peak ground velocity (PGV) from equation (1), versus hypocentral distance and local magnitude (Graham and Septimus areas, northeastern British Columbia). Squares are the mean values of residuals determined for logarithmically spaced distance and equally spaced magnitude bins and the error bars are the standard error about the mean.

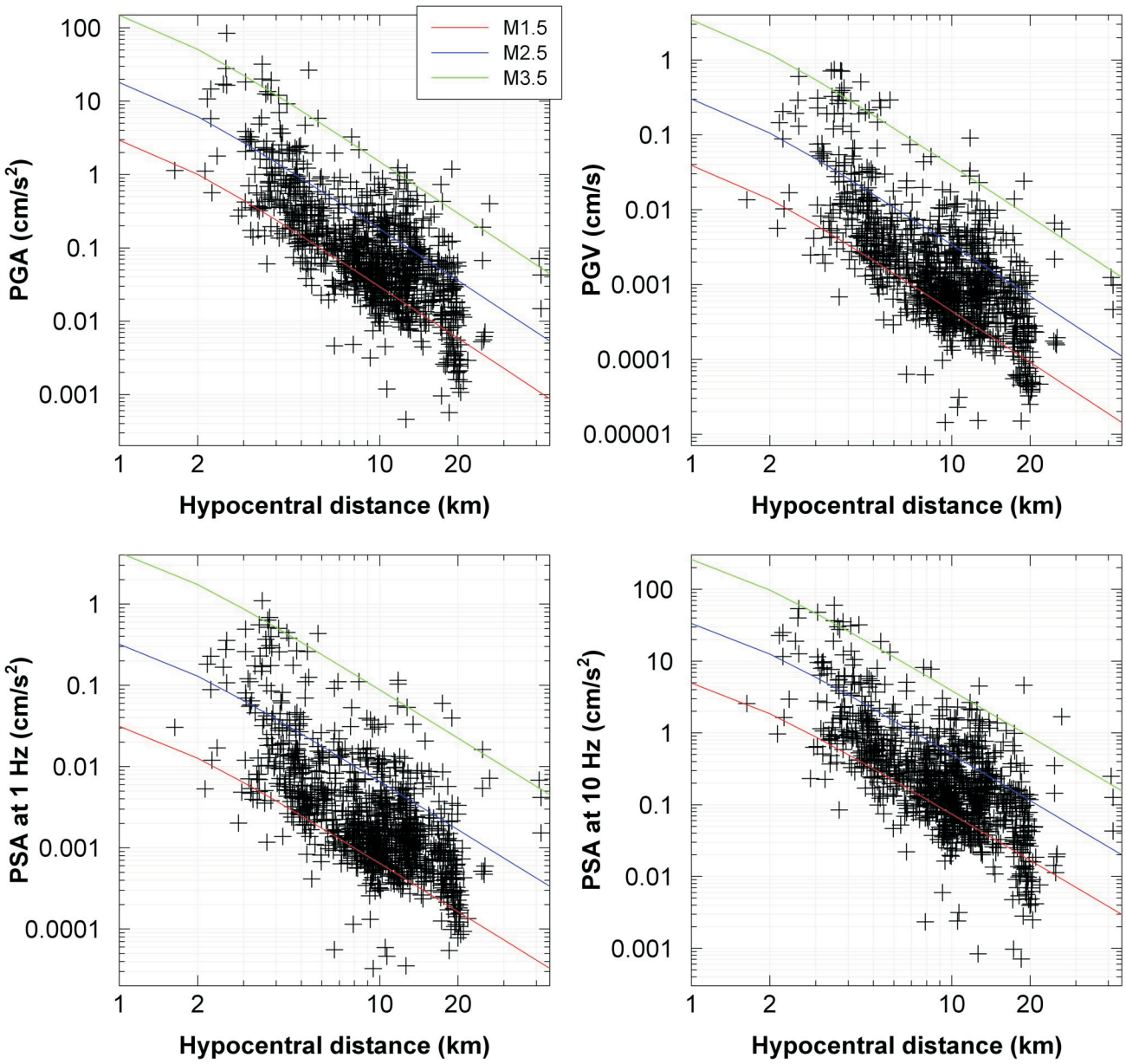

Figure 4. Geometric mean of the horizontal components of motion, corrected for the reference site condition (average shear-wave velocity in the top 30 m [Vs_{30}] of 760 m/s), for peak ground acceleration (PGA), peak ground velocity (PGV) and response spectral acceleration (PSA) at frequencies 1 and 10 hertz (Hz). Also plotted are the prediction models for different magnitudes (red, blue, green lines) using equation (1) and Table 1.

(geometric mean of the horizontal components corrected to the reference site condition) for PGA, PGV and PSA at frequencies 1 and 10 Hz. Geometrical spreading coefficients obtained for ground-motion amplitudes in this study's combined dataset suggest a higher decay rate in the amplitudes with distance than those obtained in Atkinson (2015) using the Next Generation Attenuation-West 2 database (Bozorgnia et al., 2014) for short hypocentral distance (<40 km). For example, in Atkinson (2015), the geometrical spreading coefficient of –1.75 was calculated for the attenuation of PGA whereas a value of –2.35 was obtained in this study (Table 1). The difference in the geometrical spreading attenuation between this study and Atkinson (2015) is most likely due to the different magnitude range considered in the two studies. Whereas the database in Atkinson (2015) includes earthquakes with magnitude 3–6, this study's database only contains smaller earthquakes with magnitude 1.5–3.8. This is an important observation to consider if ground-motion amplitudes from larger magnitude events (e.g., >4) are to be estimated in the Montney play area using the GMPE developed in this study (i.e., this model will likely underestimate ground motions for events with magnitudes >4).

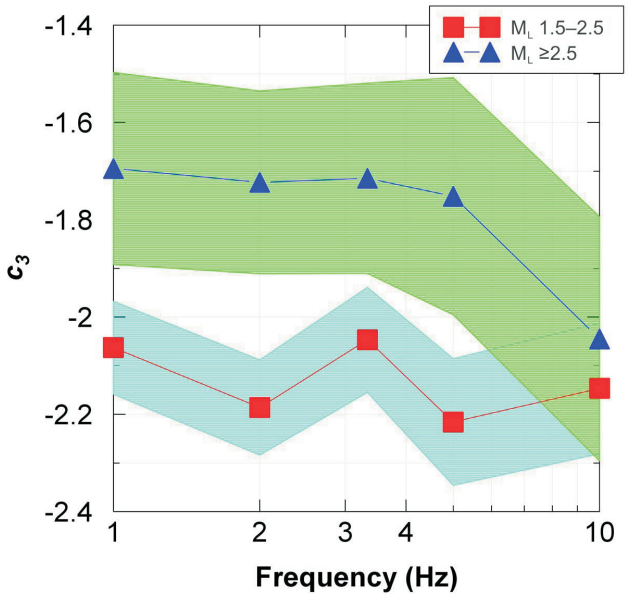

Figure 5. Coefficient of geometrical spreading attenuation (c_3 in equation 1) versus frequency (hertz [HZ]) for two local magnitude (M_L) bins, M_L 1.5–2.5 and M_L ≥2.5 (Montney play, northeastern British Columbia). Shaded regions show the 95% confidence intervals in the estimation of c_3.

To further analyze the change in the geometrical spreading attenuation of ground-motion amplitudes, its coefficient (c_3) was calculated, using equation (1), for two magnitude bins, M_L 1.5–2.5 and M_L ≥2.5, and the results are shown in Figure 5. It is clear that the ground-motion amplitudes from the lower magnitude bin (M_L 1.5–2.5) attenuate faster than those with larger magnitudes (M_L ≥2.5). The difference between the geometrical spreading attenuation becomes minimal at higher frequencies (10 Hz). This is also true for PGV and PGA (not shown).

Conclusions

Attenuation of peak ground acceleration (PGA), peak ground velocity (PGV) and response spectral acceleration (PSA) at frequencies 1, 2, 3.3, 5 and 10 Hz from potentially induced events in the Montney play of northeastern British Columbia were analyzed for this project. The dataset used included waveforms from 219 events with local magnitude (M_L) ranging from 1.5 to 3.8 recorded at hypocentral distance of <45 km. Waveforms were supplied by local seismographic stations operated by energy companies and complemented with some waveforms from the regional seismographic stations of the Canadian National Seismograph Network. The Atkinson (2015) ground-motion prediction equation (GMPE) was used and its coefficients for ground-motion amplitudes were obtained for the Montney play area. Analysis of the geometrical spreading attenuation of ground-motion amplitudes from events with magnitude ranges of M_L 1.5–2.5 and M_L ≥2.5 suggests a lower decay rate for the larger magnitude events, especially for frequencies <10 Hz. This is an important observation to consider if ground-motion amplitudes from larger magnitude events (e.g., magnitudes >4) are to be estimated in the Montney play area using the GMPE developed in this study (i.e., this model will likely underestimate ground motions for events with magnitudes >4).

Acknowledgments

This investigation would not be possible without contributions from the local oil and gas operators. The authors would like to thank N. Orr and A. Gamp from Canadian Natural Resources Limited for sharing the waveforms of more than 200 earthquakes recorded by their seismograph networks in the Graham and Septimus areas. Canbriam Energy Inc., ARC Resources Ltd. and Encana Corporation also contributed waveforms to this study. S. Venables from BC Oil and Gas Commission is especially thanked for his effort in the acquisition of waveform data. This project was supported by the BC Seismic Research Consortium (BC Oil and Gas Commission, Geoscience BC, BC Oil and Gas Research and Innovation Society, Canadian Association of Petroleum Producers and Yukon Geological Survey).

Natural Resources Canada, Lands and Minerals contribution 20170243

References

Atkinson, G.M. (2015): Ground-motion prediction equation for small-to-moderate events at short hypocentral distances, with application to induced-seismicity hazards; Bulletin of Seismological Society of America, v. 105, p. 981–992, URL <https://pubs.geoscienceworld.org/bssa/article-abstract/105/2A/981/332710/> [November 2017].

Babaie Mahani, A. and Kao, H. (in press): Ground motion from M1.5-3.8 induced earthquakes at hypocentral distance <45 km in the Montney play of northeast British Columbia, Canada; Seismological Research Letters.

Babaie Mahani, A., Kao, H., Walker, D., Johnson, J. and Salas, C. (2016): Performance evaluation of the regional seismograph network in northeast British Columbia, Canada, for monitoring of induced seismicity; Seismological Research Letters, v. 87, p. 648–660, URL <http://srl.geoscienceworld.org/content/87/3/648> [November 2017].

Boore, D.M., Stewart, J.P., Seyhan, E. and Atkinson, G.M. (2014): NGA-West2 equations for predicting PGA, PGV, and 5% damped PSA for shallow crustal earthquakes; Earthquake Spectra, v. 30, p. 1057–1085, URL <http://earthquakespectra.org/doi/10.1193/070113EQS184M> [November 2017].

Bozorgnia, Y., Abrahamson, N.A., Al Atik, L., Ancheta, T.D., Atkinson, G.M., Baker, J.W., Baltay, A., Boore, D.M., Campbell, K.W., Chiou, B.S.-J., Darragh, R., Day, S., Donahue, J., Graves, R.W., Gregor, N., Hanks, T., Idriss, I.M., Kamai, R., Kishida, T., Kottke, A., Mahin, S.A., Rezaeian, S., Rowshandel, B., Seyhan, E., Shahi, S., Shantz, T., Silva, W., Spudich, P., Stewart, J.P., Watson-Lamprey, J., Wooddell, K. and Youngs, R. (2014): NGA-West2 research project; Earthquake Spectra, v. 30, p. 973–

987, URL <http://earthquakespectra.org/doi/10.1193/072113EQS209M> [November 2017].

Novakovic, M. and Atkinson, G.M. (2015): Preliminary evaluation of ground motions from earthquakes in Alberta; Seismological Research Letters, v. 86, p. 1086–1095, URL <http://srl.geoscienceworld.org/content/86/4/1086> [November 2017].

Schultz, R., Stern, V., Gu, Y.J. and Eaton, D. (2015): Detection threshold and location resolution of the Alberta Geological Survey Earthquake Catalogue; Seismological Research Letters, v. 86, p. 385–397, URL <http://srl.geoscienceworld.org/content/86/2A/385> [November 2017].

Wald, D.J., Quitoriano, V., Heaton, T.H. and Kanamori, H. (1999): Relationships between peak ground acceleration, peak ground velocity, and Modified Mercalli Intensity in California; Earthquake Spectra, v. 15, p. 557–564, URL <http://earthquakespectra.org/doi/10.1193/1.1586058> [November 2017].

Worden, C.B., Gerstenberger, M.C., Rhoades, D.A. and Wald, D.J. (2012): Probabilistic relationships between ground-motion parameters and Modified Mercalli Intensity in California; Bulletin of Seismological Society of America, v. 102, p. 204–221, URL <https://pubs.geoscienceworld.org/bssa/article-abstract/102/1/204/349630/> [November 2017].

Collecting Ground-Motion Data for the Mitigation and Prevention of Seismicity Induced by Hydraulic Fracturing in the Montney Formation, Northeastern British Columbia

A.M.M. Bustin, The University of British Columbia, Vancouver, BC, abustin@eos.ubc.ca

M. Longobardi, The University of British Columbia, Vancouver, BC

Bustin,, A.M.M. and Longobardi, M. (2018): Collecting ground-motion data for the mitigation and prevention of seismicity induced by hydraulic fracturing in the Montney Formation, northeastern British Columbia; *in* Geoscience BC Summary of Activities 2017: Energy, Geoscience BC, Report 2018-4, p. 23–28.

Introduction

Hydraulic fracturing stimulations in the Montney Formation in northeastern British Columbia (BC) have induced the largest ever reported rate and magnitude of anomalous induced seismicity (AIS), with events of magnitudes up to M_L 4.6 recorded in five clusters within the Montney play (Figure 1; BC Oil and Gas Commission, 2014). The goal of this Geoscience BC research project is to better understand the variables and processes controlling AIS and its associated ground motions due to hydraulic fracturing in the Montney Formation, with the ultimate goal of developing protocols to reduce and mitigate the rate and magnitude of events. The research program has two components: 1) a field component, whereby hydraulic fracture completions will be densely monitored; and 2) 3-dimensional (3-D) hydrogeomechanical modelling.

Over the past year, the original five-station array has been expanded to include 12 new stations in order to densely monitor operation in the Montney. Those five stations were deployed in the spring to monitor a multilateral stimulation, providing the first dataset. The first of the new stations were also deployed during the completions program in order to test their capabilities. All 17 stations are currently deployed, many around disposal wells, as steps are being taken to organize the first dense-monitoring project. The design for these low-cost, mobile, easy-to-install stations was modified from the early-warning earthquake detectors installed in BC schools for its earthquake early-warning system. In addition to providing real-time data and ground motion parameters, algorithms for calculating near real-time hypocentres and magnitudes are being developed.

In this study, the spatiotemporal and magnitude-frequency distributions of microseismicity, AIS, and the associated ground motions will be analyzed and different mitigation techniques will be tested through 3-D numerical simulations to develop an effective AIS traffic-light protocol (TLP) based on ground motions. Developing TLPs, and combining them with research on reservoir geomechanics, has the goal of developing real-time adjustments to completion programs to prevent AIS, at the same time as optimizing the completion. The data from the monitoring array will also be used to better understand site amplification and develop attenuation relationships for predicting ground motions from the magnitude of AIS in the Montney Formation. Additionally, Earth models will be created for monitored regions, by integrating the data from the field studies with ancillary data into a 3-D hydrogeomechanical model in order to better understand the processes resulting in AIS and to develop a probabilistic model for the seismic hazard and risk to the regions.

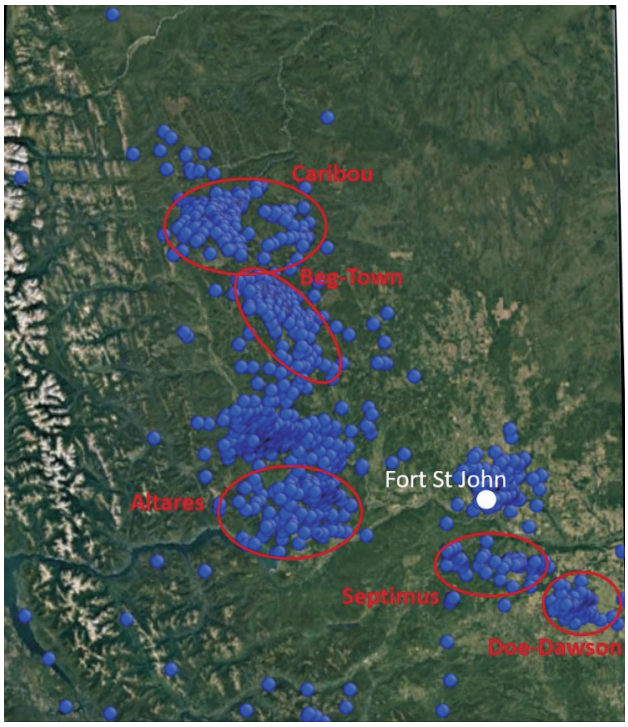

Figure 1. Seismicity recorded in the Montney Formation in northeastern BC from 1985 to present (blue circles). The five clusters linked to hydraulic fracturing are circled in red.

This publication is also available, free of charge, as colour digital files in Adobe Acrobat® PDF format from the Geoscience BC website: http://www.geosciencebc.com/s/SummaryofActivities.asp.

Methods and Approaches

The two components of the research, monitoring and modelling, will be investigated in parallel with the field studies, combined with ancillary data provided by laboratory testing and industry collaborators providing metrics for the modelling portion of the study.

Monitoring Hydraulic Fracturing Completions

The seismicity data necessary for this research is being provided by an array of accelerographs. Working with the Earthquake Engineering Research Facility (EERF) at the University of British Columbia (UBC), the authors previously designed and built five stations and, as part of this study, have now deployed an additional 12 stations. The design for the stations was modified from that developed at UBC for BC's earthquake early-warning system (Azpiri, 2016). The original stations include custom-built Tetra 2 microelectromechanical systems (MEMS) accelerometers, whereas the sensors in the new stations are commercial MEMS accelerometers and are paired with a three-axis magnetometer. Using a series of ground-motion prediction equations for induced seismicity (Dost et al., 2004; Bobbio et al., 2009; Dost et al., 2013; Atkinson, 2015), it has been conservatively estimated that, given the ambient noise recorded, the detection threshold of the stations would be M1.5 within 5 km and M–0.2 within 0.5 km. In addition to three-component (3C) accelerometers, 3C geophones are currently in the process of being added to the stations. The array will be used to densely monitor the hydraulic fracturing of 3–5 multilateral well pads in the Montney play and to obtain a dataset of reliably located events and associated ground motions.

The units are powered by a solar panel with an absorbed glass mat deep cycle battery and an uninterruptible power supply (UPS) gel battery inside a protective (weather and animal proof) case for backup. The protective case also encloses a global positioning system for timing and location, as well as a computer to store the data and run the system. Whereas the original stations use a NUC (Next Unit of Computing) with Windows, the new stations use an Advanced RISC (reduced instruction set computer) Machine processor running Linux, which considerably reduces power consumption. The sensors have individual enclosures and need only be buried under any loose materials using a shovel. The enclosure for the sensors in the original stations is a box, approximately 10 by 5 by 20 cm in dimensions, and in the new stations is a sealed tube, 80 cm in length and 7.5 cm in diameter. Telemetry is currently provided by cell-phone modems, with antennas to boost the signal. Photos of the field setups are shown in Figure 2. Depending on the length of deployment and the anticipated weather conditions, the solar panels may be mounted on an in-house–designed aluminum frame, and the protective case and battery enclosed in a secondary weatherproof box.

In addition to obtaining real-time raw data, algorithms have been added to the stations to send an alert when a threshold acceleration is recorded and to calculate ground-motion parameters for the event in real time. The raw data is first run through a 4th order Butterworth filter with a high-pass cut-off frequency of 0.1 Hz. The peak ground acceleration (PGA) is then the maximum acceleration of the filtered data during the event. The filtered acceleration data is integrated to obtain velocities and the peak ground velocity is determined (PGV; equal to the maximum velocity during the

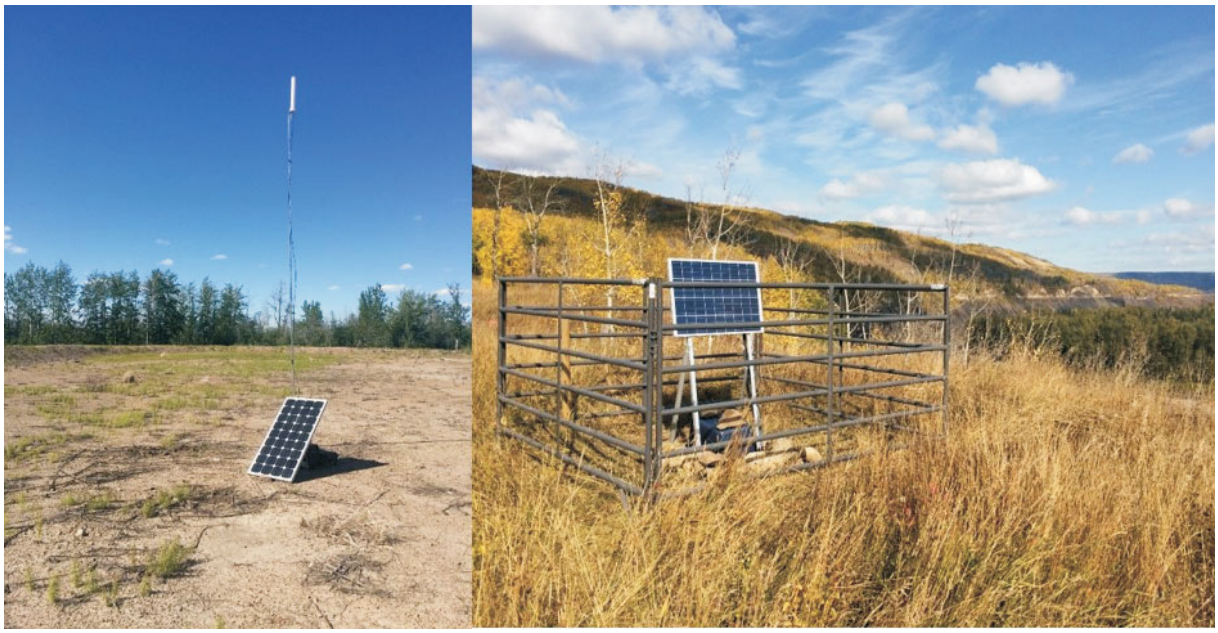

Figure 2. Field setup of a temporary (right) and a long-term station (left) used to monitor the Montney Formation.

event); then the velocities are integrated to obtain displacements and the peak ground displacement is determined (PGD; equal to the maximum displacement during the event). The ratio of the short-term average (STA) to the long-term average (LTA) is also calculated, as it provides a measure of the signal-to-noise ratio and can be used to set up the trigger threshold. The short- and long-term averages are calculated as the average squared acceleration between 1 and 10 Hz, giving a measure of the short- and long-time energy of the vibration. The raw data is first filtered through two cascading 4th order Butterworth filters, one low-pass filter at cutoff frequency of 1 Hz and one high-pass filter at 10 Hz, then the exponential average is found over 0.3 s (STA) and 30 s (LTA) time windows. Additionally, the spectral intensity (SI), which provides a measure of the damage potential to structures by events, is calculated according to A. Rosenberger (unpublished report, 2010). The authors define SI as the maximum velocity of two 20% damped single degree-of-freedom systems with resonant frequencies of 1.5 s and 2.5 s.

Currently, additional algorithms are being developed for real-time calculation of ShakeMaps, magnitudes and hypocentres. Whereas the data recorded by the geophones will allow for the calculation of magnitudes comparable to other networks, the geophone and accelerometer data will be used in conjunction to better define phases and first arrivals for estimating hypocentres.

The original five stations were deployed in the spring to monitor a multilateral stimulation, providing the first dataset, which contains 11 events recorded on multiple stations with a PGA =0.2%g. The largest recorded event had a PGA of 2.2%g (220 mm/s^2), a PGV of 2.7 mm/s, a PGD of 1 mm and a SI of 4.3 mm/s. Figure 3 shows an example of a raw waveform recorded for one of the events. The first of the new stations were also deployed during the completion program in order to test their capabilities. The original and new sensors produced very similar results, with an average difference between the PGAs for two co-located stations within 0.09%g and the new sensors producing slightly lower ambient noise measurements (Figure 4). All 17 stations are currently deployed, seven of which around disposal wells, in preparation for the first dense-monitoring project. In addition to sites obtained through operator agreements, stations have also been deployed at research sites and on a private ranch. The locations for these three sites are shown in Figure 5. It is also anticipated that the sensor package will play a role in providing reservoir surveillance against hydraulic fracturing in adjacent areas. To this end, experiments have been undertaken whereby sensors are directly mated to a suspended well in a producing field to monitor reservoir impact from adjacent operations.

Hydrogeomechanical Modelling

Hydrogeomechanical modelling provides the opportunity to evaluate the potential response of naturally stressed rock to fluid injection under various conditions. The first step of the modelling is to create a database of the parameters needed to create a hydrogeomechanical model. The necessary parameters include: 3-D stress profiles; pore pressure; rock mechanical properties (including those for fault characterization); spacing, geometry, and orientation of natural and induced fractures and faults; and bedding thickness and orientation. The modelling parameters will be obtained

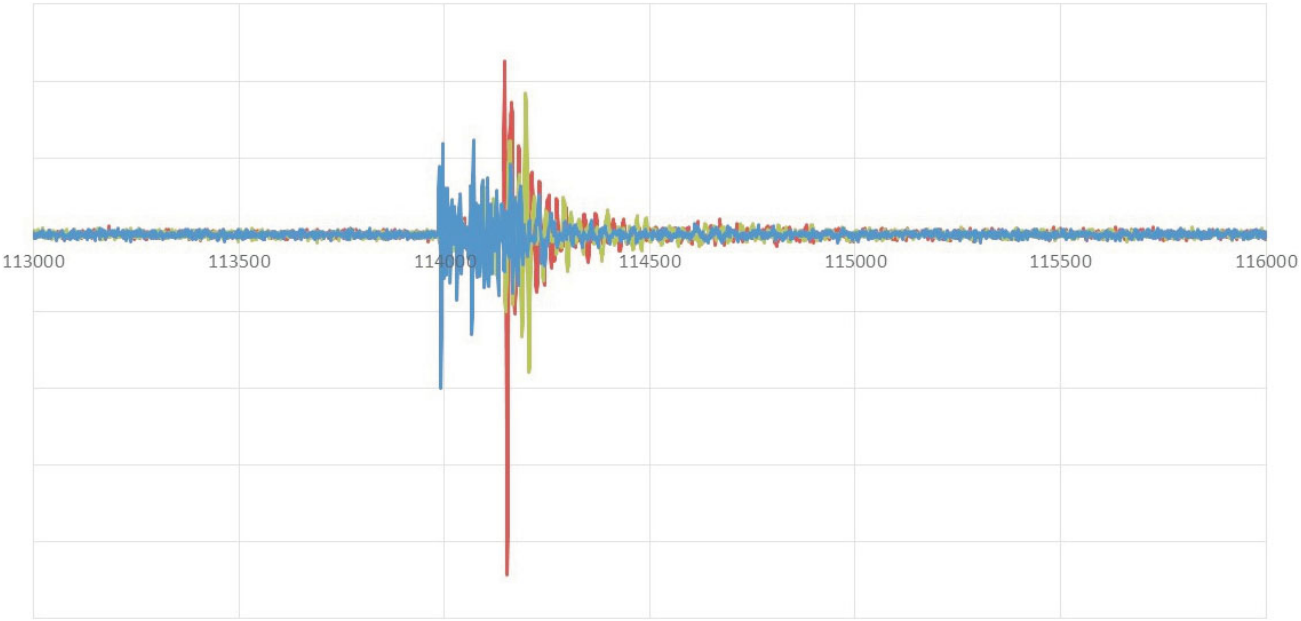

Figure 3. Example of acceleration data recorded for an event by a 3-axis accelerometer at one of the monitoring stations deployed in the Montney play. Scale and legend not included for confidentiality.

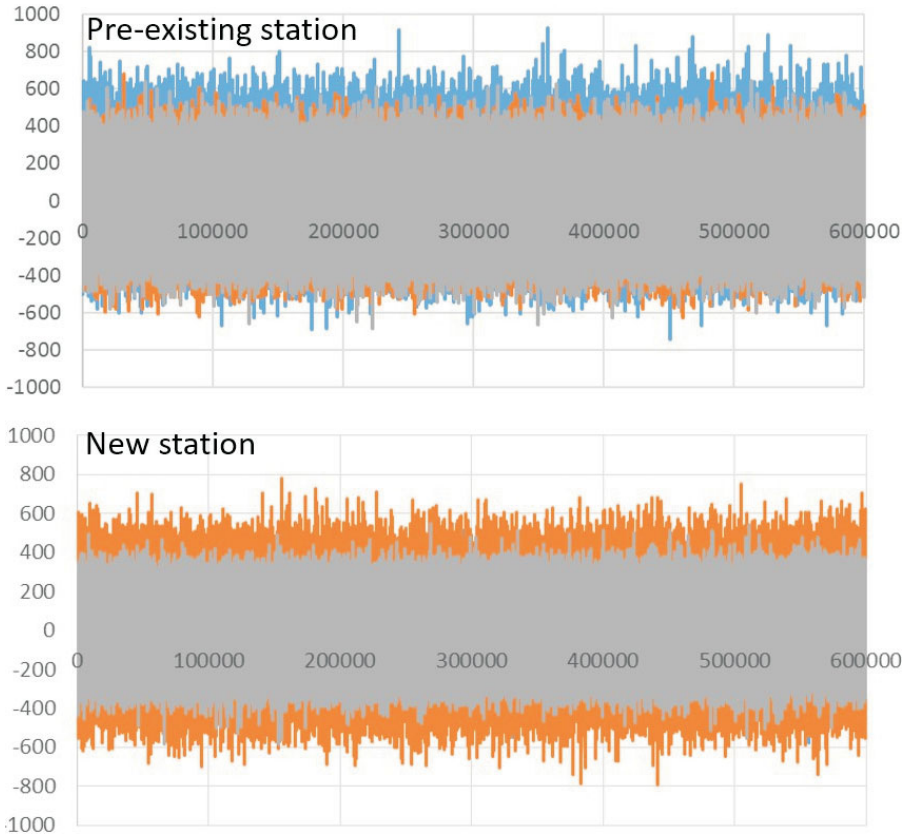

Figure 4. Example of the ambient noise recorded in µg by sensors at one of the original monitoring stations (top) and at one of the new stations (bottom), which were co-located in the Montney play.

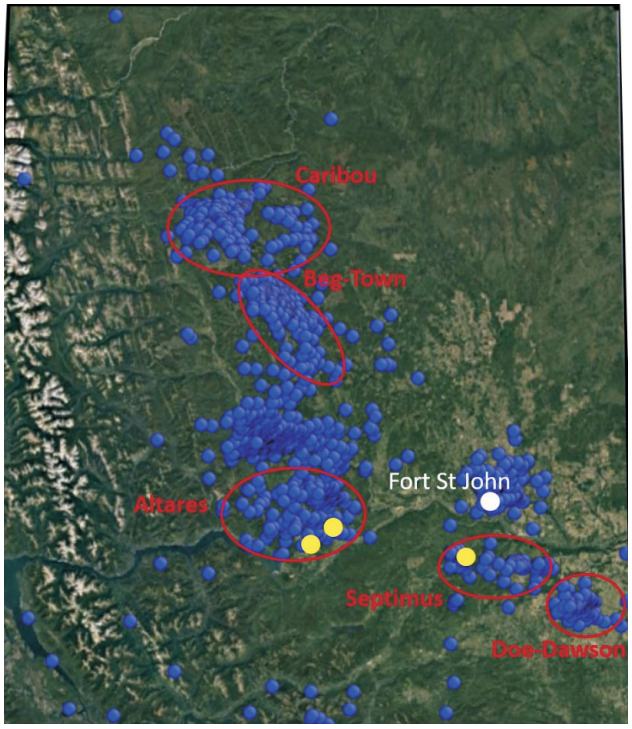

Figure 5. Locations in the Montney play where three of the new monitoring stations are deployed (yellow circles).

from the results of the seismic monitoring as well as the analysis of well logs, injection falloff tests and 'mini fracs', combined with the hydraulic-fracture stimulation parameters provided by industry partners collaborating on this project. The results from geomechanical and leakoff/imbibition tests being undertaken in sister studies at UBC will provide further metrics for the modelling. The field and laboratory data will be linked to numerical simulations incorporating advanced 3-D hydrogeomechanical bonded block distinct-element modelling (3DEC™), which uses algorithms to estimate event magnitudes from simulated induced seismicity.

For the modelling, the preferred program is 3DEC™ (version 5.2), a discontinuum-modelling code based on distinct-element method (DEM) software developed by Itasca™ Consulting Group Inc. The utility of this program was evaluated by first using UDEC™ (Universal Distinct Element Code), the two-dimensional version of the software, , to model both pore pressure build-up and its diffusion along rock discontinuities into a critically stressed fault in response to fluid injection and the subsequent changes to the effective stress field (Bustin and Bustin, 2015). The problem domain is discretized into blocks, where the boundaries represent fractures/joints/faults or

planes subject to possible failure. Failure occurs by both shear slip and dilation along the pre-specified surfaces; therefore, both shear and normal displacements can be quantified. The Mohr-Coulomb slip model with residual strength is used to quantify the displacements. The blocks are subdivided into a mesh of finite difference elements and their deformation is modelled based on the basic Mohr-Coulomb slip criterion. A coupled hydrogeomechanical analysis models the fluid flow through and between the discontinuities and the matrix blocks.

Objectives

In order to investigate the hydrogeomechanical parameters and processes controlling AIS and its associated ground motions in the Montney Formation, as well as to develop methods or protocols for reducing and mitigating AIS, this research program has two objectives, which are described below.

Develop Protocols to Manage and Mitigate AIS

One of the main objectives of this study is to develop effective TLPs for mitigating AIS based on ground motions for the Montney Formation in northeastern BC. Similar waveforms from the same fault system will first be grouped together through cross-correlations (events rupturing the same fault system will have similar waveforms), then the post-injection time-lag and magnitude increase will be quantified to better understand pore-pressure diffusion and the resulting spatiotemporal distribution. The spatiotemporal and magnitude-frequency distributions of microseismicity, AIS and the associated ground motions will then be analyzed, and different mitigation techniques, such as the impact of reducing or stopping injection at different thresholds and flow-back volumes, and controlling leakoff rates by modifying the completion-fluid chemistry, will be tested through 3-D numerical simulations. The goal of developing TLPs, when combined with current research on reservoir geomechanics, is to develop real-time adjustments to completion programs for mitigating AIS, yet, at the same time, optimize the stimulation.

The impact of site conditions on amplifying the ground motion will be investigated by estimating shear-wave–velocity profiles (e.g., Wair et al., 2012). To fully understand the ground motions resulting from AIS due to hydraulic fracturing, data will be collected from sites with varying ground conditions (i.e., bedrock to till). Comparing the geophone and accelerometer datasets will lead to a better understanding of the amplification factors, as well as the relationship between ground motions and magnitudes. The amplification and attenuation data will then be used to develop ground-motion–prediction equations.

Reducing AIS through Hydrogeomechanical Modelling

Hydrogeomechanical modelling will help prevent AIS due to hydraulic fracturing in northeastern BC by leading to a better understanding of the processes resulting in AIS, quantifying the sensitivity of the rate and magnitude of AIS to the hydrogeomechanical parameters, and by identifying regions with higher probability of hosting critically stressed faults, as well as providing insights into the maximum magnitude of events. The first stage of the hydrogeomechanical modelling involves history matching specific hydraulic-fracturing stages, laterals and/or well pads to match the spatial and temporal pattern of the seismicity and microseismicity as well as the wellbore-pressure variations that were monitored. Complete parametric analyses will then be performed on the best fit models. The modelling will investigate the re-activation of faults both inside and outside the reservoir zone. The results of the modelling will be integrated with the shake maps calculated from the monitoring data and the amplification factors to develop seismic hazard and risk maps. Earth models will also be used to test completions and well designs to optimize production; for example, the effect of zipper fracturing, simultaneous fracturing, number of stages, injection rates and pressures, fluid viscosity, as well as orientation, spacing and pattern of laterals can be investigated.

Summary

The array of inexpensive and easily deployable stations has been expanded from 5 to 17, such that it is now possible to densely monitor completions in real time. Algorithms were added to send an alert when a threshold acceleration is recorded and to calculate real-time ground-motion parameters (i.e., PGA, PGV, PGD, STA/LTA, SI). The first dataset was recorded by the original five-station array and the new stations have been thoroughly tested. All 17 stations are currently deployed, many around disposal wells, in preparation for the first dense-monitoring project. The data recorded by the monitoring projects will be integrated with ancillary data into 3-D hydrogeomechanical models to develop methods and protocols for the reduction and mitigation of AIS in the Montney Formation in northeastern BC. In addition to methods and protocols, the legacy of this research is the development of the mobile sensors that can be optimally positioned throughout field development as needed.

Acknowledgments

The authors thank Geoscience BC for their support and funding of this study. They also thank K. Johansen and C. Ventura for their help with the design and construction of the sensors and R.M. Bustin for his review of this manuscript.

References

Atkinson, G. (2015): Ground-motion prediction equation for small-to-moderate events at short hypocentral distances, with application to induced-seismicity hazards; Bulletin of the Seismological Society of America, v. 105, p. 981–992. doi: 10.1785/0120140142

Azpiri, J. (2016): Early-warning system successfully detects B.C. earthquake; Corus Entertainment Inc., Global News, January 1, 2016, URL <http://globalnews.ca/news/2429129/early-warning-system-successfully-detects-b-c-earthquake/> [December 2017].

BC Oil and Gas Commission (2014): Investigation of observed seismicity in the Montney Trend, BC Oil and Gas Commission, URL <https://www.bcogc.ca/node/12291/download> [October 2017].

Bobbio, A., Vassallo, M. and Festa, G. (2009): A local magnitude scale for southern Italy; Bulletin of the Seismological Society of America, v. 99, p. 2461–2470. doi: 10.1785/0120080364

Bustin, A.M.M. and Bustin, RM. (2015): Monitoring and risk assessment of anomalous induced seismicity in northeastern BC; presented at the Technical Meeting on the Traffic Light Protocol (TLP) for Induced Seismicity, October 6, 2015, Calgary, Alberta.

Dost, B., van Eck, T. and Haak, H. (2004): Scaling of peak ground acceleration and peak ground velocity recorded in the Netherlands; Bolletino di Geofisica Teorica e Applicata, v. 45, p. 153–168.

Dost, B., Caccavale, M., van Eck, T. and Kraaijpoel, D. (2013): Report on the expected PGV and PGA values for induced earthquakes in the Groningen area; Koninklijk Nederlands Meteorologisch Instituut De Bilt, KNMI 12-2013, 26 p.

Wair, B., DeJong, J. and Shantz, T. (2012): Guidelines for estimation of shear wave velocity profiles; Pacific Earthquake Engineering Research Center PEER Report 2012/08, 68 p.

Mapping the Amplification of Seismic Ground-Motion Hazard in the Montney Play Area, Northeastern British Columbia

P.A. Monahan, Monahan Petroleum Consulting, Victoria, BC, pmonahan@shaw.ca

V.M. Levson, Quaternary Geosciences Inc., Victoria, BC

B.J. Hayes, Petrel Robertson Consulting Ltd., Calgary, AB

K. Dorey, Petrel Robertson Consulting Ltd., Calgary, AB

Y. Mykula, Petrel Robertson Consulting Ltd., Calgary, AB

R. Brenner, Petrel Robertson Consulting Ltd., Calgary, AB

J. Clarke, Petrel Robertson Consulting Ltd., Calgary, AB

B. Galambos, Frontier Geosciences Inc., North Vancouver, BC

C. Candy, Frontier Geosciences Inc., North Vancouver, BC

C. Krumbiegel, Frontier Geosciences Inc., North Vancouver, BC

Monahan, P.A., Levson, V.M., Hayes, B.J., Dorey, K., Mykula, Y., Brenner, R., Clarke, J., Galambos, B., Candy, C. and Krumbiegel, C. (2018): Mapping the amplification of seismic ground-motion hazard in the Montney play area, northeastern British Columbia; *in* Geoscience BC Summary of Activities 2017: Energy, Geoscience BC, Report 2018-4, p. 29–38.

Introduction

The recent increase in seismicity in northeastern British Columbia (BC) has been attributed to the increase in hydraulic fracturing and subsurface fluid injection by the petroleum industry (Atkinson et al., 2016; Babaie Mahani et al., 2017). Although the increase in seismicity is well documented, the associated ground motion has not been studied until recently. Furthermore, it remains poorly understood how surficial sediments in this region could effect the amplification and attenuation of ground motions. Understanding where there is a greater likelihood of damaging ground motions to occur is paramount for public safety and protection of infrastructure. By using surface and subsurface geological and geophysical data, areas that are prone to amplified ground motion can be mapped, thereby providing key information for public safety and the natural gas sector.

Ground-motion amplification is a complex phenomenon, but can be estimated by the average shear-wave velocity (V_s) in the upper 30 m (V_{s30}). The National Earthquake Hazards Reduction Program (NEHRP) in the United States has defined five site classes based on V_{s30} (Table 1; Building Seismic Safety Council, 2003) and these have been adopted by the National Building Code of Canada. Of these, significant amplification can occur in Site classes D and E.

This publication is also available, free of charge, as colour digital files in Adobe Acrobat® PDF format from the Geoscience BC website: http://www.geosciencebc.com/s/SummaryofActivities.asp.

The objectives of this project are to

- map NEHRP site classes in the Montney play area of northeastern BC, and
- acquire sufficient V_s data in the area to develop a V_s model for shallow geological materials, for use in future earthquake studies in the region.

The project area was defined on the basis of where significant induced seismicity has been observed within the Montney play area, and where the BC Oil and Gas Commission requires seismic monitoring for hydraulic fracturing operations (Figure 1). This paper presents the results of this study to date, which include surficial geological map compilation, subsurface geological database compilation and acquisition of new V_s data.

Geological Summary

The project area lies in the plains and foothills of northeastern BC. The valleys of the Peace River and other major rivers are incised up to 200 m in this area. Bedrock consists mainly of gently dipping Cretaceous shale and sandstone (Stott, 1982; McMechan, 1994).

At least three glaciations have occurred in the area (Mathews, 1978a; Hartman and Clague, 2008; Hickin et al., 2016b). Laurentian ice extended over most of the eastern part of the area, with Cordilleran ice extending out from the Rocky Mountains front and coalescing with the Laurentide Ice Sheet during the Late Wisconsinan (Hickin et al., 2016b). Deposits of nonglacial fluvial sand and gravel (including Holocene deposits) and advance-phase deposits of

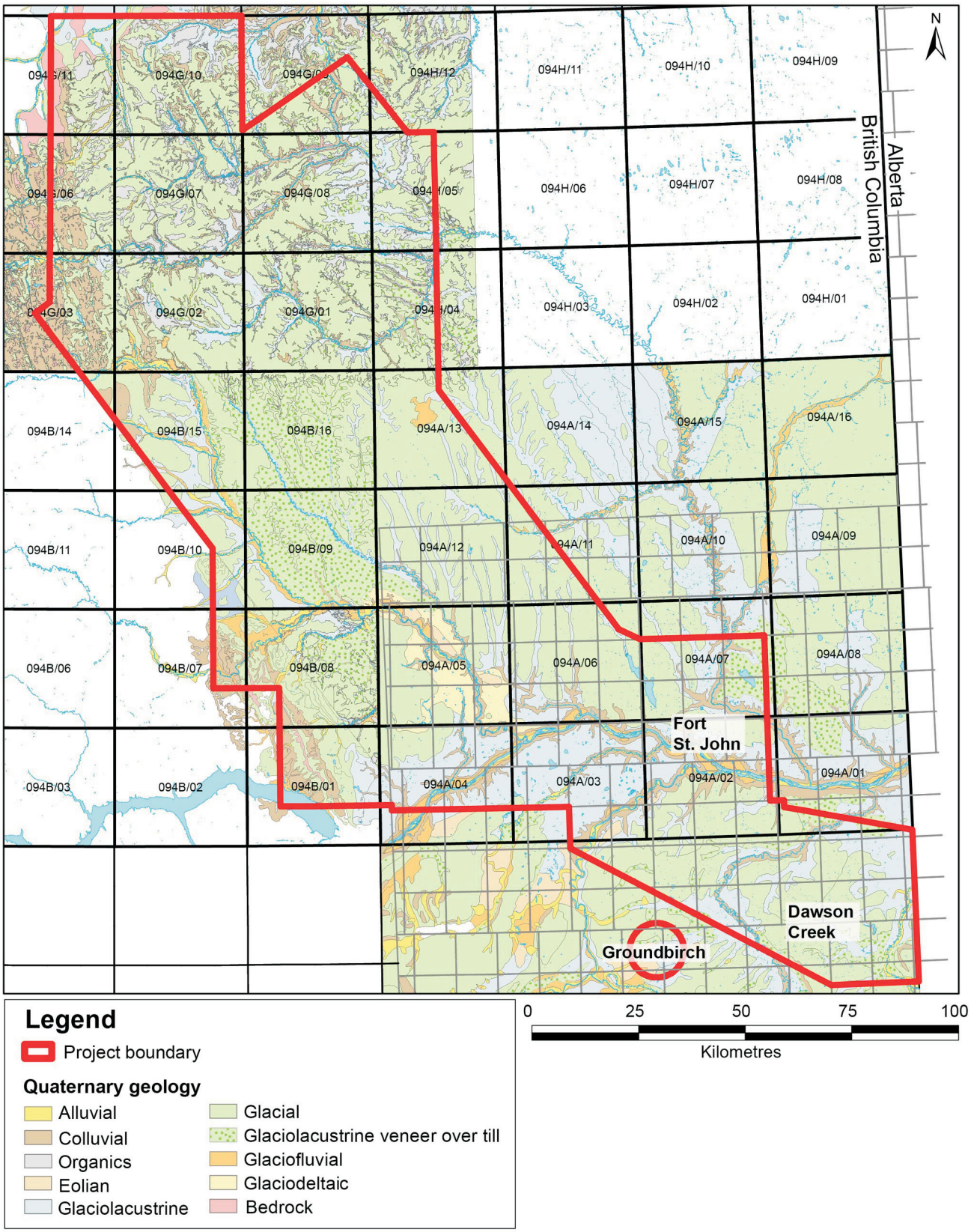

Figure 1. Surficial geological compilation map of northeastern British Columbia, assembled from existing maps (Lord and Green, 1971, 1986; Lord, 1973, 1977; Green and Lord, 1975; Mathews et al., 1975; Mathews, 1978a, b; BC Ministry of Environment, 1980, 1986, 1987, 1988a, b; Reimchen, 1980; Bednarski, 1999, 2000, 2001; Hickin and Fournier, 2011; TECO Natural Resource Group Ltd., 2011; Petrel Robertson Consulting Ltd., 2016). Project area outlined in red.

Table 1. National Earthquake Hazards Reduction Program (NEHRP) site classes (Building Seismic Safety Council, 2003).

Site Class	General description	Definition by V_{s30} (m/s)
A	Hard rock	V_{s30}>1500
B	Rock	760<V_{s30}<1500
C	Very dense soils and soft rock	360<V_{s30}<760
D	Stiff soils	180<V_{s30}<360
E	Soft soils, or soil profile with >3 m soft silt or clay	V_{s30}<180, or >3 m silt and clay with plasticity index >20, moisture content >40%, and undrained shear strength <25 kPa

the last two glaciations indicate a repetitive pattern of fluvial incision and deposition followed by deposition of glaciolacustrine silt as the drainage was blocked by advancing Laurentian ice. After retreat of the ice, renewed fluvial incision cut deeper following each glaciation, so that the modern Peace River channel is incised through the earlier Quaternary deposits into bedrock.

Most Pleistocene interglacial fluvial sediments and advance-phase glaciolacustrine deposits are restricted to paleovalleys and are exposed only in the valley walls of the Peace and other major rivers. Elsewhere, only till and recessional-phase deposits of the last glaciation and modern sediments can be mapped at the surface (Mathews, 1978a). Each surficial unit has a characteristic geomorphic expression. Upland areas, where topography is controlled by bedrock, are underlain mainly by till or colluvial deposits. Low relief areas, bordering and extending up major valleys, are underlain by recessional-phase glaciolacustrine silt, clay and fine sand and equivalent glaciodeltaic sand deposited where major drainages were blocked by retreating Laurentian ice (Figure 2). Terraces flanking major valleys are underlain by later glaciofluvial sand and gravel representing the earliest phases of postglacial fluvial incision. Modern fluvial sand and gravel occupy river valley bottoms.

Figure 2. View northward across glaciolacustrine plain toward till upland, which commences at break in slope in distance; west side of Fort St. John, adjacent to Margaret 'Ma' Murray Community School, where site SL-6 of the multichannel analysis of surface waves (MASW) program is located.

Surficial Geological Map Compilation

A surficial geological map of the study region (Figure 1, Table 2) was compiled by Quaternary Geosciences Inc. from a variety of sources, and builds on a previous compilation map completed for Petrel-Robertson Consulting Ltd.'s (2016; Hayes et al., 2016) depth-to-bedrock study. Data and map sources used in the compilation included 1:250 000 scale surficial geology maps and reports produced by the Geological Survey of Canada (Mathews, 1978a, b; Reimchen, 1980; Bednarski, 1999, 2000, 2001; Hickin and Fournier, 2011) and soils, landforms and surficial geology maps and reports produced by Green and Lord (1975), Lord (1973, 1977), Lord and Green (1971, 1986) and the BC Ministry of Environment (1980, 1986, 1987, 1988a, b) at a variety of scales ranging from 1:20 000 to 1:125 000. A regional (1:1 000 000 scale) glacial features map was also used (Mathews et al., 1975). In addition, some predictive ecosystem mapping at a scale of 1:20 000 (TECO Natural Resource Group Ltd., 2011) was used in the compilation to provide additional detail in areas originally mapped at 1:250 000, such as the Trutch map sheet (NTS 94G; Bednarski, 2000, 2001). Polygon map data for all areas were obtained digitally and compiled in GIS format. Reinterpretation of some map unit designations, grouping of map units and minor adjustments to map unit boundaries were required for overall consistency of the final compilation map and to eliminate artificial changes across map borders. In addition, some map unit designations were changed as a result of field investigations conducted in June 2017.

Subsurface Geological Data Compilation and Interpretation

There are three sources of subsurface geological data: cased-hole gamma-ray logs from petroleum wells, water well logs and geotechnical borehole logs. The distribution of these data sources is shown on Figure 3.

Gamma-ray logs run through surface casings to very shallow depths are an important source of subsurface geological data for Quaternary studies. Top of bedrock can generally be picked with reasonable confidence where highly correlative Cretaceous strata are truncated and overlain by Quaternary sediments. Normalization for surface

Table 2. Surficial geology units defined in the study area, northeastern British Columbia.

Generalized map unit	Dominant composition	Description and example subunits
Alluvial	Sand, gravel and floodplain silt	Modern river and stream deposits including floodplains (Ap) and alluvial fans (Af)
Colluvial	Poorly sorted, stratified diamict and slump deposits	Slope deposits mainly along steep valley walls (Cb, Cv); also includes minor alluvial and glaciofluvial deposits along valley bottoms
Organics	Organic-rich mud and minor peat	Mainly poorly drained fen deposits (Ov) and minor bogs (Ob)
Eolian	Well sorted sand (dunes) and silt and very fine sand (loess)	Windblown sediments; mainly eolian dunes (Er) and thin silt veneers (Ev)
Glaciolacustrine	Mainly silt, clay and fine sand; minor coarse sand and gravel	Glacial lake sediments that blanket topography (GLb) or form glacial lake plains (GLp, AGp)
Glacial	Poorly sorted, massive diamict; usually over consolidated sediments	Glacial deposits including thick till blankets (Tb), hummocky moraine (Th), till plains (Tp, Mp), fluted terrain (Tr) and thin till veneers (Tv, Mv)
Glaciolacustrine veneer over till	Sand and silt; minor clay	Thin and discontinuous cover of glacial lake sediments (LGv), usually overlying till and other glaciogenic deposits
Glaciofluvial	Sand and gravel; minor silt and diamict	Glacial outwash sand and gravel forming terraces (At, FGt, Gt), thick blankets (GFb), outwash plains (GFp), fans (GFf), hummocky or kettled outwash (GFh), kames (Agh), esker ridges (GFr), spillway floor deposits (AGp) and thin veneers (GFv)
Glaciodeltaic	Mainly fine to very fine sand	Prograding delta deposits built into glacial Lake Peace in the form of an apron (AGp, GD) in valleys such as the Halfway River and Farrell Creek valleys
Bedrock	Mainly sandstone and shale	Exposed or thinly covered bedrock outcrops (R), usually sandstone

casing effects (documented by Quartero et al., 2014) and interpretation of depth to bedrock were conducted on gamma-ray logs from 1351 petroleum wells in the north Peace region by Petrel Robertson Consulting Ltd. (2016; Hayes et al., 2016), and these have been incorporated into the present study. An additional 1076 gamma-ray logs were similarly normalized and interpreted for the current project (Figure 3). The principal advantages of this dataset are the repeatability of the data and the fact that they are in the public domain. The principal disadvantage is that each data point is a single log curve that provides only incomplete information on the Quaternary section. Furthermore, not all logs have been run continuously to surface and, in many places, attenuation of the gamma-ray signal by the conductor pipe obscures the lithological signature in the upper 10–30 m. Where the bedrock top lies above the top of the logged section, all that can be reported is a maximum depth to bedrock. Nonetheless, cased-hole gamma-ray logs provide important constraints on the Quaternary thickness and lithology, particularly when combined with other subsurface geological data.

An edited database of water well logs of northeastern BC by Hickin (2013), derived from the BC Ministry of Environment WELLS database, was included in the Petrel Robertson Consulting Ltd. (2016) study, and additional data from Hickin's database is being incorporated into the present project. Lithological descriptions in the WELLS database vary greatly in quality, and some well locations are suspect. However, the depth to bedrock is usually reliably reported, and this is the parameter of most importance for this study. Fifteen hundred and sixty water well logs from this database have been used in this project (Figure 3).

Geotechnical borehole logs provide the best data for Quaternary geological studies, because they are professionally and consistently described, reliably located, and include repeatable quantitative measurements that can be correlated to physical properties. The latter include standard penetration test (SPT) blowcount (N) values and moisture content, which are important stratigraphic indices. The SPT N value is the number of hammer blows required to drive a sample tube 305 mm (1 ft.) under standardized conditions. In the project area, N values in recessional-phase silt and clay of the last glaciation are between 2 and 15. However, N values for Quaternary sediments that have been glacially overridden are between 40 and >50 (if after 50 blows, penetration has not reached 305 mm, the test is usually terminated; this upper limit is termed refusal, and indicates a material very resistant to penetration). Till of the last glaciation is a possible exception in this area, as N values in this till range from 15 to >50. The low N values (<40) in some till may be due in part to being clay-rich, or being ablation or flow till rather than lodgment till. To date, 816 borehole logs from 174

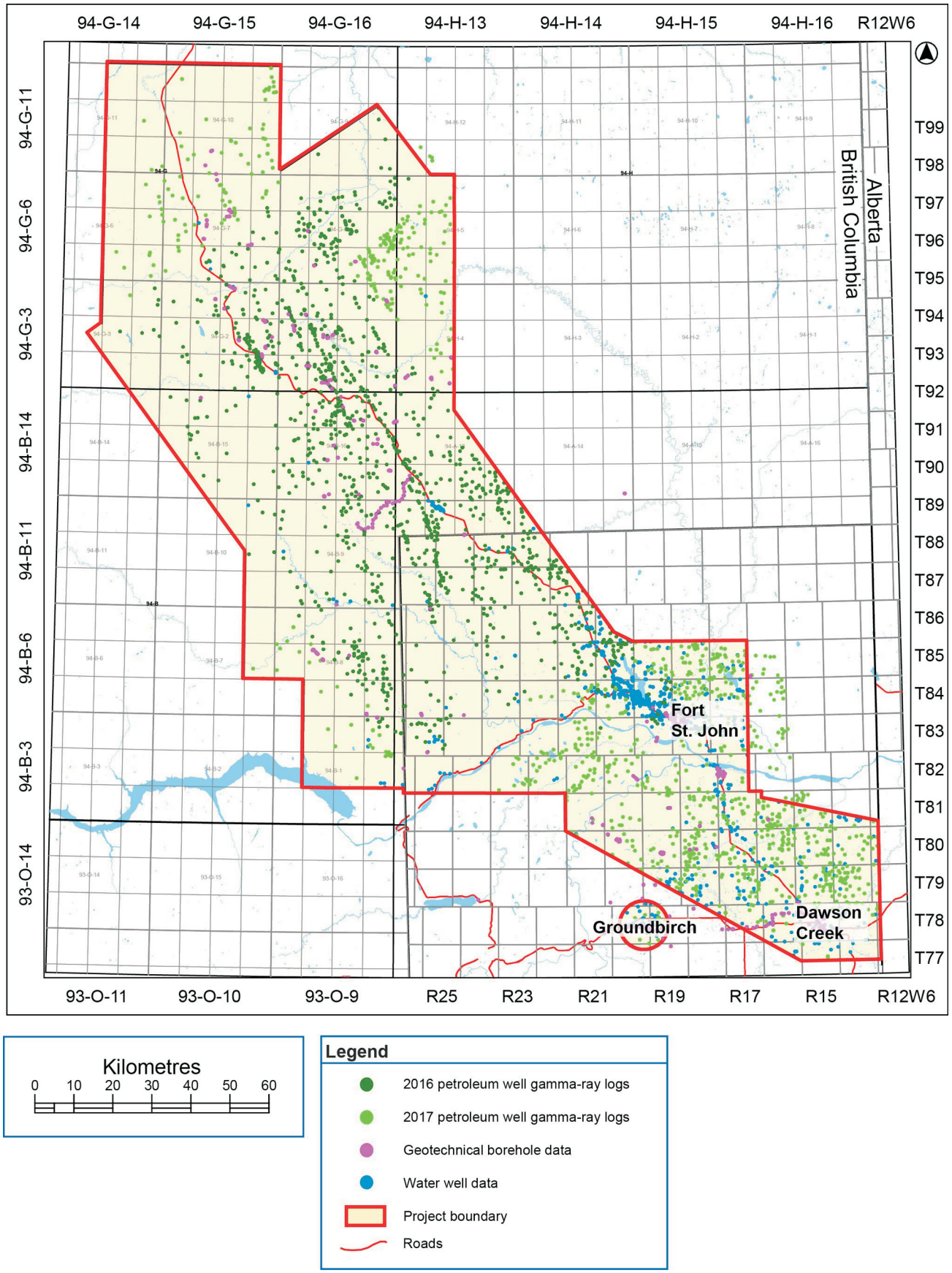

Figure 3. Petroleum well, water well and geotechnical borehole data locations in the study area, northeastern British Columbia.

sites have been obtained, of which 153 sites include borehole data deeper than 10 m. The main disadvantages of this data source are that the boreholes tend to be shallow, rarely exceeding a few tens of metres in depth, and data are proprietary, so they are labourious to collect and details cannot be routinely published.

Shear-Wave Velocity Data Acquisition

Three field programs have been conducted to date by Frontier Geosciences Inc. to determine the V_s of the shallow geological materials. Several correlations of SPT N values with V_s have been proposed (e.g., Hutchinson and Beird, 2016) but these have large uncertainties. Monahan and Levson (2001) showed that topset sand and foreset silt at the same depth in the Fraser River delta have similar V_s but greatly different N values (Monahan and Levson, 2001, Figures 5, 6, note that these figures show cone penetration test tip resistance rather than SPT N, but these correlate well). Consequently, acquisition of new V_s data specific to this area provides more reliable data than correlations.

Downhole V_s logging by the vertical seismic profile (VSP) method was conducted in six cased boreholes in the Groundbirch area (Figure 1). This method is described further by Arsenault et al. (2012). The stratigraphy of these boreholes is well described by Hickin and Best (2013) and Hickin et al. (2016a), so that the V_s of each geological unit can be readily determined. In five of these boreholes, recessional-phase deposits of the last glaciation are 26–49 m deep and overlie till, which in turn overlies bedrock or earlier glaciogenic deposits. The sixth borehole penetrated 3 m of till over bedrock. The results of this program are summarized in Table 3, and an example is shown in Figure 4.

Table 3. Summary of downhole shear-wave velocity (V_s) data acquisition in boreholes at Groundbirch, northeastern British Columbia.

Borehole	DLS location	Depth logged (m)	Thickness of recessional-phase deposits (m)	Bedrock depth (m)	Geological map unit	V_{s30} (m/s)	Site Class
GB12-2	1-13-79-20W6*	31	0	3	Glacial	806	B
GB15-1	9-17-78-19W6	112	26	82	Glaciolacustrine	290	D
GB15-2	8-17-78-19W6	149	49	>147	Glaciolacustrine	207	D
GB15-3	8-13-78-20W6	70	36	52	Glaciolacustrine	263	D
GB15-4	12-4-78-19W6	67	26	71	Glaciolacustrine	272	D
GB15-5	16-7-78-19W6	100	45	>118	Glaciolacustrine	231	D

*L.S. 1, Sec. 13, Twp. 79, Rge. 20, W 6th Mer.

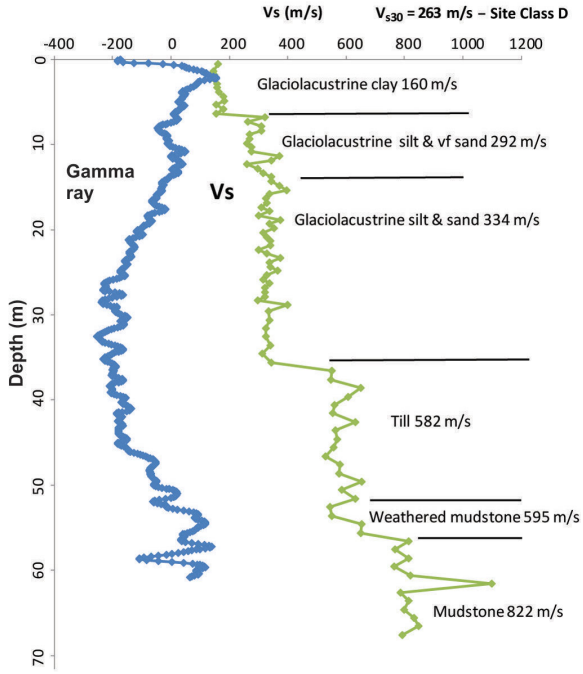

Figure 4. Shear-wave velocity (V_s) and gamma-ray logs from borehole GB15-3 at Groundbirch, northeastern British Columbia. Gamma-ray data from Weatherford, in Hickin et al. (2016a). Abbreviation: vf, very fine; V_{s30}, average shear-wave velocity in the upper 30 m.

A multichannel analysis of surface waves (MASW) program was conducted at six sites in Fort St. John and Dawson Creek, where geotechnical data was obtained. A MASW is a surface geophysical technique in which the velocities of Rayleigh waves, measured along a >100 m spread of geophones, are used to calculate a V_s profile (Phillips and Sol, 2012). The stratigraphy at these sites ranges from 5 m till over bedrock to 11 m glaciolacustrine silt over till. The results of this program are summarized in Table 4 and an example shown in Figure 5. The Vs calculations are made to 30 m depth at every geophone on the spread (except at the ends of the spread), so that multiple V_{s30} calculations can be made at each site. The averages and standard deviations of the calculated V_{s30} are shown in Table 4 for each site.

The results of these programs demonstrate that V_s in the recessional-phase deposits of the last glaciation is <350 m/s. Specifically, V_s ranges from 120 to 220 m/s in silt and clay, 200 to 290 m/s in silt and very fine sand, and 250 to 350 m/s in sand and gravel. In sediments that have been glacially overridden, V_s exceeds 400 m/s. As with the SPT data, a possible exception is till of the last glaciation, in which V_s ranges from 300 to 600 m/s. A V_s result of <400 m/s may occur because the till is clay-rich, or is ablation and flow till rather than lodgment till. In bedrock, V_s ranges from 500 to 1100 m/s. The lower values are in disturbed bedrock. Although it is often described as 'weathered bedrock', in many cases it is likely to have been disturbed by glaciotectonic processes.

As noted above, the NEHRP site classes are based on V_{s30}, which is calculated using the following formula:

$$V_{s30} = \Sigma h/\Sigma t$$

where h = each measured interval thickness, where Σh = 30 m, and t = the measured interval travel time, and $t = h/V_s$ for each interval.

The data show that sites underlain by recessional-phase deposits of the last glaciation (glaciolacustrine, glaciodeltaic and glaciofluvial units, Figure 1, Table 2), where sufficiently thick, are classified as Site Class D, and susceptible to amplification of seismic ground motions. Furthermore, where these deposits are thinner, amplification of short-period ground motions due to resonance may occur where the site period matches that of the dominant short-period ground motions. Structures with the same natural period as the site would potentially be most vulnerable to damaging ground motions. Anecdotal reports from local informants are consistent with these conclusions.

The site period (T) is calculated by the quarter wavelength rule:

$$T = 4H/V_s$$

where H = thickness of the low velocity geological unit, which may include several measured intervals, and V_s = the average shear-wave velocity of the low velocity geological unit.

The third field program is another MASW program, which is underway at the time of writing. This program is being conducted at six sites located between Parkland, south of the Peace River, and the Sikanni Chief River. The results of this and V_s data from dipole sonic logs run in boreholes drilled by Geoscience BC in 2017 (Levson and Best, 2017) will be combined with the data from this project to generate the final V_s model for the shallow geological materials.

Table 4. Summary of initial multichannel analysis of surface waves (MASW) program results. Abbreviations: N, number of hammer blows in standard penetration test; NRCan, Natural Resources Canada; V_{s30}, average shear-wave velocity in the upper 30 m.

Site	Location	Geological map unit	V_{s30} (m/s)	Site Class	Significance
SL-1	112th Avenue by Fort St. John Hospital, Fort St. John	Glacial	607 ±50	C	5–6 m till over bedrock
SL-2	94th Avenue, east of Pomeroy Sport Centre, Fort St. John	Glaciolacustrine	344 ±14	D	>7 m glaciolacustrine sediments
SL-3	10th Street bridge, Dawson Creek	Glaciolacustrine	322 ±24	D	4? m glaciolacustrine over >20 m till, N = 14–35 (thick low N till)
SL-4	Ecole Frank Ross Elementary, Dawson Creek	Glacial	469 ±23	C	8 m till over weathered bedrock
SL-5	Northern Lights College, Fort St. John	Glacial	394 ±17	C	6 m glaciolacustrine sediments over till, NRCan seismograph location NBC7
SL-6	Margaret 'Ma' Murray Community School, Fort St. John	Glaciolacustrine	355 ±11	C-D	11 m glaciolacustine silt over till

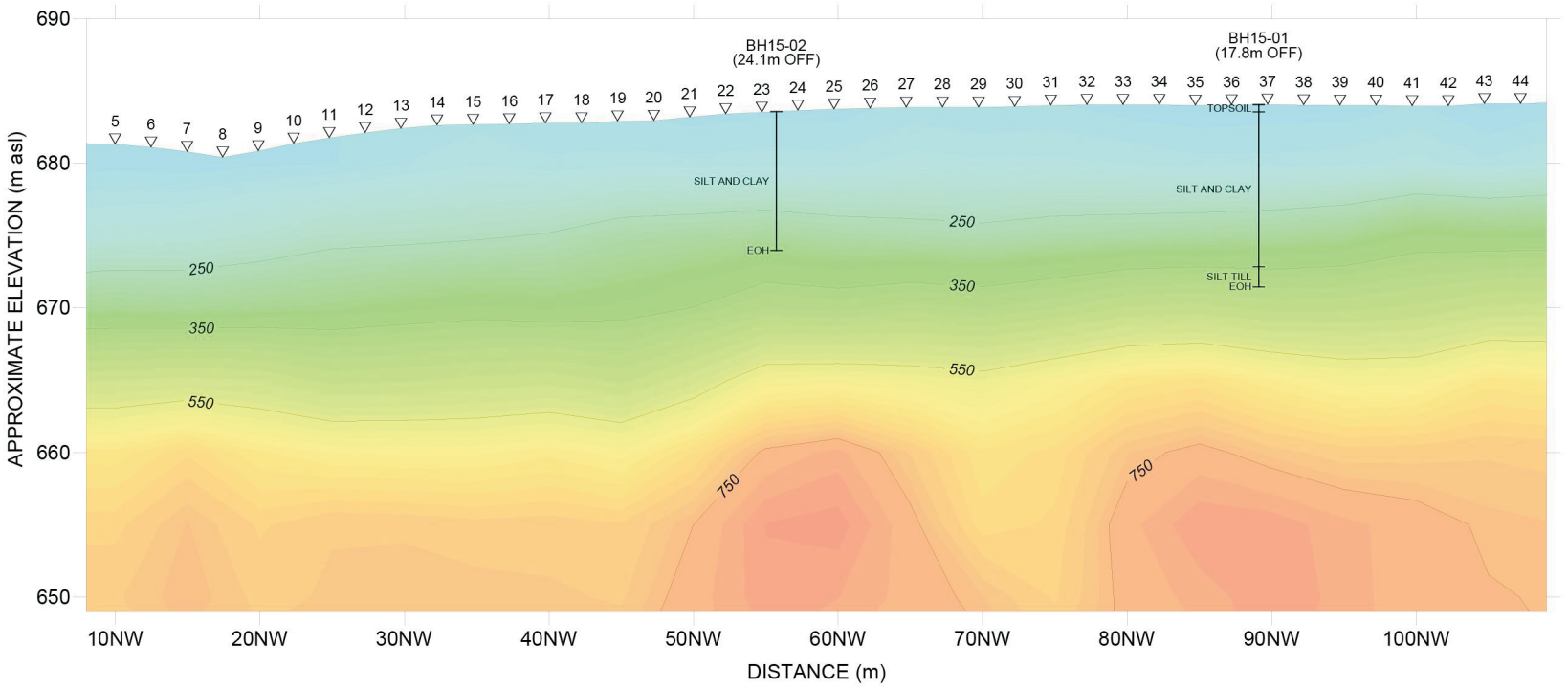

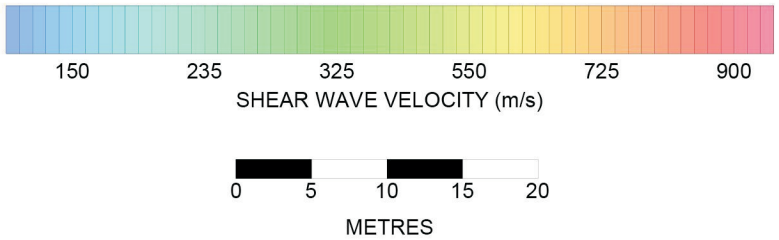

GEOSCIENCE BC FORT ST. JOHN, BC		
MASW SURVEY		
INTERPRETED MASW SECTION SL-6 (MA MURRAY SITE)		
FRONTIER GEOSCIENCES INC.		
DATE: APR. 2017	SCALE 1:500	

Figure 5. Multichannel analysis of surface waves (MASW) profile for site SL-6, Margaret 'Ma' Murray Community School, Fort St. John. Site Class C-D (Table 4) has been assigned due to shallow bedrock beneath 11 m of glaciolacustrine silt over an estimated 4–8 m of till (see also Figure 2). Abbreviation: BH, borehole; EOH, end of hole; NW, to the northwest; OFF, offset.

Summary and Conclusions

The principal results of this project to date are a) a compilation of surficial geological maps from a variety of sources; b) compilation and interpretation of a subsurface geological database comprising 2427 gamma-ray logs normalized for surface casing effects, 1560 water well logs and 816 geotechnical boreholes; and c) generation of new V_s data at 12 sites. Data obtained to date show that areas underlain by recessional-phase sediments of the last glaciation are potentially susceptible to amplification of seismic ground motions. Although data from modern sediments have not been analyzed at this time, it is anticipated that they will also be susceptible to amplification. By identifying areas where seismic ground motions may be amplified and thereby more likely to be damaging, this study is providing a tool for regional planning and mitigating the effects of induced seismicity to public safety and industrial infrastructure.

Acknowledgments

The authors gratefully thank the following organizations and individuals:

- for assistance in providing geotechnical borehole data: Northern Geo Testing and Engineering; Aurora Engineering & Construction Services Ltd.; Smith + Andersen (Kelowna); Field Engineering & Associates Ltd.; City of Fort St. John; City of Dawson Creek; Peace River Regional District; School Board 59: Peace River South; School Board 60: Peace River North; BC Ministry of Transportation and Infrastructure; BC Geological Survey; BC Hydro; Northern Health; Northern Lights College; BC Oil and Gas Commission; Progress Energy Canada Ltd.; Shell Canada Limited; Painted Pony Energy Ltd.; Black Swan Energy Ltd.; Canadian Natural Resources Limited; Saguaro Resources Ltd.; Crew Energy Inc.; and AltaGas Ltd.;
- for assistance in field operations: C. van Geloven, E. Shaw, P. Luck, D. Dunbar and B. Berg;
- for access to field sites: the cities of Fort St. John and Dawson Creek, School boards 59 and 60, Northern Lights College, Progress Energy Canada Ltd., K&L Oilfields Holdings Ltd., Buffalo Inn, Nels Ostero Ltd., BC Hydro and ARC Resources Ltd.;
- for the GIS work: M. Fournier and M. Perra;
- A. Mahani, M. Best, R. Stefik and A. Hickin for helpful discussions, L. Sears for assembling the manuscript and T. Ostero for the illuminating tour of his gravel pit;
- S. Venables, C. Salas and C. Pellett for reviewing the manuscript and making a number of helpful suggestions.

References

Arsenault, J.-L., Hunter, J.A. and Crow, H.L. (2012): Shear wave velocity logs from vertical seismic profiles; *in* Shear Wave Velocity Measurement Guidelines for Canadian Seismic Site Characterization in Soil and Rock, J.A. Hunter and H.L. Crow (ed.), Geological Survey of Canada, Open File 7078, p. 123–138.

Atkinson, G.M., Eaton, D.W., Ghofrani, H., Walker, D., Cheadle, B., Schultz, R., Shcherbakov, R., Tiampo, K., Gu, J., Harrington, R.M., Liu, Y., van der Baan, M. and Kao, H. (2016): Hydraulic fracturing and seismicity in the Western Canada Sedimentary Basin; Seismological Research Letters, v. 87, no. 3, 17 p.

Babaie Mahani, A., Kao, H., Johnson, J. and Salas, C. (2017): Ground motion from the August 17, 2015, moment magnitude 4.6 earthquake induced by hydraulic fracturing in northeastern British Columbia; *in* Geoscience BC Summary of Activities 2016, Geoscience BC, Report 2017-1, p. 9–14, URL <http://www.geosciencebc.com/i/pdf/SummaryofActivities2016/SoA2016_BabaieMahani.pdf> [October 2017].

Bednarski, J.M. (1999): Preliminary report of the Quaternary geology of the Trutch map area, northeastern British Columbia; *in* Current Research 1999A, Geological Survey of Canada, p. 35–43.

Bednarski, J.M. (2000): Surficial geology, Trutch, British Columbia (NTS 94G); Geological Survey of Canada, Open File 3885, scale 1:250 000.

Bednarski, J.M., compiler (2001): Drift composition and surficial geology of the Trutch map area (94G), northeastern British Columbia; Geological Survey of Canada, Open File D3815, 1 CD-ROM.

BC Ministry of Environment (1980): Soils and surficial geology, NTS map 94B/NE; BC Ministry of Environment, Terrain Inventory Mapping Project 4421, scale 1:100 000.

BC Ministry of Environment (1986): Soils and landforms (terrain) of the Cypress Creek map area (NTS 94B/15); BC Ministry of Environment, Terrestrial Ecosystem Information Map K15-2750, scale 1:50 000.

BC Ministry of Environment (1987): Soils, Kobes Creek, NTS map 94B/08; BC Ministry of Environment, Terrestrial Ecosystem Information Map K15-2744, scale 1:50 000.

BC Ministry of Environment (1988a): Soils and landforms (terrain) of the Blair Creek map area (NTS 94B/16); BC Ministry of Environment, Terrestrial Ecosystem Information Map K15-2752, scale 1:50 000.

BC Ministry of Environment (1988b): Soils, Dunlevy Creek, NTS map 94B/01; BC Ministry of Environment, Terrestrial Ecosystem Information Map K15-2738, scale 1:50 000.

Building Seismic Safety Council (2003): NEHRP recommended provisions for seismic regulations for new buildings and other structures (FEMA 450), part 1: provisions (2003 edition); prepared for the Federal Emergency Management Agency, 338 p., URL <http://www.nehrp.gov/pdf/fema450provisions.pdf> [October 2017].

Green, A.J. and Lord, T.M. (1975): Soils of the Nig Creek–Big Arrow Creek map areas, British Columbia; Canada Department of Agriculture, British Columbia Soil Survey Report No. 19, Terrestrial Ecosystem Information maps K15-2778 and K06-2770, scale 1:125 000.

Hartman, G.M.D. and Clague, J.J. (2008): Quaternary stratigraphy and glacial history of the Peace River valley, northeast British Columbia; Canadian Journal of Earth Sciences, v. 45, p. 549–564.

Hayes, B.J.R., Levson, V., Carey, J. and Mykula, Y. (2016): Interpretation of Quaternary sediments and depth to bedrock,

Peace Project area, northeastern British Columbia: project update; *in* Geoscience BC Summary of Activities 2015, Geoscience BC, Report 2016-1, p. 61–68, URL <http://www.geosciencebc.com/ i/pdf/SummaryofActivities2015/SoA2015_Hayes.pdf> [October 2017].

Hickin, A.S. (2013): Late Quaternary to Holocene geology, geomorphology and glacial history of Dawson Creek and surrounding area, northeast British Columbia, Canada; Ph.D. thesis, University of Victoria, Victoria, BC, 369 p.

Hickin, A.S. and Best, M.E. (2013): Mapping the geometry and lithostratigraphy of a paleovalley with a time-domain electromagnetic technique in an area with small resistivity contrasts, Groundbirch, British Columbia, Canada; Journal of Environmental and Engineering Geophysics, v. 18, p. 119–135.

Hickin, A.S. and Fournier, M.A. (2011): Compilation of Geological Survey of Canada surface geology maps for NTS 94A and 93P; BC Ministry of Energy, Mines and Petroleum Resources, Energy Open File 2011-2 and Geoscience BC Map 2011-08-1, scale 1:250 000.

Hickin, A.S., Best, M.E. and Pugin, A. (2016a): Geometry and valley-fill stratigraphic framework for aquifers in the Groundbirch paleovalley assessed through shallow seismic and ground-based electromagnetic surveys; BC Ministry of Energy, Mines and Petroleum Resources, BC Geological Survey, Open File 2016-5, 46 p.

Hickin, A.S., Lian, O.B. and Levson, V.M. (2016b): Coalescence of late Wisconsinan Cordilleran and Laurentide ice sheets east of the Rocky Mountain Foothills in the Dawson Creek region, northeast British Columbia, Canada; Quaternary Research, v. 85, p. 409–429.

Hutchinson, P.J. and Beird, M.H. (2016): A comparison of surface- and standard penetration test-derived shear-wave velocity; Environmental and Engineering Geoscience, v. XXII, p. 27–36.

Levson, V. and Best, M. (2017): Northeast BC sonic drilling project, physical logs descriptions and interpretations; Geoscience BC, Geoscience BC Report 2017-16, 35 p.

Lord, T.M. (1973): Soils of the Halfway River, British Columbia; Canada Department of Agriculture, British Columbia Soil Survey Report No. 18, Terrestrial Ecosystem Information Map K06-2757, scale 1:125 000.

Lord, T.M. (1977): Soils of the Gold Bar, Dunlevy Creek and Chinaman Lake map areas (94B/SE); Canada Department of Agriculture, Terrestrial Ecosystem Information Map K06-2763, scale 1:100 000.

Lord, T.M. and Green, A.J. (1971): Soils of the Rose Prairie–Blueberry River area of BC (94A/NW); Canada Department of Agriculture, British Columbia Soil Survey Report No. 17, Terrestrial Ecosystem Information Map K06-2718, scale 1:125 000.

Lord, T.M. and Green, A.J. (1986): Soils and landforms of the Fort St. John–Dawson Creek area, British Columbia; Canada Department of Agriculture, British Columbia Soil Survey Report 42, scale 1:125 000.

Mathews, W.H. (1978a): Quaternary stratigraphy and geomorphology of the Charlie Lake (94A) map-area, British Columbia; Geological Survey of Canada, Paper 76-20, 25 p.

Mathews, W.H. (1978b): Surficial geology, Charlie Lake, Peace River District, British Columbia (NTS 94A); Geological Survey of Canada, Map 1460A, scale 1:250 000.

Mathews, W.H., Gabrielse, H. and Rutter N.W. (1975): Glacial map, Beatton River (2139), British Columbia; Geological Survey of Canada, Open File 274, scale 1:1 000 000.

McMechan, M.E. (1994): Geology and structure cross section, Dawson Creek, British Columbia; Geological Survey of Canada, Map 1858A, scale 1:250 000.

Monahan, P.A. and Levson, V.M. (2001): Development of a shear-wave velocity model of the near-surface deposits of southwestern British Columbia; *in* Proceedings: Fourth International Conference on Recent Advances in Geotechnical Earthquake Engineering and Soil Dynamics, San Diego, California, March 26–31, 2001, Paper 11-16, 12 p.

Petrel Robertson Consulting Ltd. (2016): Interpretation of Quaternary sediments and depth to bedrock, Peace Project area, northeastern British Columbia; Geoscience BC, Report 2016-4, URL <http://www.geosciencebc.com/s/Report2016-04.asp> [October 2017].

Phillips, C. and Sol, S. (2012): Multichannel analysis of surface waves (MASW) technique for hazard studies; *in* Shear Wave Velocity Measurement Guidelines for Canadian Seismic Site Characterization in Soil and Rock, J.A. Hunter and H.L. Crow (ed.), Geological Survey of Canada, Open File 7078, p. 62–66.

Quartero, E.M., Bechtel, D., Leier, A.J. and Bentley, L.R. (2014): Gamma-ray normalization of shallow well-log data with applications to the Paleocene Paskapoo Formation, Alberta; Canadian Journal of Earth Sciences, v. 51, p. 452–465.

Reimchen, T.H.F. (1980): Surficial geology, Dawson Creek, west of the sixth meridian, British Columbia; Geological Survey of Canada, Map 1467A, scale 1:250 000.

Stott, D.F. (1982): Lower Cretaceous Fort St. John Group and Upper Cretaceous Dunvegan Formation of the foothills and plains of Alberta, British Columbia, and District of Mackenzie and Yukon Territory; Geological Survey of Canada, Bulletin 328, 124 p.

TECO Natural Resource Group Ltd. (2011): Fort St. John TSA Predictive Ecosystem Mapping (PEM) Final Report; unpublished report prepared for Canadian Forest Products Ltd., 65 p., URL <https://a100.gov.bc.ca/pub/acat/public/viewReport.do?reportId=40902> [November 2017].

Preliminary Liquid Hydrocarbon Potential Assessment of the Doig Formation, Northeastern British Columbia and West-Central Alberta, Based on Thickness, Organic Richness and Maturity

P.L. Silva, The University of British Columbia, Vancouver, BC, pablols@alumni.ubc.ca

R.M. Bustin, The University of British Columbia, Vancouver, BC

Silva, P.L. and Bustin, R.M. (2018): Preliminary liquid hydrocarbon potential assessment of the Doig Formation, northeastern British Columbia and west-central Alberta, based on thickness, organic richness and maturity; *in* Geoscience BC Summary of Activities 2017: Energy, Geoscience BC, Report 2018-4, p. 39–50.

Introduction

The Triassic section is the richest interval of the Western Canada Sedimentary Basin (WCSB) with respect to volume of oil per volume of rock (Marshall et al., 1987). Historically, the Doig and the underlying Montney formations were viewed as source rocks for other conventional reservoirs in the basin, mainly in other Triassic and Cretaceous strata (Du Rochet, 1985; Creaney and Allan, 1990; Riediger et al., 1990; Edwards et al., 1994). The Lower to Middle Triassic Doig Formation of the WCSB extends continuously across northeastern British Columbia (BC) and west-central Alberta (Figure 1). More recently, the Doig Formation has been recognized as an important unconventional reservoir for gas and natural-gas liquids (NGL), with estimates of total gas in place ranging from 1.1 to 5.6 trillion m^3 (Walsh et al., 2006). However, little is currently known about the unconventional portion of the Doig, which being a relatively new play is much less studied and understood than the Montney Formation. Basin-scale studies that focus on the entire Doig succession and the regional variation in its properties are notably absent in the literature.

The goal of the ongoing research project reported herein is to evaluate the potential of the Doig Formation through a petroleum system analysis (PSA), with focus on the distribution of producible liquids. The PSA is based on the quantification and mapping of source-rock properties, characterization of reservoir properties such as storage capacity and producibility, and backstrip modelling of the basin to reconstruct and determine the timing of thermogenic hydrocarbon generation, migration, expulsion and retention. This paper presents preliminary findings on the aspect dealing with the source-rock properties of the Doig Formation. Organic matter type, abundance and level of thermal maturity are the primary factors controlling the quantity and type of hydrocarbons generated (Welte and Leythaeuser, 1983). Combined with the spatial distribution of thickness, they are the most fundamental properties for assessing the potential of a source-rock reservoir.

This publication is also available, free of charge, as colour digital files in Adobe Acrobat® PDF format from the Geoscience BC website: http://www.geosciencebc.com/s/SummaryofActivities.asp.

Geological Framework

The Doig was deposited in the Middle Triassic, between the Anisian and Ladinian, and is part of the Diaber Group with the underlying Montney Formation (Figure 2). The sedimentation in the Triassic of the WCSB is marked by a transition from carbonate-dominated intra-cratonic and passive-margin conditions, predominant during the Paleozoic, to a siliciclastic-dominated relatively active embryonic foreland basin. The structural elements that influenced the distribution of the interval were the underlying Devonian Leduc reef and the Mesozoic reactivation of the Mississippian Dawson Creek graben complex (Marshall et al., 1987; Davies, 1997). The Doig Formation consists of mudstone, siltstone and subordinate sandstone, bioclastic packstone and grainstone, deposited under marine conditions in environments ranging from shoreface through offshore (Evoy and Moslow, 1995). The Doig can be informally subdivided into three units, as proposed by Chalmers and Bustin (2012): the basal unit, Doig A, corresponding to the also informal but widely used Doig Phosphate Zone (DPZ), composed of organic-rich radioactive dark mudstone with common phosphate granules and nodules, and generally very distinguishable in well logs by its high gamma-ray signature; the intermediate Doig B, primarily composed of medium to dark grey argillaceous siltstone and mudstone intercalated with localized sandstone; and the upper Doig C, composed of relatively organic-lean siltstone and argillaceous fine sandstone.

Methods

Cuttings samples from the Doig Formation were analyzed for total organic carbon (TOC) and temperature of maximum rate of hydrocarbon generation (T_{max}), as well as other standard pyrolysis-derived parameters. Existing pyrolysis data for the Doig in the public domain were compiled and thoroughly reviewed for consistency. As opposed to public

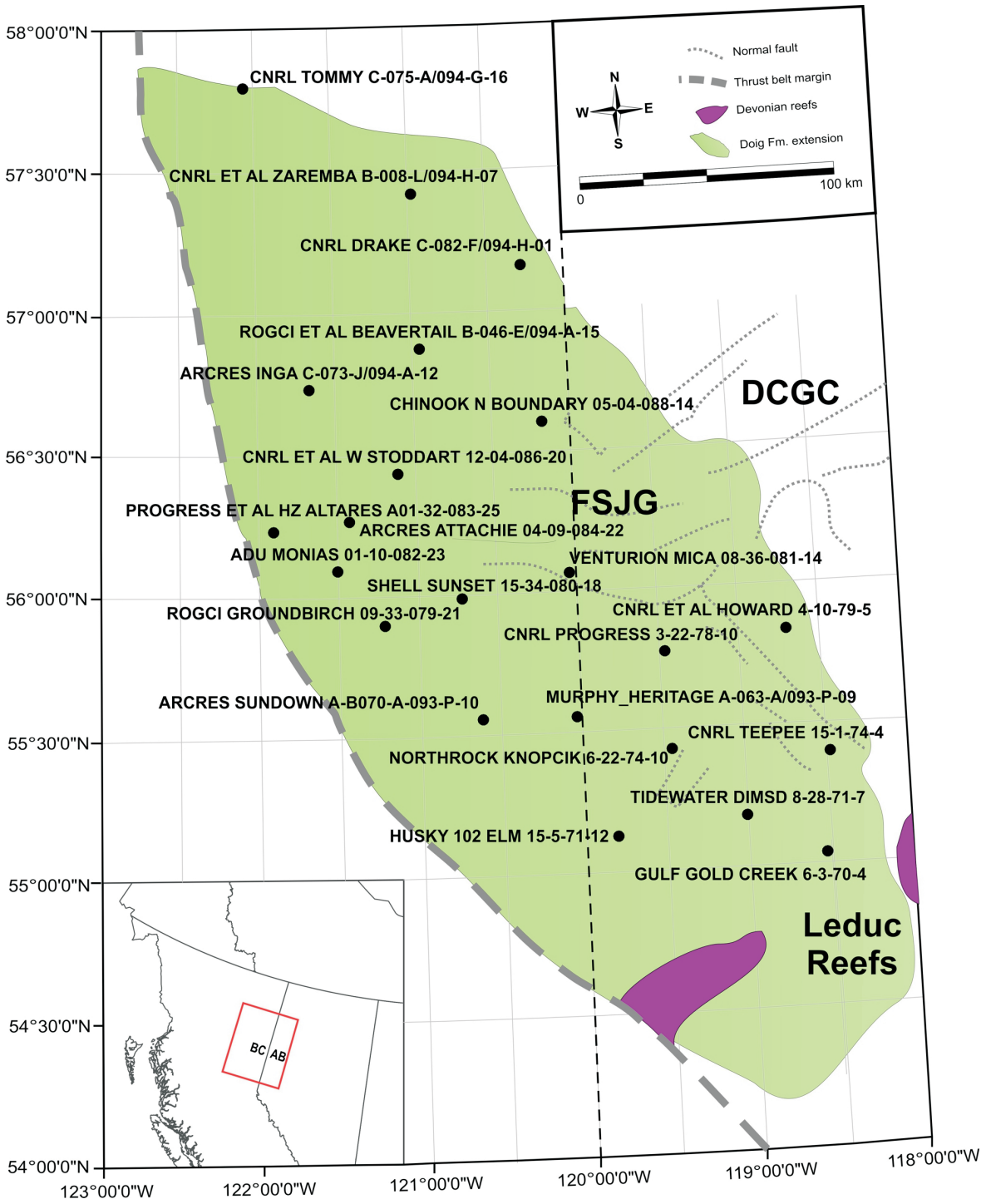

Figure 1. Location of the Doig Formation, main structural elements and wells analyzed in the study area in northeastern British Columbia and west-central Alberta. Abbreviations: DCGC, Dawson Creek graben complex; FSJG, Fort St. John graben.

data, for which no pyrograms or signal quality indicators were available, the data generated for this study was ranked according to signal quality and thus served as high-confidence control points, against which publicly available data was then compared. Between the public data and the analyses conducted for the purpose of this study, nearly 1500 data points from approximately 200 wells were used. The TOC from pyrolysis was used to derive and calibrate continuous TOC logs from compressional sonic slowness and resistivity well logs for all the wells. These logs were calibrated to the laboratory data to map the spatial distribution of the average values in the sequence. Structural, thickness,

average TOC and maturity maps were then created and interpreted, with a focus on defining thick organic-rich areas in the liquid-hydrocarbon–rich generation window.

Pyrolysis

A total of 252 cuttings samples from 24 wells distributed across the entire extent of the Doig Formation were analyzed using the whole-rock pyrolysis method. The samples were selected at an average vertical spacing of 10 m and prepared as bulk rock samples (i.e., not high-graded toward clay-rich fractions). This decision was made in order to avoid overestimation of TOC, which is expected to have a positive correlation with clay; however, the clear trade-off was that the decision was made at the expense of a more pronounced kerogen conversion (S2) peak, and hence a better quality T_{max} value. The analyses were performed using a HAWK™ instrument from Wildcat Technologies with the standard pyrolysis method after Espitalié et al. (1977). Pyrograms were individually reviewed and the T_{max} values were ranked in quality according to the intensity and sharpness of S2. This resulted in the exclusion of 38% of the data for the purpose of maturity assessment as they were deemed unusable, due to being overmature or having low TOC content. Almost 26% of the data were ranked as 'poor' and thus have a low degree of reliability; the remaining 36% of the data was ranked 'good' or better.

A total of 1200 pyrolysis analyses for 170 wells from the public domain were compiled. Due to the unavailability of pyrograms, these data points were reviewed for consistency within each well and for regional agreement. From these data, 12% were beyond a reasonable range expected for T_{max} (400 to 550 °C); another 28% were considered outliers due to either deviating more than 5 °C from the well average or, in the case of wells with less than three data points, disagreeing with the regional trend so as to create bull's-eye patterns on the map. The remaining data were internally and/or regionally consistent, and thus used in the mapping.

Well-Log–Derived TOC

In regional studies involving a large number of wells, laboratory TOC data is sparse relative to the large volume being studied and therefore is of limited utility for regional mapping. Various methods have been developed for extrapolating laboratory data and creating a continuous record of TOC through the entire wellbore using well logs. The most commonly used logs are bulk density, compressional sonic slowness, resistivity and gamma ray. Whereas the use of sonic and density is based on kerogen having substantially lower density than the mineral matrix, gamma ray works on the assumption that organic matter has an affinity with uranium. Because well logs are sensitive to various changes in rock and fluid properties, and thus show non-unique responses, the most dependable methods for estimating TOC

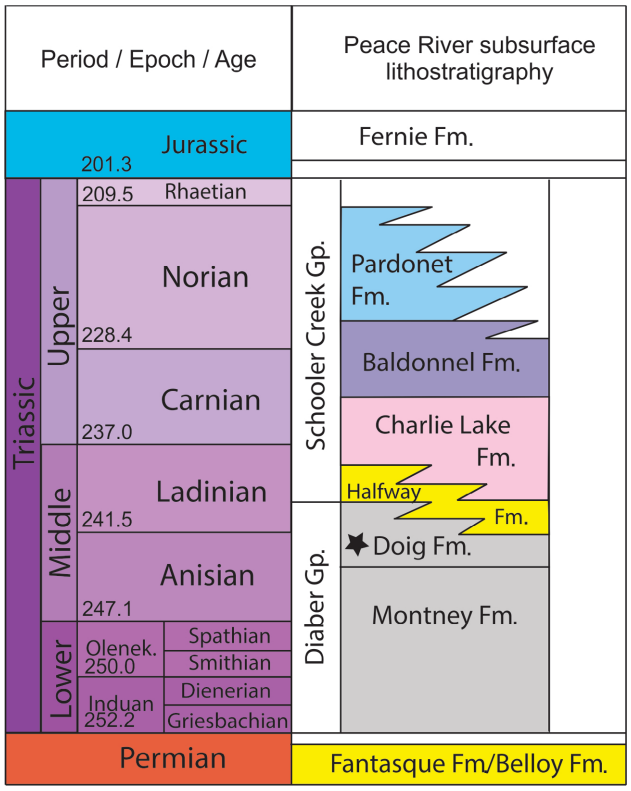

Figure 2. Stratigraphic chart of the Triassic, illustrating lithostratigraphic and chronostratigraphic relationships of the Peace River arch, northeastern British Columbia (after Golding et al., 2016). Abbreviations: Fm., Formation; Gp., Group; Olenek., Olenekian.

rely on a combination of sonic or density with resistivity. For the purpose of this study, two such methods were tested, one described in Passey et al. (1990) and the other in Carpentier et al. (1991), the latter also known as the CARBOLOG® method. Their individual calculations and assumptions differ slightly; however they both use sonic and resistivity in tandem, relying on the slower acoustic velocity of kerogen in less mature rocks and the increase in resistivity with maturity due to generation of hydrocarbons, which displace connate brine. The ΔlogR method proposed in Passey et al. (1990) is computed in two steps: firstly, for every depth, the separation between the sonic and resistivity curves, or ΔlogR, is calculated according to the equation

$$\Delta\log R = \log\left(\frac{R_t}{R_b}\right) + 0.02 \times (\Delta t - \Delta t_b) \quad (1)$$

where R_t and R_b are the true formation resistivity and the baseline resistivity in non-source, clay-rich rocks in ohm·m, respectively; and Δt and Δt_b are formation slowness and baseline slowness in non-source, clay-rich rocks in microseconds per metre (µs/m), respectively. In this study the values used for R_b and Δt_b were 23 ohm·m and 171 µs/m (52 µs/ft.), respectively.

Secondly, TOC was calculated using the formula

$$TOC = (\Delta\log R) \times 10^{(2.297 - 0.1688 \times LOM)} \quad (2)$$

as a function of ΔlogR and level of maturity (LOM), which in turn was calculated for all the wells as a linear function of depth of burial. The calculated LOM values are between 2 and 8 with a median of 4.6.

The CARBOLOG® method TOC computation is also based on sonic slowness and resistivity and can be represented in a crossplot of sonic slowness on the x axis and the inverse of the square root of resistivity on the y axis (Figure 3). The volume of organic matter is calculated according to the distance between lines of equal TOC defined by three end points. End members are defined as matrix, organic matter and brine. Both matrix and organic matter points are assumed to be infinitely resistive and thus lie along the x axis, where y equals zero. The matrix point and the slope of the 0% organic matter line are determined by the distribution of the data, which is naturally bound by a linear slope when plotted as described. The projection of the line on the opposite end of the pure-matrix point is the theoretical pure-brine point. The lines of same organic-matter content are then drawn parallel to, and equally spaced from, the first line to a theoretical 100% organic-matter point on the slow-velocity side of the crossplot, which is determined in an empirical, iterative way.

The TOC is then calculated for each depth frame according to their distance between the 100% matrix and organic-matter lines in the Cartesian plane. Due to the difference in density of mineral matrix and kerogen, the values calculated correspond to volume percentage and hence must be converted into weight fraction as per the equation

$$TOC = V_{om} \times \left(\frac{\rho_{om}}{\rho_m}\right) \times \frac{1}{k} \quad (3)$$

where V_{om} is the volume percentage of organic matter, ρ_{om} and ρ_m are the densities of organic matter and mineral matrix, set as constant values at 1.2 and 2.71 g/cm^3, respectively; and k is a unitless organic-carbon conversion factor, with an empirically determined value of 1.25. The TOC calculated by both methods was extrapolated to approximately 200 wells that had slowness and resistivity logs available for the entire Doig interval, as well as pyrolysis laboratory data, to assess the accuracy of the methods and adjust the parameters where necessary. The parameters were adjusted iteratively to minimize the difference between laboratory and log TOC.

Mapping

Formation picks for the top and base of the Doig were obtained from the database in geoSCOUT™ for approximately one thousand wells. Due to the time-consuming nature of individually checking every well, quality control of formation picks for the purpose of this study was limited to repicking or deleting wells that caused bull's-eye patterns on the structural maps. Gross-thickness isochore maps were then calculated between the top of the Montney and top of the Doig. Grids of the average CARBOLOG® method TOC values for the entire Doig interval in each well and T_{max} were created using simple regression kriging. The search radius for each grid was determined through experimental variograms at 25 km for TOC and 100 km for T_{max}. The larger radius for T_{max} is due to the smoother trend in maturity caused by the regional dip, relatively to the more random nature of TOC distribution. The map boundaries are the Doig subcrop edge to the northeast and the deformation front of the Cordilleran foreland fold-and-thrust belt to the southwest. Data in the deformation belt were not used at this stage, as it would require structural restoration to their original location relative to the undeformed portion.

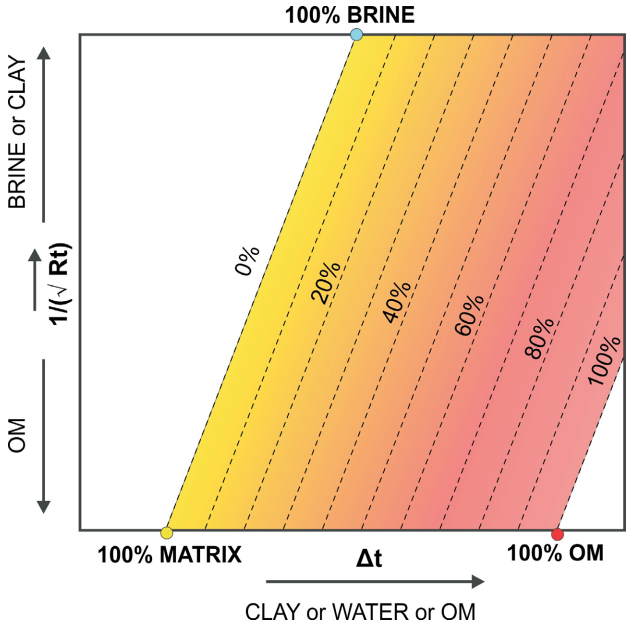

Figure 3. Crossplot showing a graphical representation of the CARBOLOG® method of total organic carbon (TOC) computation (dashed lines) in terms of three end members (poles) according to their compressional slowness and inverse of square root of resistivity relationship (after Carpentier et al., 1991), using well-log data from the Doig Formation, northeastern British Columbia and west-central Alberta. Abbreviations: OM, organic matter; Rt, true resistivity; Δt, compressional sonic slowness.

Pyrolysis

The 80% confidence interval of TOC content for the Doig is between 0.8% and 4.8%, with a median of 2% and a maximum of 14.7% (Figure 4). However, this maximum is from the public data and may not be completely reliable since it was not possible to obtain their raw files. The highest value observed in the samples analyzed for this study is 8.6%. There is a large range of values for the hydrogen index (HI), spanning from nearly 0 to almost 500, over a wide range of thermal maturity from immature to overmature (Figure 5). This range of HI values for similar T_{max} values through the oil window suggests that multiple types of kerogen are present in the Doig, from type II, through type II-III to type III. In the samples analyzed for this study, which were

properly calibrated and quality checked, and hence carry a higher degree of confidence, there was only type II-III and type III kerogen observed. This observation differs substantially from other studies that found mostly type II kerogen in the Doig (Riediger et al., 1990; Ibrahimbas and Riediger, 2004; Walsh et al., 2006). Thermal maturity within wells does not show any increasing trend with depth, despite section thicknesses in excess of 300 m.

TOC Transform

Overall, both the CARBOLOG® method and the method proposed by Passey et al. (1990) had acceptable results in estimating TOC content, on average showing good agreement with the laboratory data. The quality of the match was assessed by subtracting the log-derived TOC value from the laboratory-derived TOC (Figure 6). If the method was completely accurate, the subtraction would be null. Due to log resolution, depth shifts, imperfect assumptions, analytical errors and other factors, the subtraction results in a residual error. Although both methods employed to estimate TOC from well logs use resistivity and compressional sonic slowness, CARBOLOG® yielded superior results when compared to the ΔlogR (Passey et al., 1990) method. The median of the laboratory and log difference for the CARBOLOG® and ΔlogR (Passey et al., 1990) methods were 0.47 and 0.96, with standard deviations of 2.65 and 3.36, respectively (Figure 6). The larger average error and higher standard deviation for the ΔlogR (Passey et al., 1990) method is likely due to the fact that, unlike the CARBOLOG method, it weights resistivity higher relative to sonic and the resistivity logs have lower vertical resolution. Additionally, migrated hydrocarbons will tend to increase the resistivity above the baseline in cleaner rock types and hence result in erroneously high calculated TOC (Figure 7).

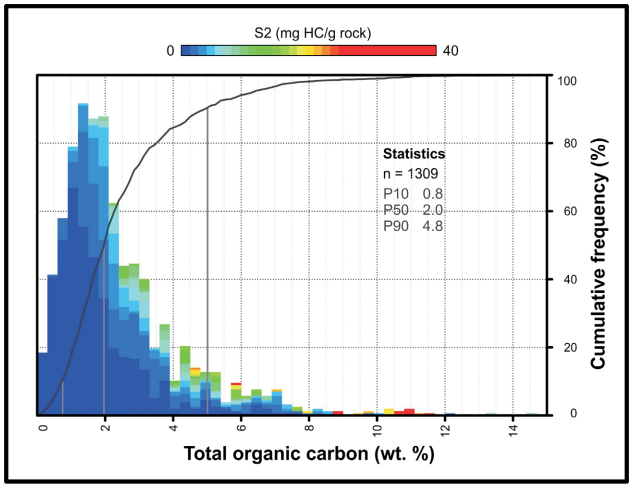

Figure 4. Histogram and key statistical parameters of all total organic carbon (TOC) from the public data and samples analyzed for this study of the Doig Formation, northeastern British Columbia and west-central Alberta, coloured by intensity of the kerogen conversion peak (S2). Abbreviations: n, sample size; P, probability.

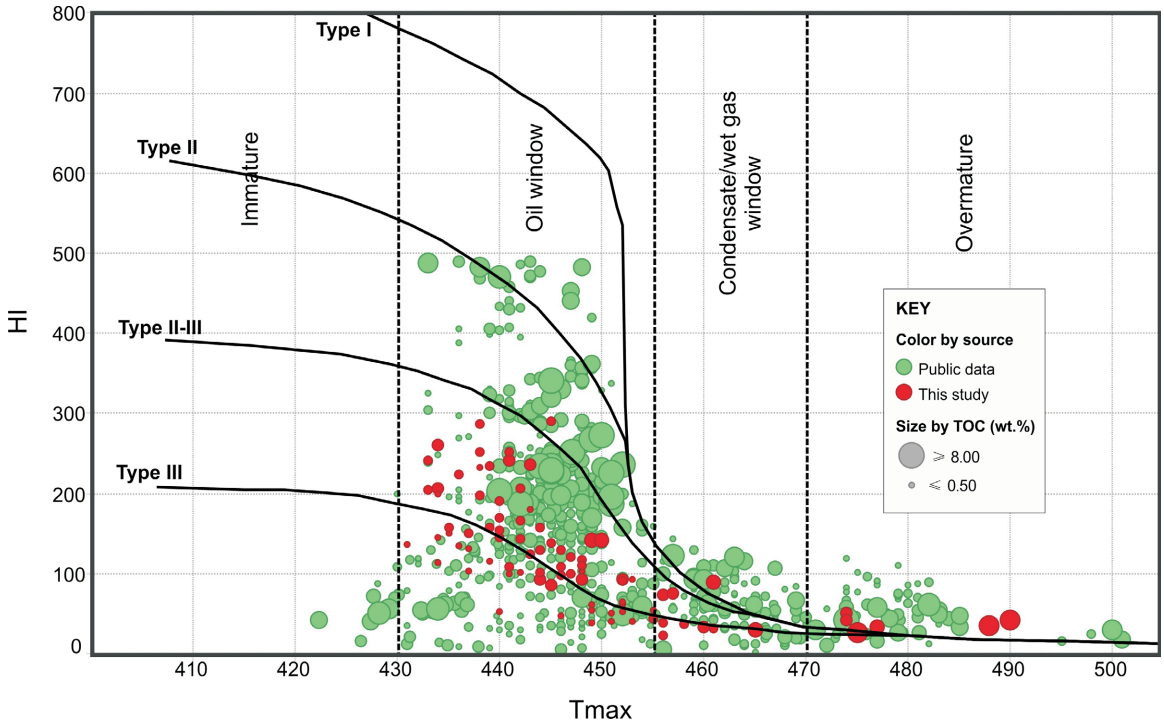

Figure 5. Hydrogen index (HI) versus temperature of maximum rate of hydrocarbon generation (T_{max}) of pyrolysis data from public domain and generated for this study of the Doig Formation, northeastern British Columbia and west-central Alberta, colour coded by data source and sized by total organic carbon (TOC). Only data points that either presented a good quality kerogen conversion peak (S2) or consistent T_{max} values are shown.

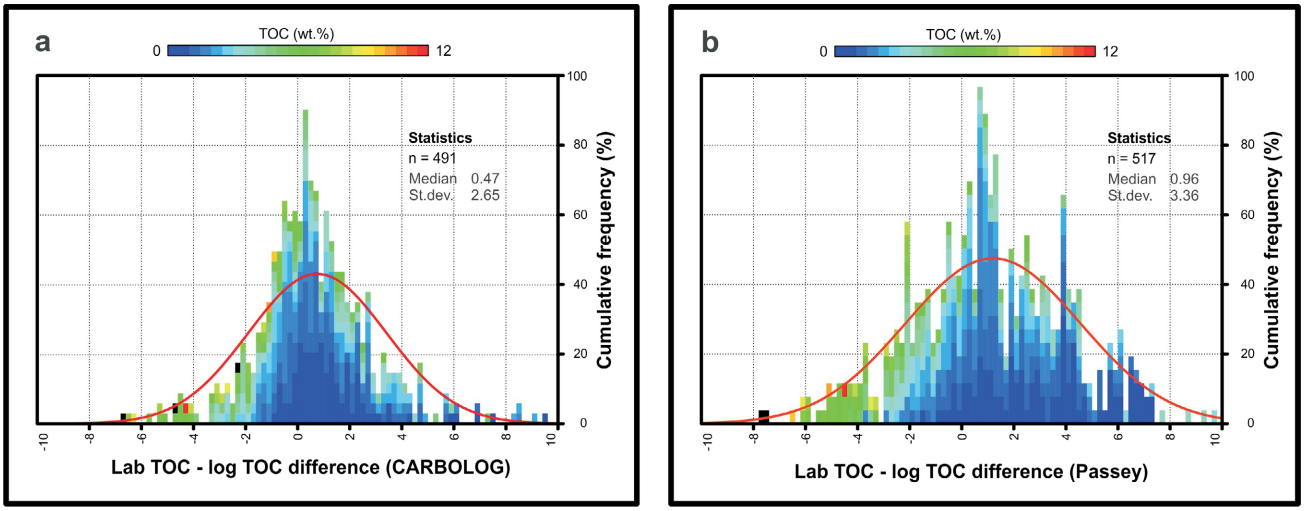

Figure 6. Histograms of the difference between laboratory- and log-derived (lab-log) total organic carbon (TOC) values from both **a)** the CARBOLOG® and **b)** the ΔlogR methods using data from the Doig Formation, northeastern British Columbia and west-central Alberta, showing a symmetric and narrow distribution centred about zero. Abbreviations: n, sample size; Passey, ΔlogR (Passey et al., 1990) method; St. dev., standard deviation.

Structure and Isochore

The top and base (top of the Montney Formation; Figure 2) structures of the Doig Formation are subparallel and follow the general southwest-trending dip of the Phanerozoic in the basin (Figure 8). A slight increase in dip angle is evident south of a line defined by the southern edge of the Monias and Progress oilfields. The dip of both top and base change from 0.4° in the northeast portion of the basin, to approximately 0.7° through a slope 40 km wide following the regional strike, and revert back to a gentler dip of 0.3° in the distal part of the basin. This relatively steep-dipping slope

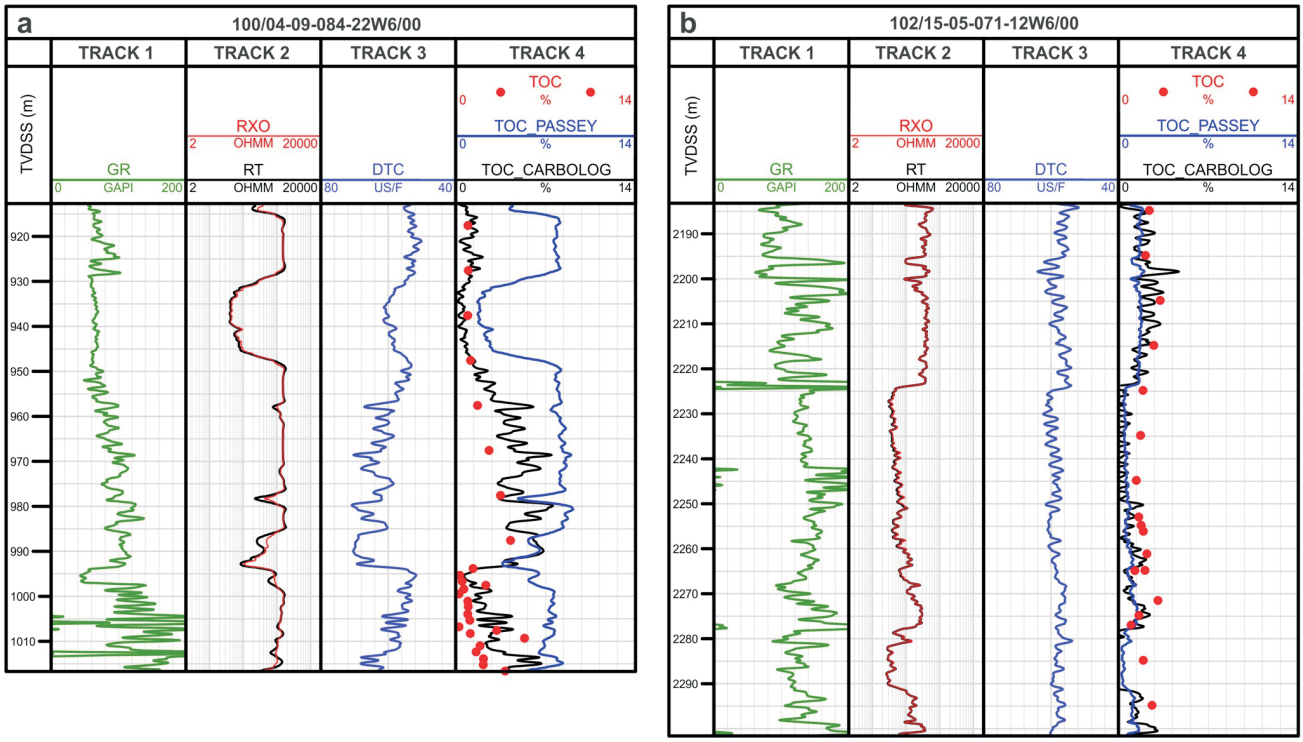

Figure 7. Log plots of two wells (a and b) in northeastern British Columbia and west-central Alberta showing, from left to right on each well: vertical depth below sea level (TVDSS), gamma ray (GR) in track 1, resistivity (RT) in track 2`, compressional sonic slowness (DTC) in track 3, total organic carbon (TOC) in track 4. CARBOLOG® TOC shows good agreement with laboratory data (red circles) in both wells, whereas the ΔlogR (Passey et al., 1990) method has a good match on well b, but largely overestimates TOC on well a.

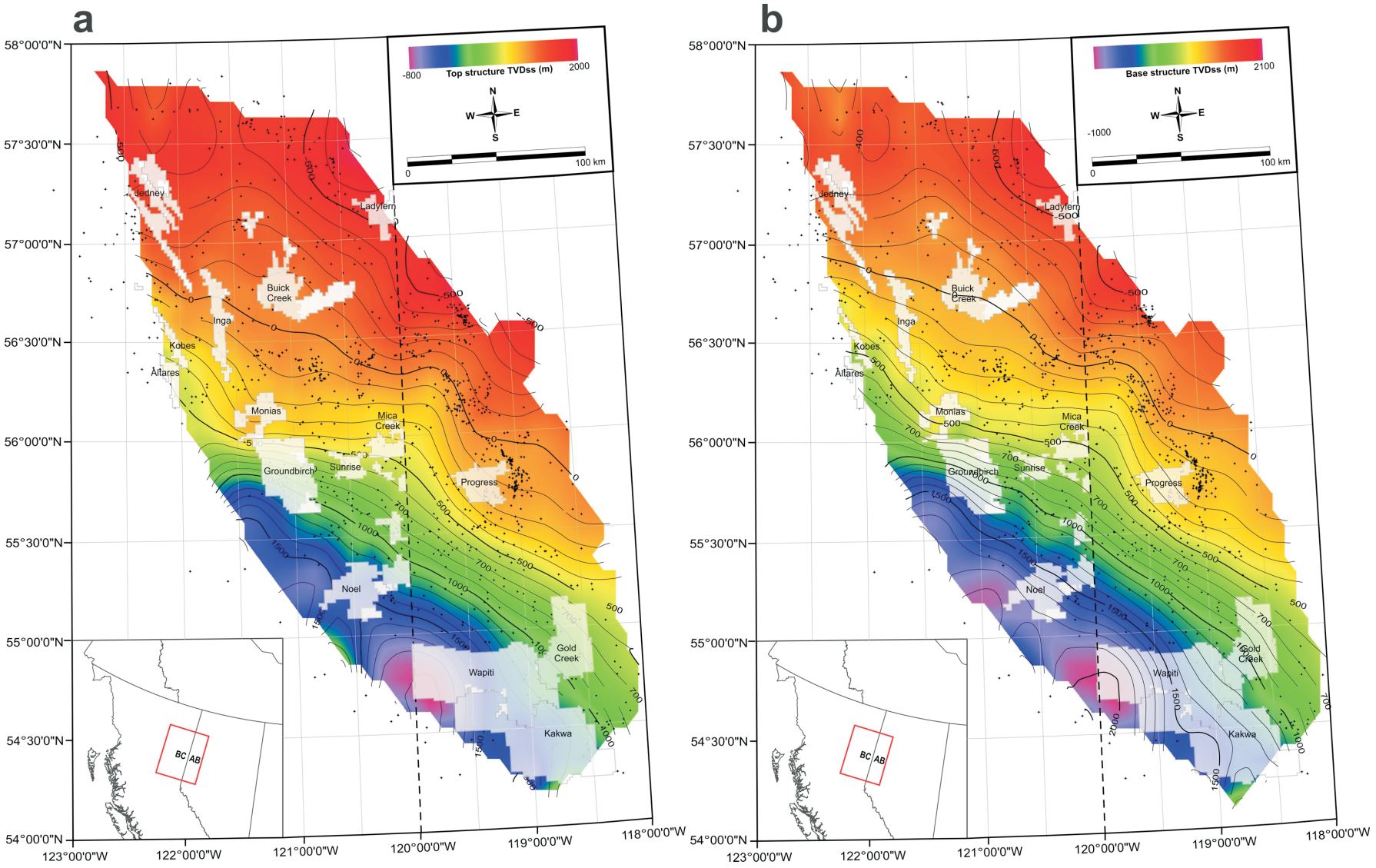

Figure 8. Structure maps of the Doig Formation **a)** top and **b)** base (Montney Formation top) in northeastern British Columbia and west-central Alberta, with elevations expressed in vertical metres below mean sea level (TVDss) permanent datum.

is interpreted as the paleoshelf break and likely represents an important facies boundary between coarser-grained shelf sediments to the northeast and finer-grained sediments to the southwest.

A southwest-trending linear feature of negative relief exists between the Mica Creek and Progress fields. This feature is approximately coincident with the Fort St. John graben complex (Figure 1) and is associated with increased accommodation space, as evidenced by the thickening of the Doig interval northwest of the Progress field (Figure 9). The trough may have also served as a sediment conduit into the deeper part of the basin showing anomalous thicknesses in excess of 160 m immediately southwest of the trough, around the vicinity of the Noel field in BC up to the border with Alberta. The average thickness of the Doig interval is 84 m with an 80% confidence interval between 25 and 175 m. Other regions of anomalous thicknesses in excess of 240 m are located in the west-central part of the basin, in a semi-circular shape around the Monias and Groundbirch fields and thickening to the west, and in the northwest of the Inga field.

The average interval TOC from CARBOLOG® has a background of 3% in weight, ranging from 1.2% to 7.5% in weight (Figure 10). One of the areas with the highest average TOC coincides with the anomalous thickness on, and immediately adjacent to, the depression associated with the Fort St. John graben. This area is bounded on both sides by regions of TOC lower than the background. Another area of high TOC associated with a thick gross interval occurs on and around the Sunrise oilfield, immediately east of the Groundbirch field. Elevated average TOC values are also observed with no association to increased thickness in the relatively shallow dipping platform near the Altares, Kobes, Inga and Buick Creek fields.

The maturity map reveals T_{max} values from the early oil window, using the zones for petroleum generation for type II kerogen from Dow (1977) as a reference, in the eastern and southwestern portions of the basin, through condensate/wet gas, to peak dry gas in the western edge against the deformation front (Figure 11). Approximately 76% of the area is in the oil window, with 22% in the condensate/wet gas and 2% in the dry gas window (Table 1). In terms of gross rock volume within each region, the numbers are slightly skewed toward condensate/wet gas and dry gas, as the thickness increases westward, so that approximately 60% of the total rock volume is in the oil window, 34% in the condensate/wet gas, and over 5% in the dry gas. Within the southern portion of the basin, on the eastern side of the Wapiti field, there is an area of increased maturity in the peak oil window. There is a broad area in the west-central region lying in the condensate/wet gas window, which roughly coincides with the alignment of the Jedney, Inga, Groundbirch and Sunrise fields.

Conclusions

The work presented here is based on a preliminary assessment of source-rock properties and will serve as the foundation for a PSA of the Doig Formation, incorporating an evaluation of its reservoir properties and a reconstruction of its thermal history through basin modelling. The data provide insights for evaluating the additional potential of currently developed areas as well as new prospects. The combination of maturity and thickness maps suggests that one third of the Doig gross rock volume lies within the condensate/wet gas window for type II kerogen. The vast majority of this area is in BC. By combining the isochore with the average TOC map, total carbon thickness maps may be calculated and used for further assessing hydrocarbon prospectivity.

Ongoing work will improve the quality of the results presented in this preliminary update, as well as integrate these data into a basin model. The picks for top and base of the Doig will be more thoroughly reviewed for consistency, improving the accuracy of the thickness maps. The DPZ top and its correlative surface will be picked across the entire distribution of the Doig, subdividing the mapping in two intervals. This subdivision will highlight differences in thickness and TOC distribution of the more organic-rich basal interval. The log-derived TOC estimation for this work was performed only in wells for which laboratory data was available, so that the quality of the model could be checked, and served as a proof of concept. Additional log-based TOC methods will be evaluated, and the existing models will be refined. With increased confidence in the models, all wells with a minimum log suite will ultimately be used in the mapping of TOC, resulting in a denser grid of data and a TOC map with enhanced resolution and accuracy. Historic production data will be integrated into the analysis and cross-correlated with the maturity maps. Integrating the production data will be particularly useful for the investigation of the influence of kerogen type on the type of hydrocarbons generated. If there are multiple types of kerogen present in the Doig, as pseudo-van Krevelen and T_{max} versus HI crossplots suggest, they are expected to play an important role in the type of hydrocarbon generated and produced. In that case, kerogen type will have to be taken into account when delineating liquid-rich areas, by means of defining regional trends in the type of kerogen and establishing correlations with lithofacies.

Acknowledgments

The authors would like to acknowledge financial support from Geoscience BC, Canadian Natural Resources Limited, Chevron Canada Limited, Devon Energy Corporation, Encana Corporation, geoLOGIC Systems ltd., Husky Energy Inc. and Trican Geological Solutions Ltd. This study would not have been possible without the generous lending

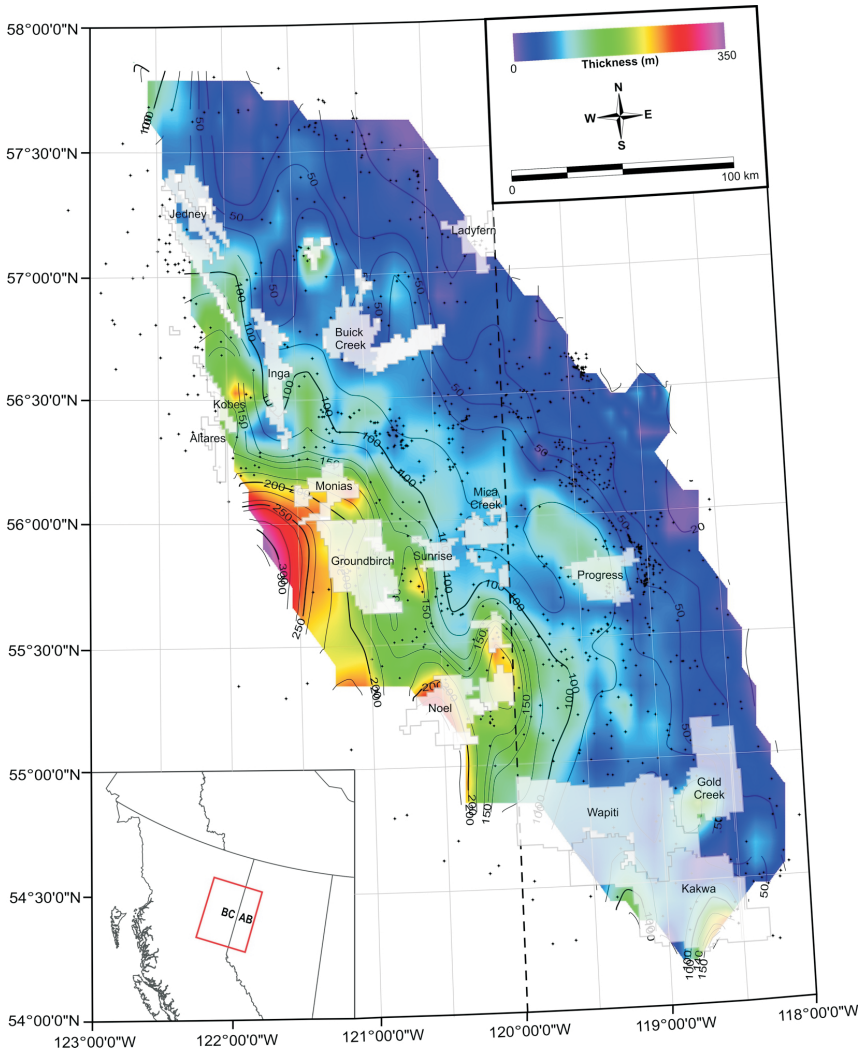

Figure 9. Gross isochore map of the Doig interval in northeastern British Columbia and west-central Alberta, with thicknesses expressed in metres.

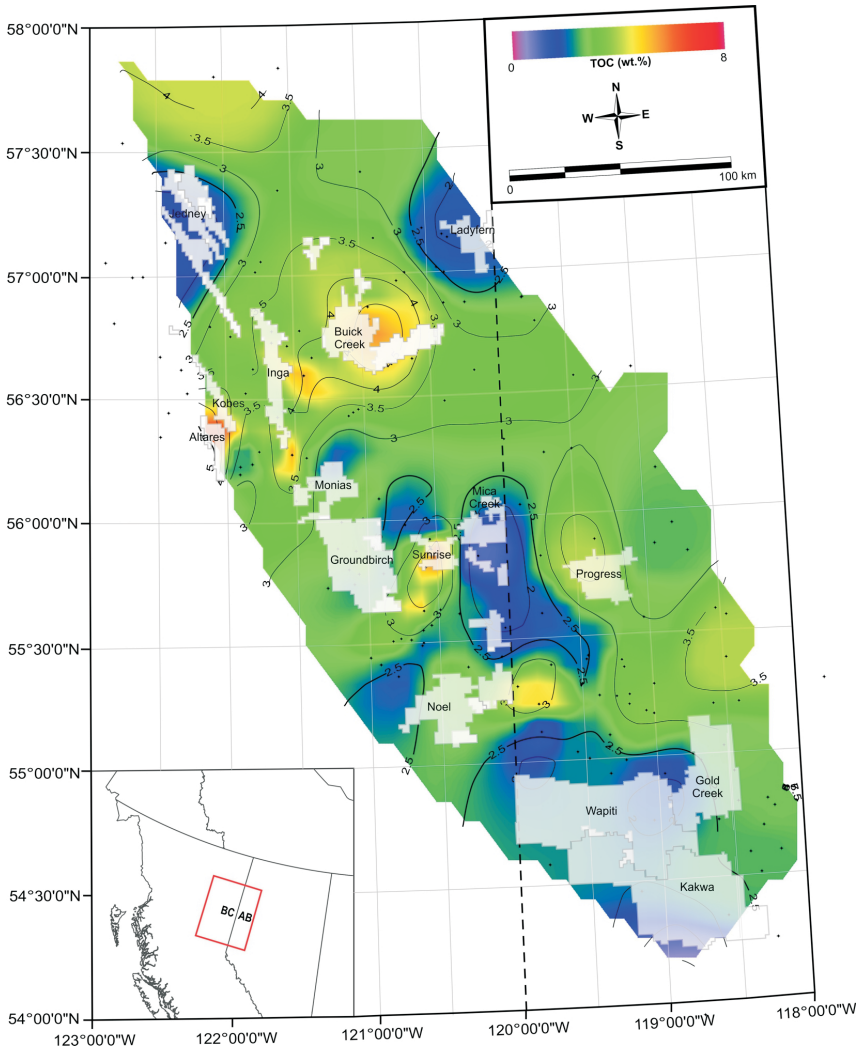

Figure 10. Average total organic carbon (TOC) map for the Doig interval in northeastern British Columbia and west-central Alberta, with TOC content expressed in weight percentage.

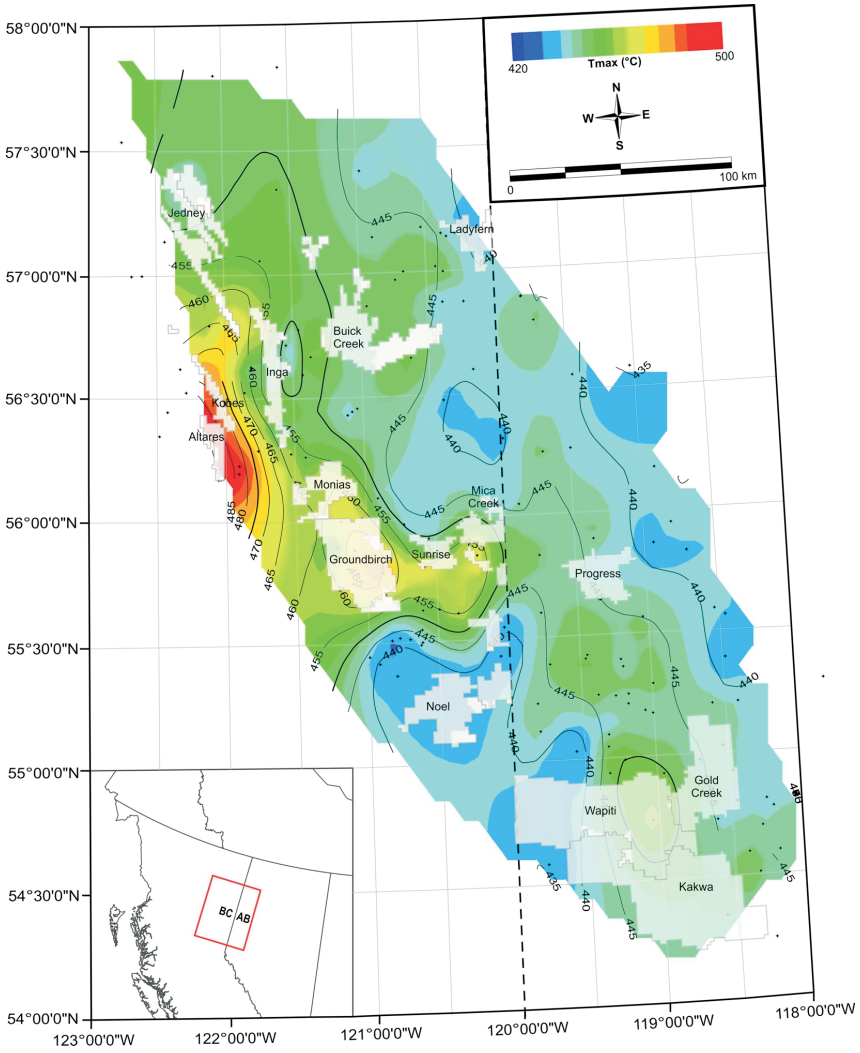

Figure 11. Generalized thermal maturity map of the Doig interval in northeastern British Columbia and west-central Alberta, expressed by temperature of maximum rate of hydrocarbon generation (T_{max}).

of instruments by, and valuable expertise of, Trican's staff, especially B. Nassichuk, C. Twemlow and S. Tu. Also essential for this study and greatly appreciated was the kind donation of software by geoLOGIC Systems ltd. and Paradigm Geophysical Canada Ltd. The authors would also like to thank D. Mare for his efforts in finding and compiling public domain data and, last but not least, they acknowledge the time and effort dedicated to the thorough review of the manuscript by E. Letham, Ph.D. candidate at The University of British Columbia.

Table 1. Area and gross rock volume of the Doig Formation in northeastern British Columbia and west-central Alberta, within each hydrocarbon generation window.

Window (Tmax)	Area ($x10^{10}$ m^2)	Area (%)	Volume ($x10^{12}$ m^3)	Volume (%)
Oil (430–455°C)	5.003	75.7	3.021	60.3
Condensate/wet gas (455–470°C)	1.448	21.9	1.717	34.3
Dry Gas (>470°C)	0.155	2.3	0.269	5.4

References

Carpentier, B., Huc, A.Y. and Bessereau, G. (1991): Wireline logging and source rocks – estimation of organic content by CARBOLOG® method; The Log Analyst, v. 32, no. 3, p. 279–297.

Chalmers, G.R.L. and Bustin, R.M. (2012): Geological evaluation of Halfway-Doig-Montney hybrid gas shale-tight gas reservoir, northeastern British Columbia; Marine and Petroleum Geology, v. 38 p. 53–72.

Creaney, S. and Allan, J. (1990): Hydrocarbon generation and migration in the Western Canada Sedimentary Basin; *in* Classic Petroleum Provinces, J. Brooks (ed.), Geological Society Special Publication 50, p. 189–203.

Davies, G.R. (1997): The Triassic of the Western Canada Sedimentary Basin: tectonic and stratigraphic framework, paleogeography, paleoclimate and biota; Bulletin of Canadian Petroleum Geology, v. 45, no. 4, p. 434–460.

Dow, W.G. (1977): Kerogen studies and geological interpretations; Geochemical Exploration Journal, v. 7, p. 79–99.

Du Rouchet, J. (1985): The origin and migration paths of hydrocarbons accumulated in the Lower Cretaceous sandstone "giant" tar accumulations of Alberta – Part II; Journal of Petroleum Geology, v. 8, no. 1, p. 101–114.

Edwards, D.E., Barclay, J.E., Gibson, D.W., Kvill, G.E. and Halton, E. (1994): Triassic strata of the Western Canada Sedimentary Basin; Chapter 16 *in* Geological Atlas of the Western Canada Sedimentary Basin, G.D. Mossop and I. Shetsen (ed.), Canadian Society of Petroleum Geologists and Alberta Research Council, Edmonton, Alberta, p. 257–275.

Espitalié, J., Madec, M. Tissot, B., Mennig, J.J. and Leplat, P. (1977): Source rock characterization method for petroleum exploration; Offshore Technology Conference, 2–5 May 1977, Houston, Texas, Paper 2935.

Evoy, R.W. and Moslow, T.F. (1995): Lithofacies associations and depositional environments in the Middle Triassic Doig Formation, Buick Creek Field, northeastern British Columbia; Bulletin of Canadian Petroleum Geology, v. 43, no. 4, p. 461–475.

Golding, M.L., Mortensen, J.K., Ferri, F., Zonneveld, J.-P., Orchard, M.J. and Rygel, M. (2016): Determining the provenance of Triassic sedimentary rocks in northeastern British Columbia and western Alberta using detrital zircon geochronology, with implications for regional tectonics; Canadian Journal of Earth Sciences, v. 53, no. 2, p. 140–155.

Ibrahimbas, A. and Riediger, C.L., (2004): Hydrocarbon source rock potential as determined by Rock- Eval 6/TOC pyrolysis, northeast British Columbia and northwest Alberta; *in* Summary of Activities, BC Ministry of Energy, Mines and Petroleum Resources, Oil and Gas Division, Resource Development and Geoscience Branch, p. 7–18.

Marshall, G.M., Noble, I.A. and Tang, R.C.W. (1987): Triassic/Jurassic fields; Chapter 7 *in* Geophysical Atlas of Western Canadian Hydrocarbon Pools, N.L. Anderson, L.V. Hills and D.A. Cederwall (ed.), Canadian Society of Exploration Geophysicists and Canadian Society of Petroleum Geologists, p. 187–215, URL <http://www.cspg.org/cspg/documents/Publications/Atlas/geophysical/L_Chap ter_7.pdf> [November 2016].

Passey, Q.R., Creaney, S., Kulla, J.B., Moretti, F.J. and Stroud, J.D. (1990): A practical model for organic richness from porosity and resistivity logs; American Association of Petroleum Geologists Bulletin, v. 74, no. 12, p. 1777–1794.

Riediger, C.L., Fowler, M. G., Brooks, P. W. and Snowdon, L. R. (1990): Triassic oils and potential Mesozoic source rocks, Peace River Arch area, Western Canada Basin; Organic Geochemistry, v. 16, no. 1–3, p. 295–306.

Walsh, W., Adams, C., Kerr, B. and Korol, J. (2006): Regional "shale gas" potential of the Triassic Doig and Montney formations, northeastern British Columbia; BC Ministry of Energy, Mines and Petroleum Resources, Oil and Gas Division, Resource Development and Geoscience Branch, Petroleum Geology Open File 2006-02, 19 p., URL <http://www2.gov.bc.ca/assets/gov/farming-natural-resources-and-industry/natural-gas-oil/petroleum-geoscience/petroleum-open-files/pgof20062.pdf> [November 2016].Welte, D.H. and Leythaeuser, D. (1983): Generation of hydrocarbons in source rocks; Naturwissenschaften, v. 70, p. 53–59.

Regional Variability of Reservoir Properties of the Devonian Shales of Northeastern British Columbia

T.K. Wilson, The University of British Columbia, Vancouver BC, twilson@eoas.ubc.ca

R.M. Bustin, The University of British Columbia, Vancouver BC

Wilson, T.K. and Bustin, R.M. (2018): Regional variability of reservoir properties of the Devonian shales of northeastern British Columbia; *in* Geoscience BC Summary of Activities 2017: Energy, Geoscience BC, Report 2018-4, p. 51–64.

Introduction

Organic-rich Devonian mudrocks with proven unconventional-resource potential are prevalent throughout the Western Canada Sedimentary Basin (WCSB). In northeastern British Columbia (BC) the Devonian Muskwa and Horn River formations host economically significant volumes of gas within the Horn River and Liard basins, and Cordova Embayment. Despite the proven gas reserves, exploitation and production of these reservoirs has not reached the prolific levels of other noteworthy shale plays due to market access and, arguably, a lack of natural-gas liquids, and thus the study of the variation in reservoir properties and hydrocarbons in place has received little attention.

The objective of this study is to contribute to the prediction of hydrocarbon distribution, reservoir quality and producibility of Devonian shales in the Horn River and Liard basins, and Cordova Embayment. Specifically, the goal is to determine the geological factors controlling the distribution of gas and condensate/natural-gas liquids. This multifaceted study uses petroleum systems analysis ground truthed with fluid analysis, and petrophysical and organic geochemical analyses of cuttings and core samples to predict the types and volumes of generated and retained hydrocarbons throughout the basins' evolution (Figure 1). This paper provides an update on the study, focusing on the characterization of various reservoir properties such as organic content, thermal maturity and mineralogy, their regional variations, and how the evolution of the basin may have affected the distribution of such properties.

Geological Background

During the Devonian and Mississippian periods, northeastern BC was situated along the edge of the North American protocontinent. As in other parts of the WCSB, the stratigraphy during that time was dominated by shale and carbonate packages, which were related to major transgressive and regressive cycles. The basinal setting of the study area resulted in the deposition of thick packages of fine-grained sedimentary rocks, whereas stratigraphically equivalent carbonate units further to the east were deposited in shallower water (Figure 2). Extensional block faulting, synchronous with the Antler orogeny, further influenced Paleozoic deposition by creating salient features such as the Liard Basin and Fort St. John graben (Wright et al., 1994). Subsequent evolution of the region was heavily affected by the formation and development of the Cordilleran foreland fold-and-thrust belt.

This study focuses on the BC portion of the Horn River and Liard basins, and Cordova Embayment (Figure 3). The Horn River Basin (HRB) is bounded by the Bovie fault zone to the west and terminates against the Presqu'ile barrier reef to the south and east; this same carbonate complex surrounds the Cordova Embayment. There is an overall shallowing of the basin and general thinning of Devonian shale units from the southwest to the northeast.

The overall depositional environment of the Devonian shale sequence is dominated by deep-water embayments (HRB and Cordova Embayment), representing two second-order sea level cycles in which the Muskwa Formation and Evie Member represent transgressive systems tracts (Potma et al., 2012). The Muskwa Formation is an especially significant event, which represents a basin-wide transgression that inundated the basin and led to extensive deep-water sedimentation throughout northeastern BC and western Alberta. (Switzer et al., 1994). Geochemical analysis data suggest that the organic-rich Devonian–Mississippian interval represents deep-basinal deposition with regional upwelling and connectivity to the open ocean. In addition, based on geochemical markers, as well as the lack of any substantial bioturbation, the environment is interpreted as having been anaerobic to dysaerobic (Fowler et al. 2001; Ross and Bustin, 2009; Bunnell and Hillier, 2014).

The Devonian shales are dominated by black siliceous mudstones, with rare pyritic laminae (Figure 4a–e). The siliceous nature of these rocks is of biogenic origin, due to the accumulation of pelagic radiolarians in an otherwise sedi-

This publication is also available, free of charge, as colour digital files in Adobe Acrobat® PDF format from the Geoscience BC website: http://www.geosciencebc.com/s/SummaryofActivities.asp.

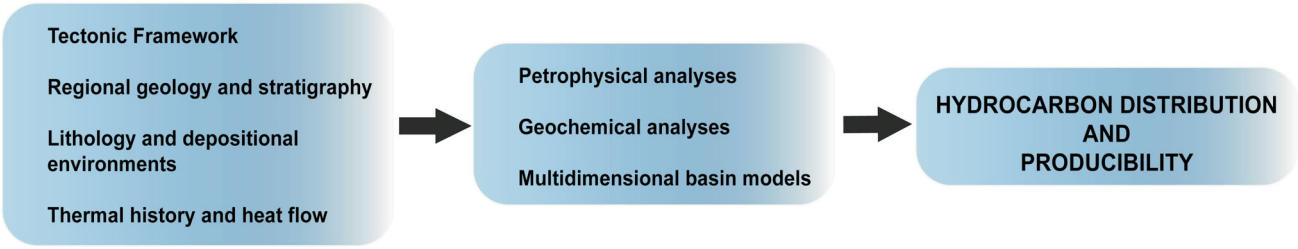

Figure 1. Flowchart illustrating the protocol for this study (from Wilson and Bustin, 2017).

ment-starved basin (Ross and Bustin, 2008). Subordinate lithofacies include grey silty mudstones, laminated grey mudstones, carbonate mudstones, and carbonate grainstone. Overall, sedimentary structures are rare, and bioturbation is sparse and diminutive, particularly within the Muskwa Formation (Dong et al., 2015). The shales generally become increasingly argillaceous from east to west (Ross and Bustin, 2008).

Materials and Methodology

Core and cuttings samples were collected from 20 wells along two southwest-trending transects. Where possible, these samples were collected at consistent intervals, while still making an effort to sample all major lithofacies present in the core. The cuttings were collected at 30 to 50 m intervals along the entire length of each well. Core samples were

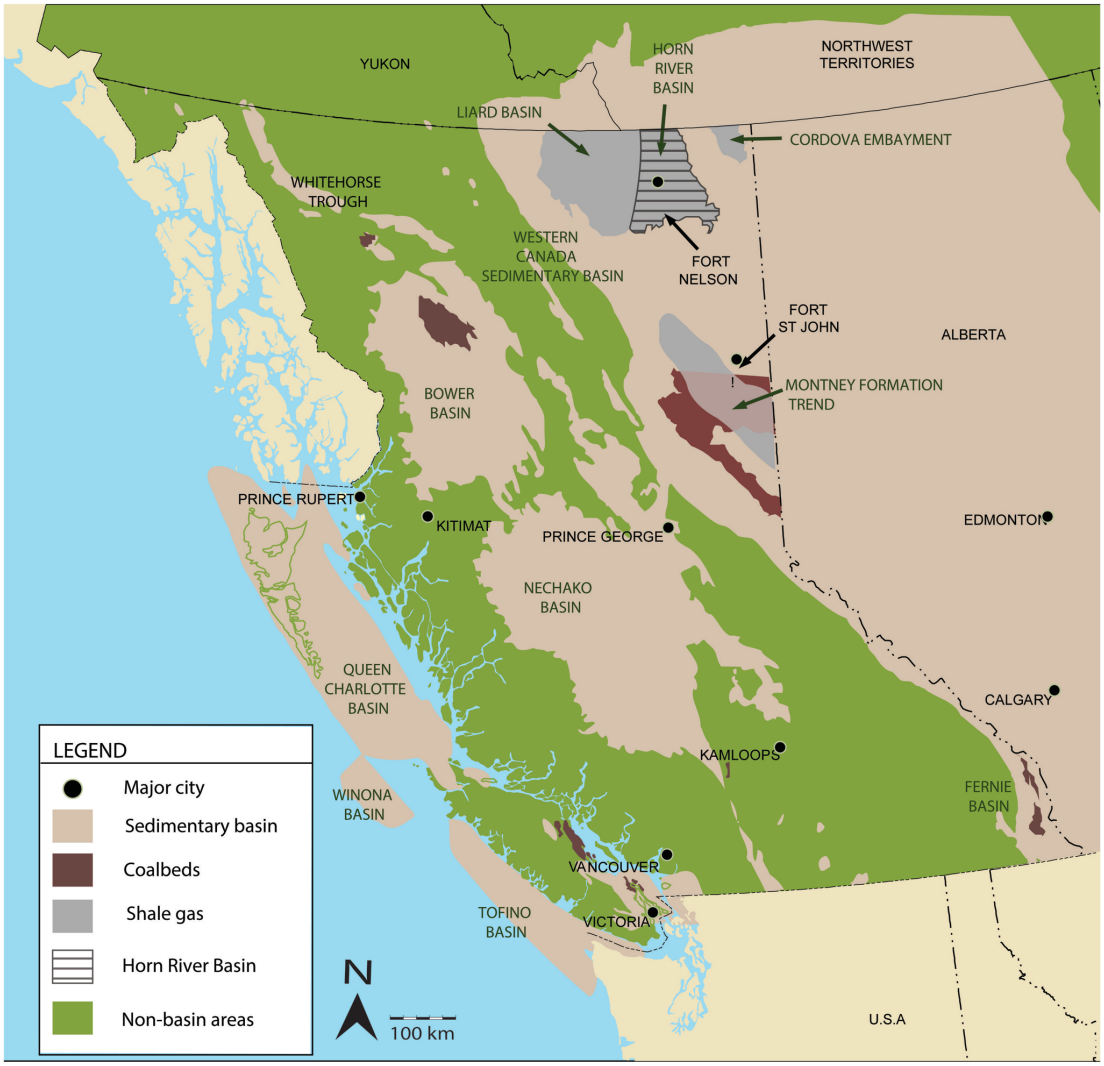

Figure 2. Location of the Liard and Horn River basins, and Cordova Embayment, in northeastern British Columbia (modified from BC Ministry of Energy, Mines and Petroleum Resources and National Energy Board et al., 2011).

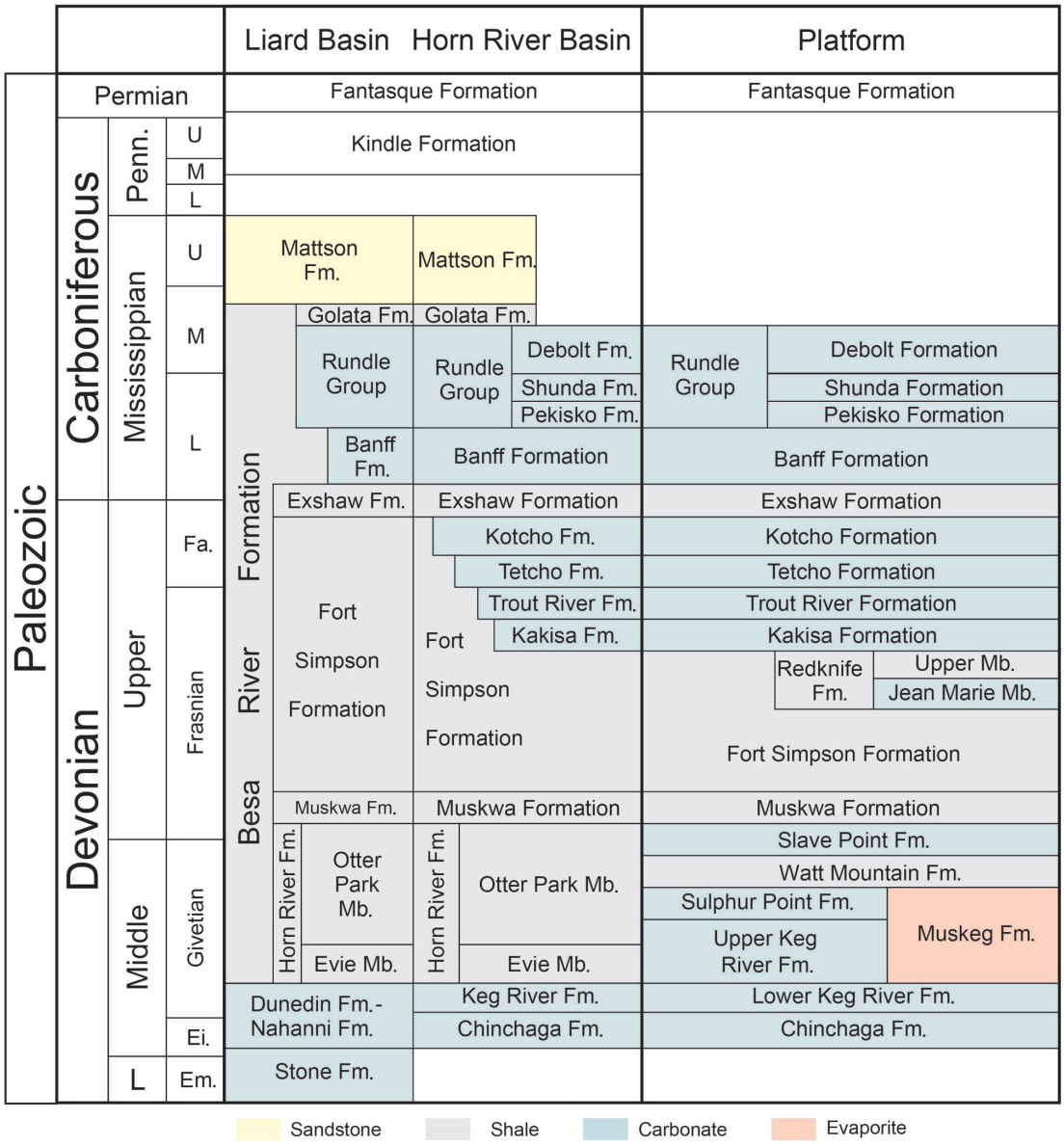

Figure 3. Upper Paleozoic stratigraphy for northeastern British Columbia (modified from Ferri et al., 2011). Abbreviations: Ei., Eifelian; Em., Emsian; Fa., Fammenian; Fm., formation; L, lower; M, middle; Mb., member; Penn, Pennsylvanian; U, upper.

analyzed using Rock-Eval pyrolysis, helium pycnometry, mercury intrusion porosimetry, X-ray diffraction, and low pressure N_2 and CO_2 gas adsorption. Additionally, pyrolysis was also completed for all of the collected cuttings samples, including samples from western Alberta. The location of the wells was selected to capture the variation in depth of burial and thermal history across the basins, and therefore the associated variability in reservoir quality (Figure 5). Only the methods employed in organic geochemistry and mineralogy analyses are described in this update.

Organic Geochemistry

Total organic carbon (TOC) contents and temperature of maximum rate of hydrocarbon generation (T_{max}) values from pyrolysis were determined using a HAWK™ pyrolysis instrument from Wildcat Technologies for all of the cuttings samples and 27 of the Muskwa Formation core samples. All samples were crushed to powder (<60 mesh) and approximately 100 mg of sample was analyzed. These analyses were used to complement regional data in public domain and data in the University of British Columbia database.

Mineralogy

Sample preparation for quantitative mineralogy determination followed the modified smear-mount method for X-ray diffraction analysis (Munson, 2015). Data were collected using a normal-focus Bruker® D8 FOCUS diffractometer

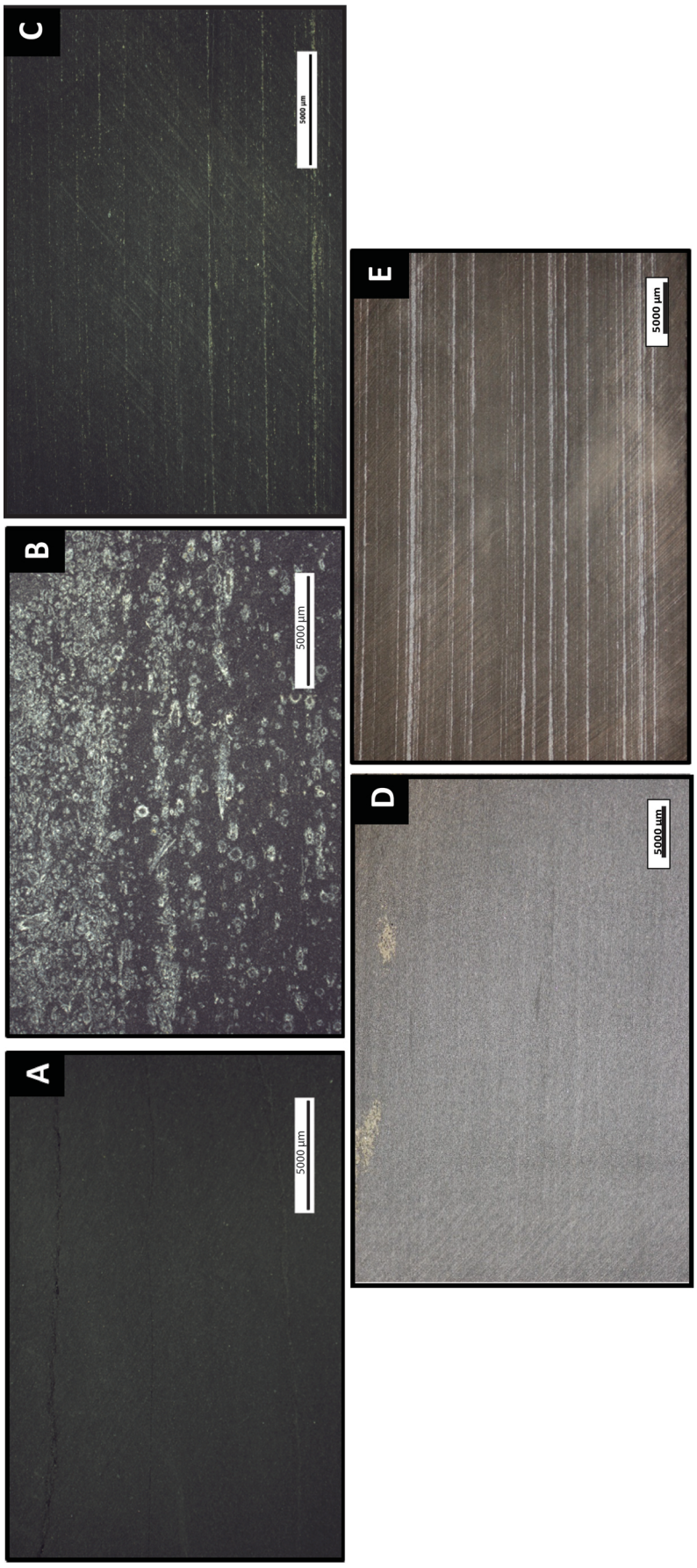

Figure 4. Examples of facies from the Muskwa and Horn River formations from core samples collected in northeastern British Columbia, showing **a)** siliceous black mudstone; **b)** skeletal lime mudstone containing mainly sponge spicules and radiolarians; **c)** siliceous black mudstone with pyritic laminations and lenses; **d)** carbonate mudstone; **e)** laminated mudstone.

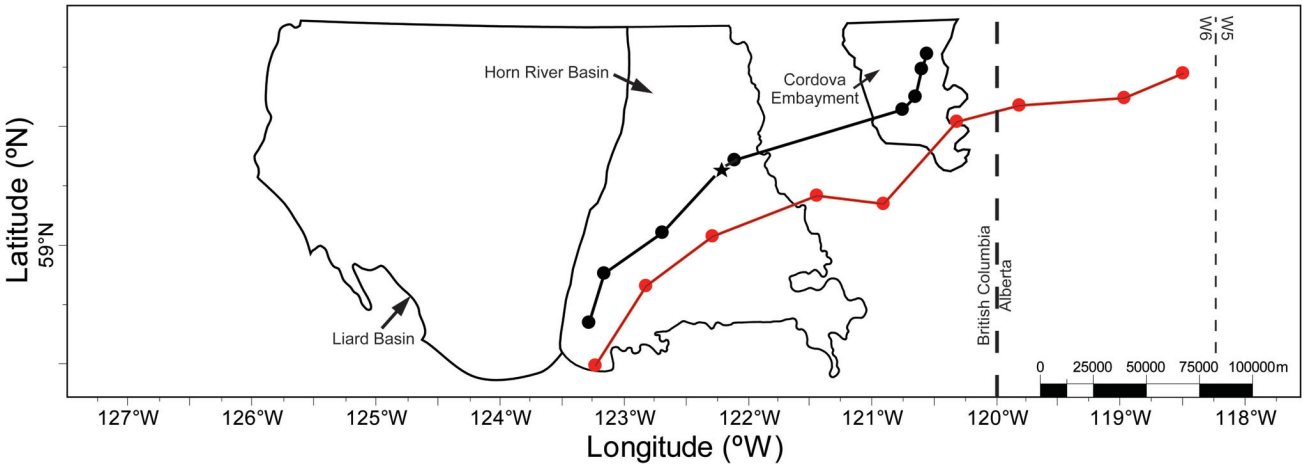

Figure 5. Top of the Muskwa Formation in northeastern British Columbia; the two cross-sections represent the location of wells from which core (black dots) and cuttings (red dots) samples were collected, and the star indicates the location of the well used for showing log-TOC calibration.

(CoKα radiation), with diffraction patterns obtained over a range of 3–70° 2θ at a scanning step of 0.03° 2θ and a counting time of 0.8 s/step. Diffraction patterns were quantified using the Rietveld full-pattern fitting method with the TOPAS software from Bruker AXS.

Results and Discussion

Maturity

Pyrolysis Results

Devonian shales in northeastern BC are generally overmature. Trends in T_{max} versus depth are rarely informative since the kerogen conversion (S2) peaks are low and indistinct for nearly all Devonian samples within northeastern BC, leading to anomalous T_{max} values (Figure 6a). Pyrolysis results for the Alberta samples exhibit more reliability due to lower maturity and more distinct S2 peaks. Maturity within western Alberta ranges from immature to the upper oil window (T_{max} values of 426 to 471 °C) and a general increase in T_{max} versus depth can be observed (Figure 6b). The following discussion on maturity will focus on the Muskwa Formation; however, similar trends exist in the more spatially constrained Horn River Formation.

Maturity Trends

Pyrolysis results from the two southwest–northeast transects (T_{max}, pyrograms, hydrogen and oxygen indices) demonstrate that overmaturity of Devonian shales persists throughout NTS areas 094J, 094O and 094P of northeastern BC. Vitrinite reflectance measurements are sparse in northeastern BC, with measured values ranging from 1.75 to 3.2 %Ro. The southwest to northeast increase in maturity extends into northeastern BC with the lowest vitrinite reflectance values of <2 %Ro occurring in the eastern portions of NTS areas 094I and 094P (Figure 7). Maturity generally tends to increase toward the north and northwest across the Cordova Embayment, Presqu'ile barrier and HRB, with the highest maturities occurring in the northwestern corner of the HRB.

Although Devonian strata are approximately 1500 m deeper on the western side of the Bovie fault, %Ro values are similar to those in the HRB (2.6 to 3.1 %Ro) to the east. Both to the east and west of the Bovie fault, there is a northward trend of increasing maturity. Considering the few reliable data points, they seem to suggest that maximum thermal exposure (and hence peak maturity) of the Devonian strata across northeastern BC predates the extensive displacement along the Bovie fault that occurred during the Late Cretaceous and Tertiary[1] (MacLean and Morrow, 2004).

Total Organic Carbon

TOC Results

The public database was used along with additional data acquired for this study to analyze TOC trends. Kerogen type for the Devonian shales is inferred to be type II, based on pseudo-van Krevelen plots for the lower maturity Alberta samples. The organic content of the Devonian shales in northeastern BC is generally greater than 1% in weight in the HRB and Cordova Embayment. Combining all available data for the Muskwa and Horn River formations, TOC averages around 3% in weight, with the Muskwa Formation and Evie Member generally exhibiting higher values than the Otter Park Member. Due to potential caving and mixing from organic-lean units within cuttings samples, the average values for cuttings are generally lower than

[1] *'Tertiary' is an historical term. The International Commission on Stratigraphy recommends using 'Paleogene' (comprising the Paleocene to Oligocene epochs) and 'Neogene' (comprising the Miocene and Pliocene epochs). The author used the term 'Tertiary' because it was used in the source material for this paper.*

core samples, with values of 2.07 and 2.88% in weight, respectively, for the Muskwa Formation.

Petrophysical Analysis – Log TOC

In the study area, spatial distribution of TOC data is limited and thus well logs calibrated with measured TOC were utilized. There are many methods that have been developed to calculate TOC from calibrated logs, all of which have limitations (Schmoker, 1980; Passey et al., 1990; Passey et al., 2010; Sondergeld et al., 2010; Ariketi, 2011; Herron et al., 2011). In this study, the modified ΔlogR method developed by Passey et al. (1990) and Sondergeld et al. (2010) has

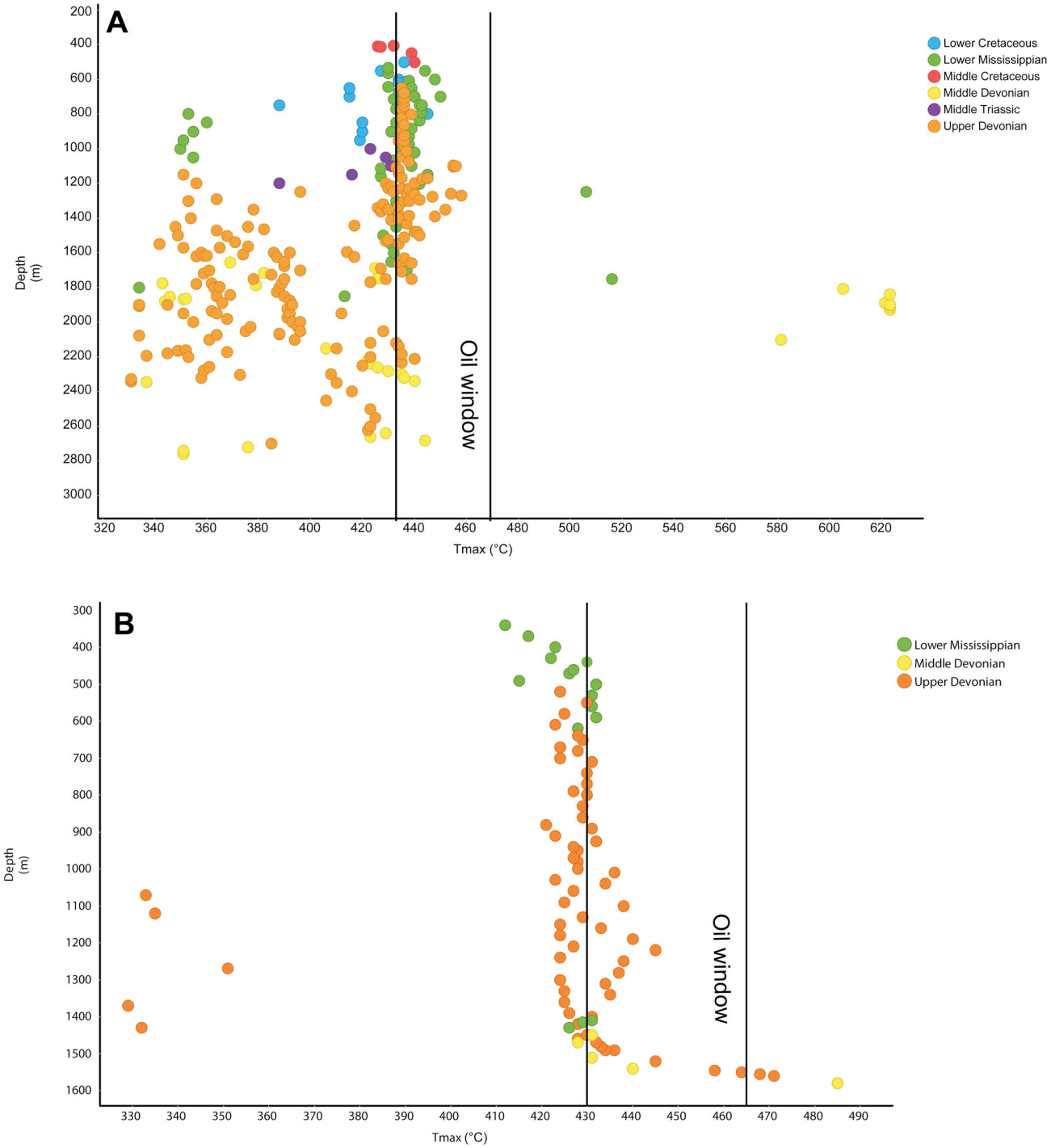

Figure 6. Depth versus temperature of maximum rate of hydrocarbon generation (T_{max}; °C) from pyrolysis analyses on cuttings samples from **a)** British Columbia (Horn River Basin and Cordova Embayment) and **b)** western Alberta. The colours correspond to the period of deposition (for sample locations, refer to Figure 5).

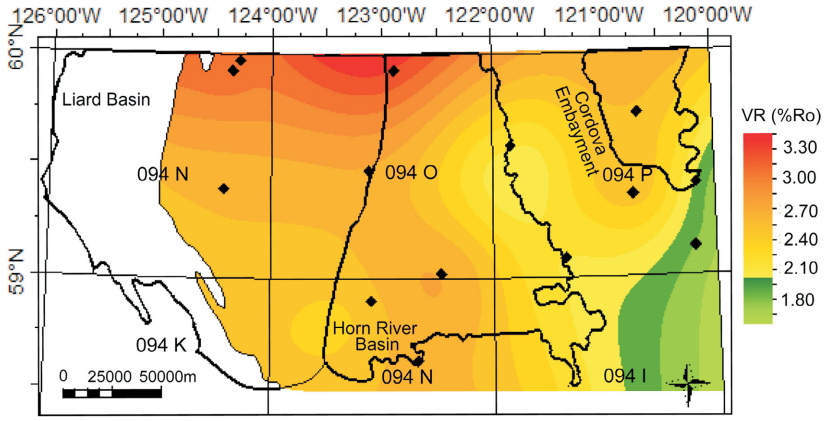

Figure 7. Isoreflectance map for the Muskwa Formation in northeastern British Columbia, based on publicly available vitrinite reflectance (VR) analyses. Areas of potential wet gas are represented by green and are related to %Ro values <2. Maturity generally increases to the northwest.

been used to calculate log-derived TOC (equations 1 and 2):

$$\Delta \log R = \log_{10}\left(\frac{R}{R_o}\right) - 1.4(\rho - \rho_o) \quad (1)$$

$$TOC = (\Delta \log R) \times 10^{(2.297 - 0.1688 \times LOM)} \quad (2)$$

where R is the resistivity log values; ρ is the bulk density log values; R_o is the resistivity log baseline value; ρ_o is the bulk density log baseline value; 1.4 represents the scale ratio factor; LOM is the level of organic maturity; and C is the high maturity modification factor. The high maturity of the HRB requires the use of the modified method, with the additional term, C, to account for underestimation of TOC in formations exceeding 10.5 on the level of organic maturity (LOM) scale. For this study, a LOM value of 14 to 16 was used along with a C of 4 to 5 to correct for the high maturity of the HRB and to achieve a higher level of correlation with the laboratory values. Figure 8 shows measured TOC plotted alongside calculated-log TOC for a well in the central portion of the HRB. The difference between measured and calculated TOC values is <0.5% in weight for most wells.

Regional TOC Trends

The regional maps of TOC for the Muskwa and Horn River formations (Otter Park and Evie members) show a similar trend of higher levels of organic richness within the central HRB, and further to the north and west (Figure 9a–d). This trend is most obvious within the more spatially extensive Muskwa Formation. Along the reef complex, TOC content drops to near zero and increases significantly to the east and west of the platform within the Cordova Embayment and HRB.

The Presqu'ile barrier reef persisted throughout the deposition of the Muskwa and Horn River formations, creating a restricted basin environment within the two depocentres (Dong, 2016). The shallow-water environments near or along the carbonate trends caused the shales to thin (Muskwa) and pinch out (Horn River), and would not have been a conducive environment for the accumulation and preservation of organic matter. However, reducing conditions would have formed further basinward. Coupled with low levels of detrital influx, it would have created a favourable environment for organic accumulation (Dong, 2016), which is supported by the increase in TOC. Eustatic sea-level changes also played an important role in the distribution of organic content. The distal portions of the basin were within a deep-water anoxic environment for the entirety of this depositional period. A rise in sea level, as the one interpreted to have occurred during the Muskwa Formation and Evie Member deposition (Potma et al., 2012), would have expanded anoxia and further restricted high influxes of detrital matter to the basin edge (Dong, 2016). Dong (2016) interpreted the Muskwa Formation and Evie Member as corresponding to a 3rd order transgressive systems tract, and the Otter Park Member, to a 2nd order lowstand systems tract The transgressive nature of the Muskwa and Evie units allowed for increased productivity and preservation of organic matter, and thus led to the elevated TOC content observed within the basin today.

The delineation of highly organic-rich zones required an understanding of the interplay between proximity to the surrounding platform and eustatic sea-level changes. The ongoing mapping of separate zones within these main shale units will provide further information on smaller scale basin influences and localized variability.

Mineralogy

The mineralogy of the Muskwa and Horn River formations comprises quartz, feldspar, clay and carbonate minerals, with minor amounts of pyrite. Quartz and feldspar (mainly albite) dominate the mineralogy in the Muskwa Formation, ranging in amount from 7 to 95 wt. % and averaging

71 wt. %; with quartz being overwhelmingly dominant in this fraction. The average contents of carbonate (calcite and dolomite, with minor ankerite) and clay (illite/muscovite and chlorite groups) components are of 8 and 19 wt. %, respectively. In comparison to the Muskwa Formation, the Horn River Formation contains less quartz and feldspar and more carbonate minerals. In the Evie Member, the carbonate component (calcite, dolomite, ankerite) is dominant, with a range of 18 to 97 wt. % and an average of 52 wt. %. Total quartz and feldspar averages 41 wt. % and clay content (illite/muscovite) is minor, with an average of 5.7 wt. %. The Otter Park Member is the most clay rich with an average of 18 wt. % clay, and 46 and 34 wt. % for quartz/feldspar and carbonate minerals, respectively.

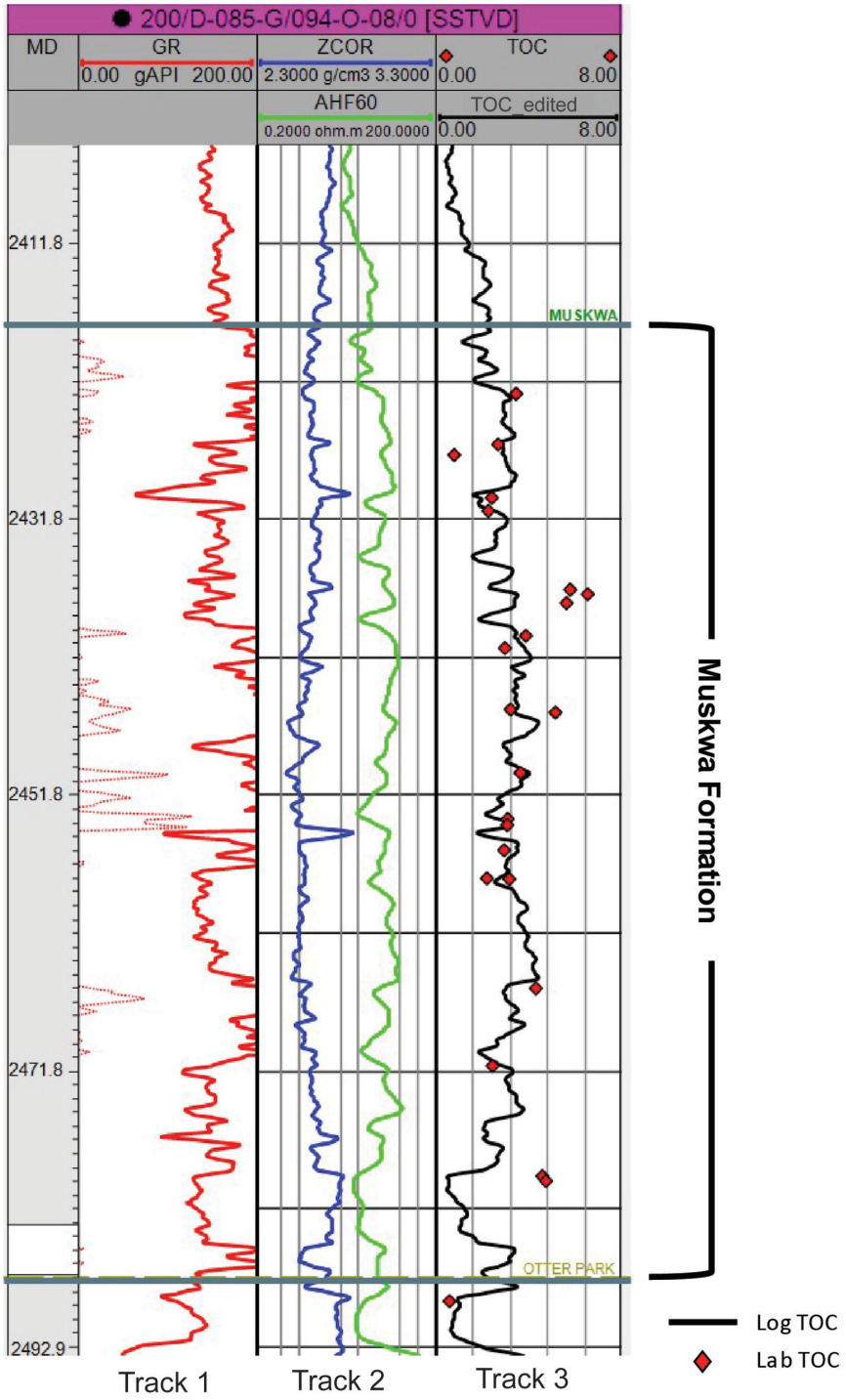

Figure 8. Example of the calibration of log TOC using the modified ΔlogR method (Passey et al., 1990; Sondergeld et al., 2010). For the location of this well refer to Figure 5.

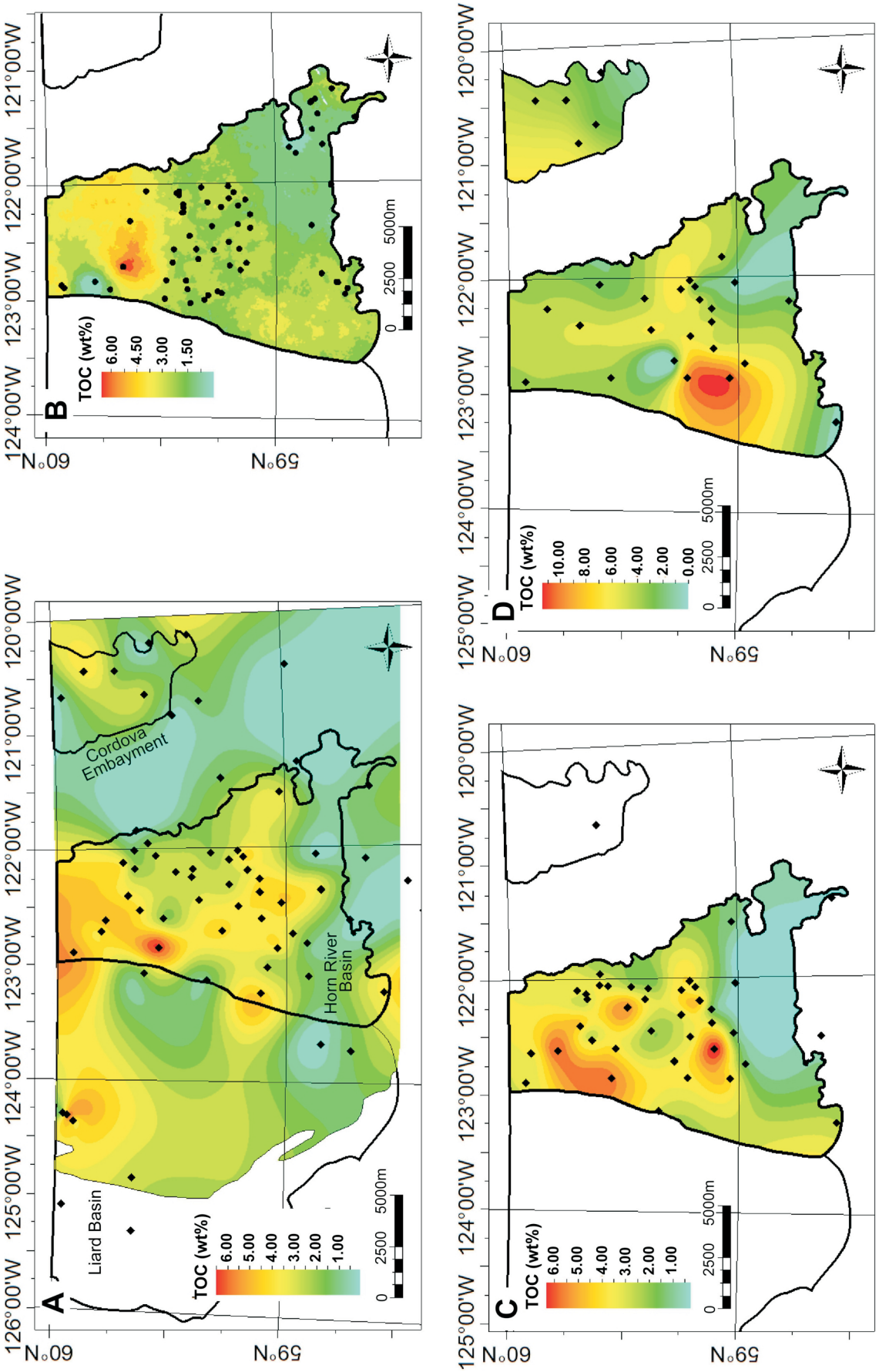

Figure 9. Regional total organic carbon (TOC) variability for the Muskwa and Horn River formations in northeastern British Columbia: **a)** Muskwa Formation (and equivalent mark in the Liard Basin); **b)** log-derived TOC for the Muskwa Formation within the Horn River Basin (note the similarity with the trends exhibited by laboratory data); **c)** Otter Park Member; **d)** Evie Member.

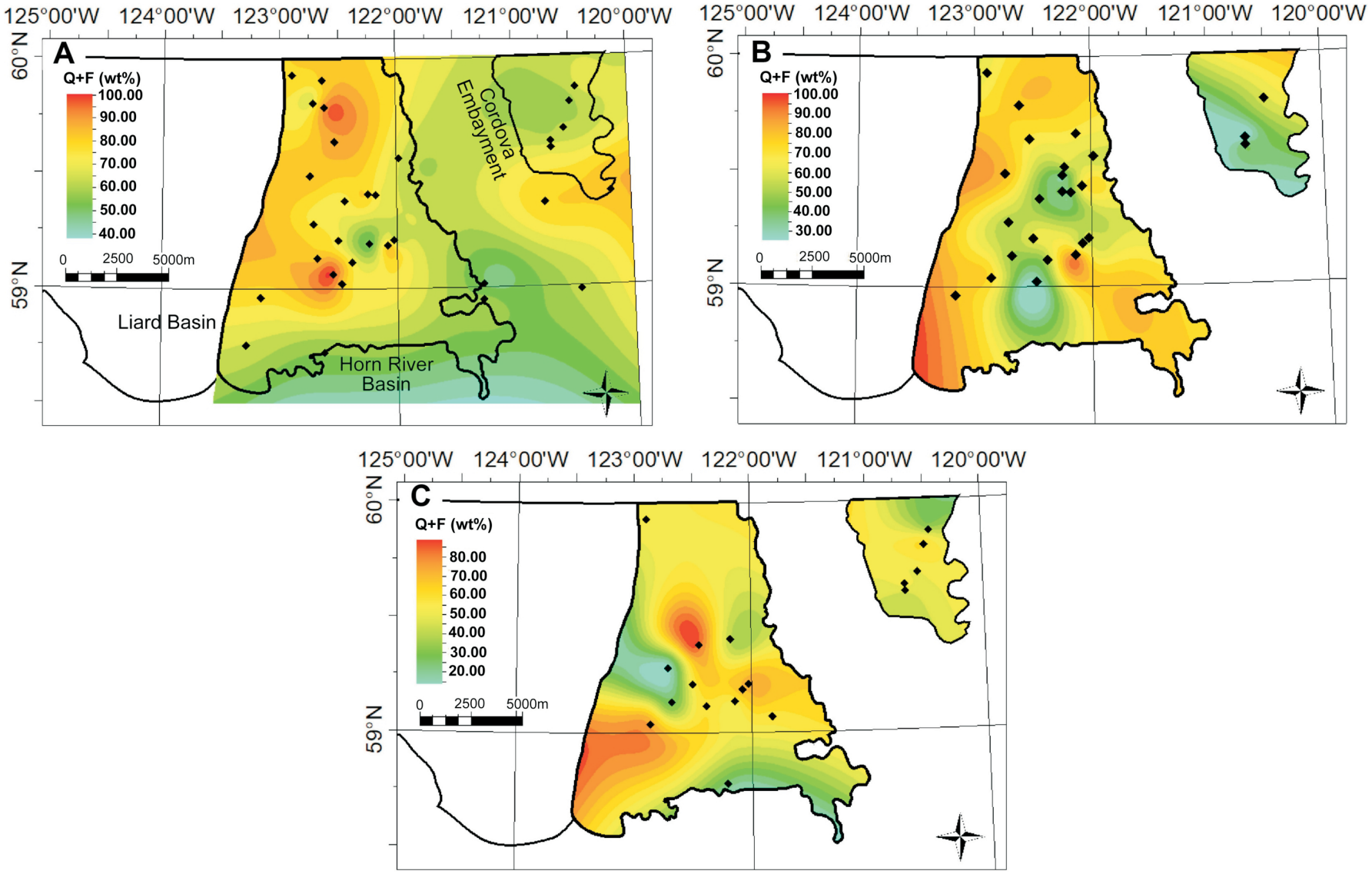

Figure 10. Regional quartz (Q) and feldspar (F) variability for the Muskwa and Horn River formations In northeastern British Columbia: **a)** Muskwa Formation; **b)** Otter Park Member; **c)** Evie Member.

Regional Mineralogical Trends

The quartz content of the Muskwa and Horn River formations increases to the north and west within the HRB (Figure 10a–c). This trend is similar to that of TOC, due to the strong correlation exhibited between organic accumulation and pelagic radiolarian accumulation within the distal portions of the HRB (Ross and Bustin, 2008). Away from the carbonate platform, carbonate and detrital clay are anticipated to decrease. The Muskwa and Evie units have a lower clay content as a result of the increased sea level, causing accommodation space to move shoreward, which led to less clastic material settling within the basin. Analyzing mineralogical trends and eventual anomalies in more detail may reveal additional insights on the paleogeometry of the basin and delineate more local trends.

Condensate Potential

The potential for the occurrence of producible liquid hydrocarbons in unconventional reservoirs is dependent on the complex interplay between the maturation, migration pathways, kerogen type and abundance, and retention of hydrocarbons during generation and production.

Production data from the Jean Marie Member and Muskwa Formation have been analyzed. The Jean Marie Member is likely sourced from the underlying Muskwa Formation (Ferri and Griffiths, 2014) and can provide additional insight into liquid-hydrocarbon potential and distribution. The bubble map of produced condensate for the Jean Marie Member and Muskwa Formation from the first month of production shows higher levels of condensate within NTS area 094I in northeastern BC (Figure 11). The higher condensate production correlates with lower levels of maturity determined by vitrinite reflectance. Minor volumes of condensate have been produced from the Jean Marie Member and Muskwa Formation within the eastern and central HRB, respectively. Gas-wetness ratios can be calculated to further constrain condensate potential; in this study, gas wetness is calculated using the formula developed by Unrau and Nagel (2012)

$$\text{Wetness ratio} = \frac{C2 + C3 + C4 + C5}{C1 + C2 + C3 + C4 + C5} \times 100 \qquad (3)$$

where <0.5 indicates light, dry gas.

In the HRB, all values for the wetness ratio fall below 0.4 (average = 0.12), indicating dry gas, and wetness shows a general decrease toward the west (Figure 12).

In general, condensate production corresponds to observed maturity trends, with the largest volumes of condensate being produced from the area to the southeast of the HRB. The single well producing directly from the Muskwa Formation within NTS area 094I is at a depth of 1850 m, with a reservoir temperature of approximately 80 °C. Similar reservoir temperatures occur throughout the southeastern corner of the study area; therefore, further potential for condensate production from the Muskwa Formation within this area is likely. Minor condensate is present in the Jean Marie Member and Muskwa Formation throughout the HRB, pointing toward hydrocarbon migration from the south.

Conclusions and Future Work

The purpose of this research is to further understand the Devonian petroleum systems within northeastern BC, including a regional understanding of reservoir properties. The central portion of the HRB is the most organic and quartz rich, and is associated with a deep anoxic environment. This environment is further influenced by eustatic sea level, causing preferable zones to be more common within transgressive systems, such as the Muskwa Formation and Evie Member. The majority of the study area is within the dry-gas window, due to significant burial depths and peak maturation during tectonic events in the Canadian Cordillera.

Based on production and gas-composition data, it is evident that condensate potential is minor, with maximum burial depths and temperatures during foreland subsidence having ultimately created a dry-gas environment in the study area. The Muskwa Formation does contain producible condensate in the southern portion of NTS area 09I, possibly extending along the Jean Marie Member subcrop in BC, due to migration. In the northwestern corner of Alberta, there is also some potential for oil production. The organic-rich Devonian–Mississippian Exshaw Formation is significantly less mature (often ~1000 m shallower) throughout the study area and may be a prospective formation for condensate production.

Future work will include analyzing the maturity, organic richness and mineralogy in more detail, along with an analysis of variability in porosity. A detailed study of reservoir properties, both stratigraphically and spatially, will help to further elucidate trends and lead to a more comprehensive understanding of the basin petroleum system(s). Basin modelling in progress will contribute to the understanding of hydrocarbon generation and migration, and will assess the impact of basin history on the type and quantity of migrated and retained hydrocarbons, and ultimately their producibility.

Acknowledgments

The authors thank Trican Geological Solutions for their logistic support and generosity in providing laboratory analyses. Financial support from Geoscience BC, Encana Corporation, Devon Energy Corporation, Husky Energy Inc., Chevron Canada Limited., Canadian Natural Resources Limited, and geoLOGIC systems ltd. are greatly appreciated. This paper benefited from a careful review by P.L. Silva.

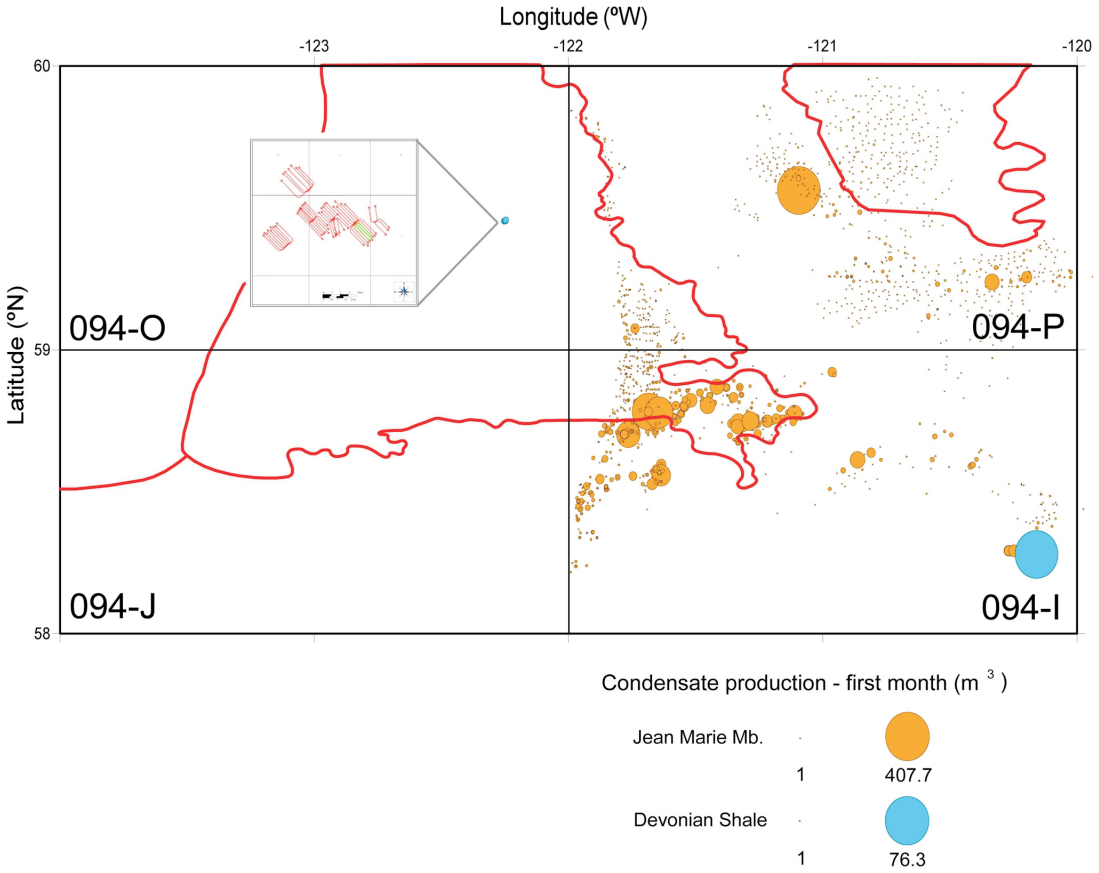

Figure 11. Bubble map showing the first month of condensate production from Devonian shales (blue) and the Jean Marie Member (orange). Note that the scales differ between the two units. The largest condensate potential is located in the southeastern corner of the map. The insert represents the horizontal wells within NTS area 094O that have reported minor condensate production. Abbreviation: Mb., Member.

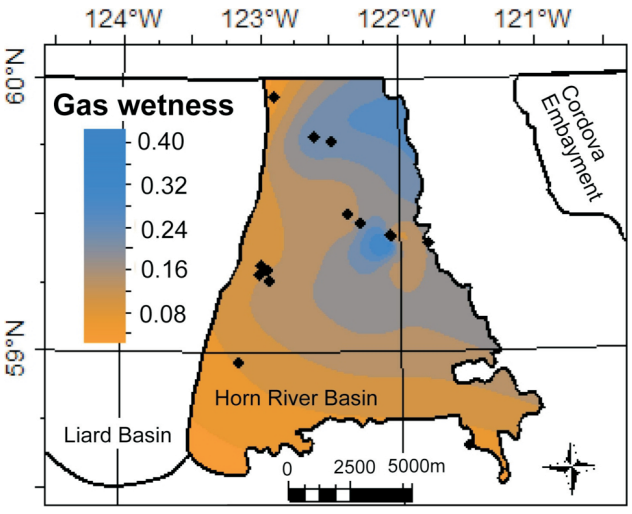

Figure 12. Gas wetness for the Muskwa Formation within the Horn River Basin in northeastern British Columbia. Wetness was calculated using the equation developed by Unrau and Nagel (2012).

References

Ariketi, R. (2011): Estimation of level of organic maturity (LOM) and total organic carbon (TOC) in absence of geochemical data by using resistivity and density logs – example from Cambay Shale, Tarapur area, Cambay Basin, India; Journal of the Indian Association of Sedimentologists, v. 30, p. 55–63.

BC Ministry of Energy, Mines and Petroleum Resources and National Energy Board (2011): Ultimate potential for unconventional natural gas in northeastern British Columbia's Horn River Basin; BC Ministry of Energy, Mines and Petroleum Resources and National Energy Board Report, Oil and Gas reports 2011-1, 50 p.

Bunnell, C. and Hillier, C. (2014): Integration of lithofacies and natural fractures in a Nexen Horn River shales gas core; Canadian Society of Petroleum Geologists, GeoConvention 2014, May 12–16, 2014, Calgary, Alberta, extended abstract, 5 p.

Dong, T. (2016): Geochemical, petrophysical and geochemical properties of stratigraphic sequences in Horn River shale, Middle and Upper Devonian, northeastern British Columbia, Canada; Ph.D. thesis, University of Alberta, Edmonton, 258 p.

Dong, T., Harris, N.B., Ayranci, K., Twemlow, C.E. and Nassichuk, B.R. (2015): Porosity characteristics of the Devonian Horn River shale, Canada: insights from lithofacies

classification and shale composition; International Journal of Coal Geology, v. 141-142, p. 74–90.

Ferri, F. and Griffiths, M. (2014): Thermal maturity and regional distribution of the Muskwa Formation, northeastern British Columbia; *in* Geoscience Reports 2014, BC Ministry of Natural Gas Development, p. 37–45.

Ferri, F., Hickin, A.S. and Huntley, D.H. (2011): Besa River Formation, western Liard Basin, British Columbia (NTS 094N): geochemistry and regional correlations; *in* Geoscience Reports 2011, BC Ministry of Energy, Mines and Petroleum Resources, BC Geological Survey, p. 1–18.

Fowler, M.G., Stasiuk, L.D., Hearn, M. and Obermajer, M. (2001): Devonian hydrocarbon source rocks and their derived oils in the Western Canada Sedimentary Basin; Bulletin of Canadian Petroleum Geology, v. 48, p. 117–148.

Herron, M.M., Grau, J.A., Herron, S.L., Kleinberg, R.L., Machlus, M., Reeder, S.L., Vissapragada, B., Burnham, A.K., Day, R.L. and Allix, P. (2011): Total organic carbon and formation evaluation with wireline logs in the Green River oil shale; Society of Petroleum Engineers, Annual Technical Conference and Exhibition, October 30, 2011, Denver, Colorado, paper for presentation, SPE 147184, 20 p.

MacLean, B.C. and Morrow, D.W. (2004): Bovie structure; its evolution and regional context; Bulletin of Canadian Petroleum Geology, v. 52, p. 302–324.

Munson, E.O. (2015): Reservoir characterization of the Duvernay Formation, Alberta: a pore to basin-scale investigation; Ph.D. thesis, University of British Columbia, Vancouver, 289 p.

Passey, Q.R., Bohacs, W.L., Esch, W.L., Klimentidis, R. and Sinha, S. (2010): From oil-prone source rock to gas-producing shale reservoir – geological and petrophysical characterization of unconventional shale-gas reservoirs; Society of Petroleum Engineers, International Oil and Gas Conference and Exhibition, June 8-11, 2010, Beijing, China, paper for presentation, SPE 13150, 29 p.

Passey, Q.R., Creaney, S., Kulla, J.B., Moretti, F.J. and Stroud, J.D. (1990): A practical model for organic richness from porosity and resistivity logs; American Association of Petroleum Geologists Bulletin, v. 74, p. 1777–1794.

Potma, K., Jonk, R., Davie, M. and Austin, N. (2012): A mudstone lithofacies classification of the Horn River Group, British Columbia: integrated stratigraphic analysis and inversion from wireline log and seismic data; Canadian Society of Petroleum Geologists, GeoConvention 2012, May 14–18, 2012, Calgary, Alberta, extended abstract, 3 p.

Ross, D.J.K. and Bustin, R.M. (2008): Characterizing the shale gas resource potential of Devonian–Mississippian strata in the Western Canada Sedimentary Basin: application of an integrated formation evaluation; American Association of Petroleum Geologists Bulletin, v. 92, p. 87–125.

Ross, D.J.K. and Bustin, R.M. (2009): Investigating the use of sedimentary geochemical proxies for paleoenvironment interpretation of thermal mature organic rich strata: examples from the Devonian–Mississippian shales, Western Canadian Sedimentary Basin; Chemical Geology, v. 260, p. 1–19.

Schmoker, J.W. (1980): Determination of organic-matter of Appalachian Devonian shales from gamma ray logs; American Association of Petroleum Geologists Bulletin, v. 64, p. 2156–2165.

Sondergeld, C.H., Newsham, K.E., Comisky, J.T., Rice, M.C. and Rai, C.S. (2010): Petrophysical consideration in evaluating and producing shale gas resources; Society of Petroleum Engineers, Unconventional Gas Conference, February 23–25 2010, Pittsburgh, Pennsylvania, paper for presentation, SPE 131768, p. 34.

Stasiuk, L.D. and Fowler, M.G. (2002): Thermal maturity evaluation (vitrinite and vitrinite reflectance equivalent) of Middle Devonian, Upper Devonian, and Mississippian strata in the Western Canada Sedimentary Basin; Geological Survey of Canada, Open File 4341, 1 CD-ROM.

Switzer, S.B., Holland, W.G., Christie, D.S., Graf, G.C., Hedinger, A.S., McAuley, R.J., Wierzbicki, R.A. and Packard, J.J. (1994): Devonian Woodbend–Winterburn strata of the Western Canada Sedimentary Basin; *in* Geological Atlas of the Western Canadian Sedimentary Basin, G.D. Mossop and I. Shetsen (comp.), Canadian Society of Petroleum Geologists, Calgary, Alberta and Alberta Research Council, Edmonton, Alberta, p. 165–202.

Unrau, S. and Nagel, B. (2012): Using compositional gas data for horizontal drilling and practical detection of natural gas liquids (NGL); Canadian Society of Petroleum Geologists, GeoConvention 2012, May 14–18,2012, Calgary, Alberta, extended abstract, 4 p.

Wilson, T.K. and Bustin, R.M. (2017): Unconventional petroleum systems analysis of Upper Devonian organic-rich shale units in the Horn River and Liard basins, northeastern British Columbia, and adjacent western Alberta: preliminary report; *in* Geoscience BC Summary of Activities 2016, Geoscience BC, Report 2017-1, p. 29–36.

Wright, G. N., McMechan, M.E. and Potter, D.E.G. (1994): Structure and architecture of the Western Canadian Sedimentary Basin; *in* Geological Atlas of the Western Canadian Sedimentary Basin, G.D. Mossop and I. Shetsen (comp.), Canadian Society of Petroleum Geologists, Calgary, Alberta and Alberta Research Council, Edmonton, Alberta, p. 25–39.

Establishment of Field Stations for the Multidisciplinary Study of Fugitive Gas, Northeastern British Columbia

A.G. Cahill, The University of British Columbia, Vancouver, BC, acahill@eoas.ubc.ca

J. Chao, The University of British Columbia, Vancouver, BC

O. Ford, The University of British Columbia, Vancouver, BC

B. Ladd, The University of British Columbia, Vancouver, BC

E. Prystupa, The University of British Columbia, Vancouver, BC

K.U. Mayer, The University of British Columbia, Vancouver, BC

D. Tannant, The University of British Columbia, Okanagan, BC

A. Black, The University of British Columbia, Vancouver, BC

S. Crowe, The University of British Columbia, Vancouver, BC

S. Hallam, The University of British Columbia, Vancouver, BC

B. Mayer, University of Calgary, Calgary, AB

C. van Geloven, British Columbia Ministry of Forests, Lands, Natural Resource Operations and Rural Development, Prince George, BC

L.A. Welch, British Columbia Oil and Gas Commission, Kelowna, BC

V. Levson, Quaternary Geosciences Inc., Victoria, BC

R.D. Beckie, The University of British Columbia, Vancouver, BC

Cahill, A.G., Chao, J., Ford, O., Ladd, B., Prystupa, E., Mayer, K.U., Tannant, D., Black, A., Crowe, S., Hallam, S., Mayer, B., van Geloven, C., Welch, L.A., Levson, V. and Beckie, R.D. (2018): Establishment of field stations for the multidisciplinary study of fugitive gas, northeastern British Columbia; *in* Geoscience BC Summary of Activities 2017: Energy, Geoscience BC, Report 2018-4, p. 65–76.

Introduction

Fugitive gas, comprising primarily methane, can be unintentionally released from upstream oil and gas development either at surface from leaky infrastructure or in the subsurface through failure of well bore integrity. For the latter, compromised cement seals around well casings can permit flow of natural gas into the subsurface, tending toward ground surface and potentially into the atmosphere. Concerns associated with fugitive gas release at surface and in the subsurface include contributions to greenhouse gas emissions, subsurface migration of gas leading to accumulation in nearby infrastructure and impacts to groundwater quality. Current knowledge of fugitive gas is incomplete, including how to best detect and monitor it over time and, particularly, its migration and fate in the subsurface at the individual event scale. Consequently, an experimental field observatory has been established to evaluate surface and subsurface fugitive gas leakage in an area that hosts historic and ongoing hydrocarbon resource development—the Montney play of the Western Canada Sedimentary Basin, northeastern British Columbia (BC). At the field laboratory, natural gas has and will be intentionally released at various low rates (<10 m^3/day [d]), durations and configurations. Resulting migration patterns and impacts will be evaluated through examination of the geology, hydrogeology, hydrogeochemistry, isotope geochemistry, hydrogeophysics, vadose zone and soil gas processes, microbiology and atmospheric conditions. The use of unmanned aerial vehicles and remote sensors for monitoring and detecting methane will also be assessed as environmental monitoring tools. Herein the progress to date is outlined, including significant successful efforts undertaken to leverage the base funding provided by Geoscience BC to enhance the multidisciplinary nature of the research program. Activities undertaken in order to select and secure suitable locations for the field observatory and then develop detailed site conceptual models are also described. Ongoing research, which will take place at the newly established field observatory, will a) create rigorous, evidence-based

This publication is also available, free of charge, as colour digital files in Adobe Acrobat® PDF format from the Geoscience BC website: http://www.geosciencebc.com/s/SummaryofActivities.asp.

knowledge to inform surface gas flux and groundwater monitoring approaches with respect to fugitive gas, b) aid in quantifying and reducing greenhouse gas emissions, and c) help to guide changes to associated regulatory and technical guidance policies.

Background

Over the last decade the combination of well stimulation by hydraulic fracturing and horizontal drilling has led to rapid and unprecedented tight-rock–derived natural gas extraction across the United States and Canada (Kerr, 2010). Consequently, tens of thousands of energy wells have been drilled across regions underlain by gas-bearing shales (e.g., 7226 wells were drilled in Pennsylvania between 2005 and 2013; Brantley et al., 2014). Following such intense unconventional resource development, cases of environmental impacts were alleged and investigated (Osborn et al., 2011; Fontenot et al., 2013; Jackson et al., 2013; Hammond, 2015) resulting in significant controversy and various regional bans and moratoria. One of the main issues of concern is accidental leakage of natural gas, often termed fugitive methane (CH_4; Vengosh et al., 2013, 2014; Vidic et al., 2013). Although hydraulic fracturing brought attention to the issue, fugitive CH_4 is a historic engineering challenge associated with all petroleum resource development and associated activities (e.g., underground gas storage; Dusseault et al., 2000; Robertson et al., 2012). In general, two key configurations of fugitive CH_4 leakage can occur in the context of upstream petroleum development: 1) surface or 2) subsurface leakage, for which there are multiple conduits (Figure 1). Surface fugitive CH_4 can originate at the well head either by leakage from associated distribution infrastructure or from within or along the well casing (e.g., surface casing vent flow) leading to direct emission to atmosphere (Kang et al., 2014). Subsurface fugitive CH_4 has several potential origins, including subsurface well casing failure or mobilization of intermediate in situ gas pockets during or after drilling. Regardless of source, subsurface leakage results in entry of gas into the adjacent geological media, which is followed by three generalized outcomes: 1) subsurface migration through the geological profile and efflux to atmosphere; 2) free-phase gas migration and entrapment in the subsurface; and 3) dissolution into groundwater, aqueous-phase migration and attenuation. Likely, a

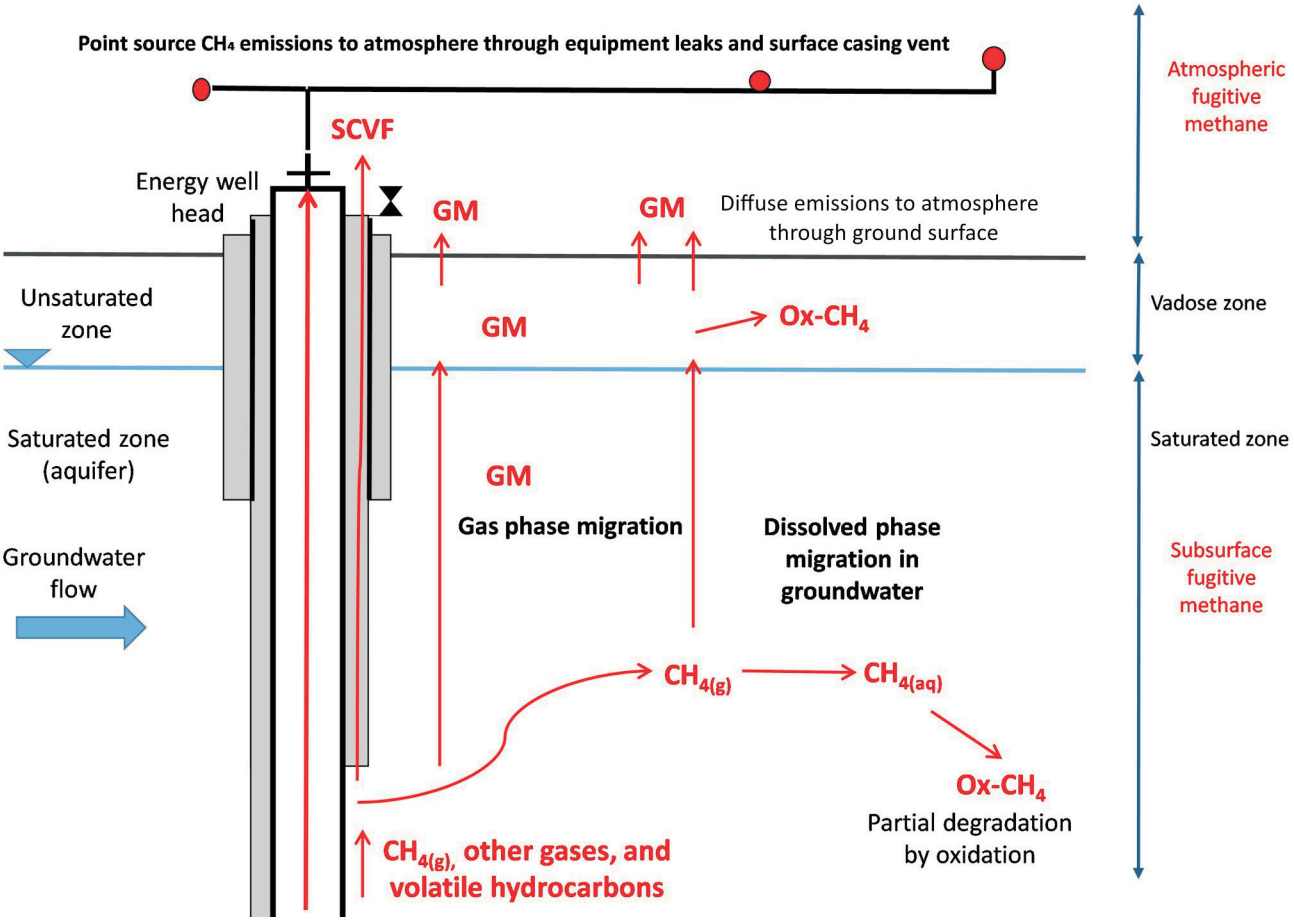

Figure 1. Conceptual model (not to scale) showing fugitive gas release from a gas well. Abbreviations: $CH_{4(aq)}$, dissolved/aqueous methane; $CH_{4(g)}$, gas phase methane; GM, gas migration; Ox-CH_4, oxidation of methane; SCVF, surface casing vent flow. Modified from Cahill et al. (2017).

combination of these processes occur dependent on site-specific conditions, however, detailed knowledge on how to predict or estimate this is lacking.

Fugitive CH_4 causes concern as it poses three potential risks to human health and/or the environment. Firstly, fugitive CH_4 poses an explosion hazard (lower explosive limit of 5% in air; LeBreton, 2009) if released into a confined space. Secondly, CH_4 is a potent greenhouse gas (a factor of 25 times greater in a 100-year period than CO_2; United States Environmental Protection Agency, 2010). Considering emissions of CH_4 from energy resource development (particularly shale gas operations) have been identified as potentially significant to overall greenhouse gas emissions (Caulton et al., 2014), fugitive CH_4 therefore has potential to contribute significantly to climate change (Shindell et al., 2009; Stocker et al., 2013). Thirdly, fugitive CH_4 can impact groundwater resources by migrating in the aqueous phase and forming an explosion risk following extraction, and also following microbial attenuation (based on availability of electron acceptors, according to the redox sequence; Christensen et al., 2000; Le Mer and Roger, 2001) where it may generate undesirable byproducts (e.g., H_2S, Fe^{2+}, Mn^{2+}) or potentially induce the release of trace metals (Bennet and Dudas, 2003; Van Stempvoort et al., 2005, 2007; Amos et al., 2012; Ng et al., 2015). Although much research has recently been undertaken with respect to fugitive CH_4, it has for the most part taken the form of retrospective environmental forensic studies to assess if detectable impacts to groundwater have occurred. Unfortunately, little research has comprehensively assessed migration, impacts and fate of fugitive CH_4 in a holistic manner or at the single event scale. Exceptionally, a recent multidisciplinary study, upon which the current study builds, monitored groundwater, soil gas and surface efflux at high spatiotemporal resolution during release of a small volume of natural gas into a shallow (i.e., ~9 m depth) unconfined aquifer system. Results from this study showed that although a significant proportion of injected gas reached the surface and emitted to atmosphere with some oxidation observed in the unsaturated zone, a large portion remained in the saturated zone where it created a dispersed and laterally extensive volume of impacted groundwater (Cahill et al., 2017). Although this study provided important and detailed insights regarding fugitive CH_4, it forms only a single site specific study and its overall applicability and relevance to regions of resource development (e.g., the Western Canada Sedimentary Basin) is limited. Consequently, many knowledge gaps remain and more studies such as this are needed in a range of geological settings where petroleum resource development takes place in order to improve an understanding of the fugitive CH_4.

In March 2017, Geoscience BC entered into a contribution agreement with The University of British Columbia's Energy and Environment Research Initiative (UBC EERI; directed by R. Beckie and A. Cahill), located at the Department of Earth, Ocean and Atmospheric Sciences, in order to address the paucity of field data concerning fugitive gas. Based on a proposal submitted in 2016, Geoscience BC agreed to provide $0.5 million funding in order for UBC EERI to undertake a groundwater-focused, controlled natural gas release investigation at a field station to be located in the Peace region of northeastern BC. This paper has a description of the progress on this project beginning with the significant successful efforts enacted by UBC EERI to leverage the base funding provided by Geoscience BC in order to increase the multidisciplinary nature of the research program (i.e., above and beyond groundwater alone). Progress on site selection and field station characterization and setup undertaken during 2017 is also presented.

Summary of Activities and Progress

Leveraging and Increase of Project Scope

Although UBC EERI recognized that the $0.5 million awarded by Geoscience BC to conduct a groundwater-focused study (hereafter referred to as 'the base funding') was a significant award, it was quickly identified that this would be insufficient for a fully comprehensive multidisciplinary investigation, which has been seen to be required to truly advance knowledge on fugitive gas (Cahill et al., 2017). Consequently, UBC EERI rapidly formulated and enacted a successful strategic plan in order to enhance the multidisciplinary aspects of the research program through leveraging the base funding wherever possible. Two leveraging opportunities were identified and successfully advanced after significant development and efforts. The major leveraging opportunity took the form of the Clean Energy Innovation component of the Energy Innovation Program administered by Natural Resources Canada (NRCan). A proposal was formulated and submitted seeking to leverage the base funding by approximately 3:1 and attain an additional $1.617 million to include enhanced geological investigations, soil gas and surface efflux, eddy covariance, microbial and geophysical components to the study program. This proposal was ultimately successful and a full contributions agreement signed between UBC EERI and NRCan on August 24, 2017. Additionally, a proposal and work plan to include drone measurements and remote sensors during the project was formulated and submitted to the BC Oil and Gas Research and Innovation Society (BC OGRIS) with an additional value to project of $93 000 in April 2017. This proposal was subsequently confirmed as successful May 12, 2017. These leveraging opportunities led by UBC EERI and its collaborators have brought the overall project cash value to >$2.2 million; meaning the base funding has been leveraged by 3.4 to 1 (Table 1).

Identification and Characterization of Field Sites

As part of a Geoscience BC groundwater mapping project (which took place in the primary area of interest for the current study), a series of aerial geophysical surveys were conducted in 2015 (i.e., airborne transient electromagnetic measurements by SkyTEM; Brown et al., 2016). These surveys were used to aid in the identification of two areas close to Hudson's Hope as potentially suitable to host the fugitive gas investigations. At first it was envisioned that one site could be representative of the Peace region and would include both a saturated aquifer and a significant unsaturated zone. However, this was ultimately not possible and instead two separate sites were identified near Hudson's Hope: one a saturated aquifer or the saturated zone (SZ; with no unsaturated zone) and the other a dry soil site or the unsaturated zone (USZ) field research sites (FRS; Figure 2a, b).

Having both dry and saturated soil systems into which natural gas could be released was deemed a critical design requirement of the research program. The USZ FRS is located on the west side of Lynx Creek (a tributary of the Peace River), which has incised approximately 50 m into the local relief at an elevation of ~800 m asl. The airborne survey identified the USZ area as having a low resistance surface layer (inferred to be glacial till) underlain by a highly resistive material (inferred to be unsaturated glacial outwash sand, silt and gravel; Figure 2b). Sonic core drilling confirmed this to be the case with ~10 m of glacial diamict (gravel suspended in a matrix of clay and/or silt) overlying a fine to very fine dry sand. Based on the airborne SkyTEM data, the SZ FRS appeared to be located in a buried paleovalley with a layer of low resistance overlying a channel of moderate resistance suggesting a confined aquifer, typical in the area. This hypothesis was confirmed by drillcores, which showed glacial diamictic clay overlying a saturated glacial outwash deposit; albeit this time the glacial deposits appeared more heterogeneous being composed of interbedded layers of sand, silt and gravel. The two sites are typical of the Quaternary geology found within the Peace region's Montney play and ideal for simulating how fugitive gas may manifest.

Table 1. Funding structure for project including increased multidisciplinary components achieved through leveraging of Geoscience BC funding.

Project funding component	Value	Project component
Geoscience BC (i.e., base funding)	$0.5 million	Identify field site, obtain release, setup infrastructure
		Groundwater
Natural Resources Canada	$1.617 million	Enhanced geological data
		Soil gas and surface efflux
		Microbiology
		Surface geophysics
		Enhanced isotope geochemistry
		Eddy covariance
BC Oil and Gas Research and Innovation Society	$93 000	Drone (aerial) measurements

Initial Results

Unsaturated Zone Field Research Site

Following identification of the USZ FRS as potentially suitable for controlled release investigations, a drilling campaign was undertaken in order to better characterize site geology (e.g., assess heterogeneity) and to install multilevel soil gas monitoring wells and a gas injection well. An auger capable geoprobe rig was used to drill nine boreholes to 12 m depth (Figure 3a) with full geological logging and a range of depth discrete sampling undertaken for a variety of parameters (e.g., grain size distribution; Figure 3b). Boreholes were subsequently installed with depth discrete soil gas sampling systems made 'in house' using polyethylene tubing with geotextile screens, backfilled with sand pack and hydrated bentonite chips. A short duration gas release experiment was then planned to be rapidly implemented in September 2017 in order to precede the onset of winter, during which a slowdown in field activities is inevitable. Consequently, many activities were rapidly initiated including setting up a full surface efflux monitoring system, including seven continuous measuring chambers and ~100 additional spatially discrete survey collars (Figure 3a), installation of a $20 000 solar power system to provide continuous power to the site, and collection of several background soil gas samples (Figure 4). Subsequently 29 m^3 of compressed natural gas was injected at a constant rate at the site at 12 m depth over five days with monitoring of gas migration and fate (i.e., where it ultimately goes: being either released to atmosphere; oxidized by bacteria; or remaining trapped in the subsurface) ongoing. Results from this experiment are still being collected and are yet to be processed thus are not reported here. They will, however, be reported in next year's reporting phase.

Saturated Zone Field Research Site

Following identification of the SZ FRS as potentially suitable for controlled release investigations, a further drilling campaign was undertaken in order to better characterize site geology (e.g., assess heterogeneity) and to install groundwater monitoring wells and a gas injection well. These initial monitoring wells would allow the UBC EERI team to collect initial water samples for assessing baseline conditions, including groundwater quality, flow direction and magnitude, and to advance the design of the

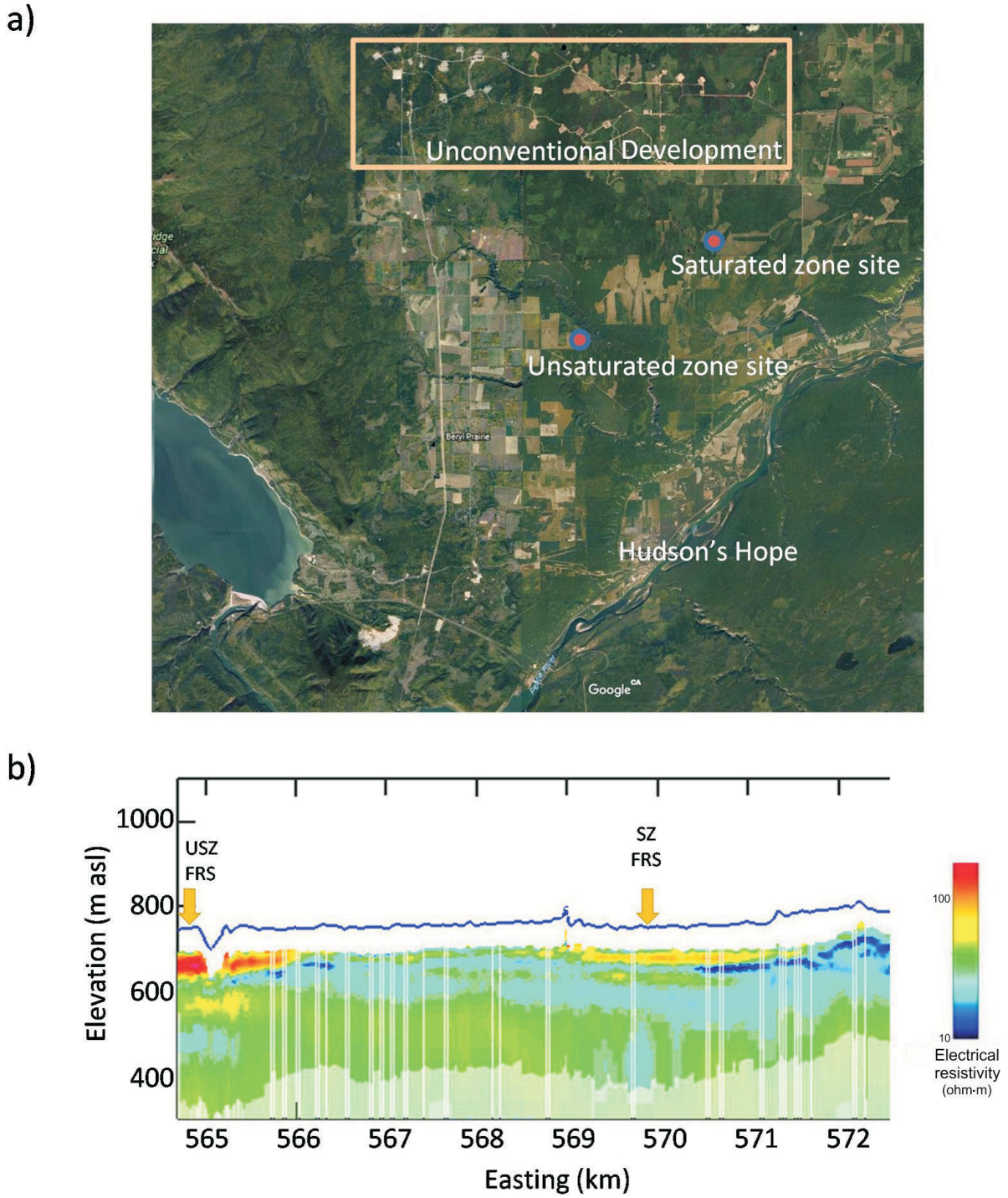

Figure 2. a) Image of study area showing location of unsaturated and saturated zone field research sites. Significant unconventional resource development is underway approximately 2 km north of the study area demonstrating relevance of site setting. Red dashed line between sites indicates approximate location of the aerial geophysics SkyTEM survey line, initially used to identify the sites as potentially suitable for investigation. Imagery ©2017 Landsat/Copernicus, map data ©2017 Google, Canada. **b)** Airborne geophysics (electromagnetic) survey line, flown as part of a separate Geoscience BC Peace project (Aarhus Geophysics ApS, 2016), showing inferred resistivity of the subsurface geology, with warm colours indicating higher resistivity and cool colours lower resistivity. Blue line indicates flight line of sensor. Abbreviations: FRS, field research site; SZ, saturated zone; USZ, unsaturated zone.

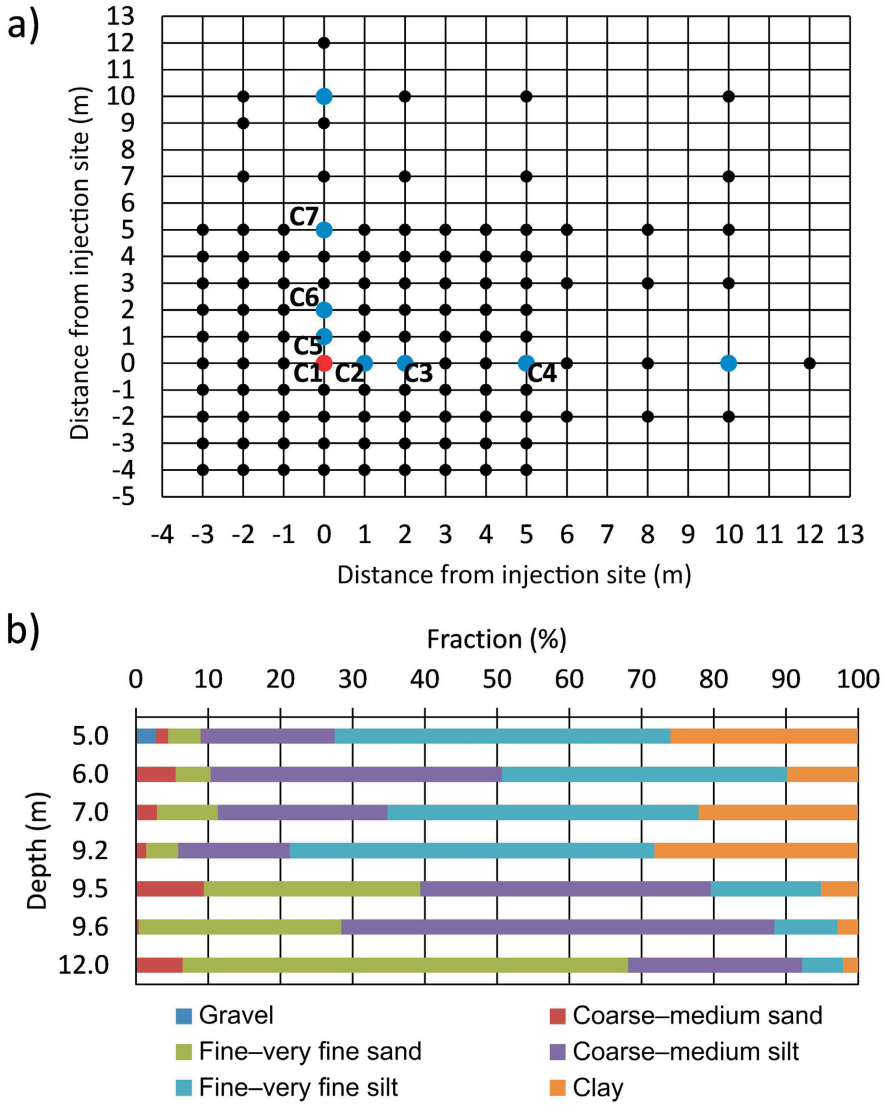

Figure 3. a) Monitoring network installed at the unsaturated zone field research site. The red circle indicates the injection location and the blue circles indicate the locations of the multilevel soil gas monitoring wells. Continuous flux chambers, indicated by C1 through C7, are co-located with selected multilevel wells. Spatial flux measurements were collected at locations indicated by the black circles. **b)** Grain size distribution with depth for sediments in the multilevel well next to C6, 2 m from the injection location.

experiment. Drilling of five monitoring wells and an inclined gas injection well to approximately 25 m depth (Figure 5a, b) was conducted using a Sonic coring rig. These investigations confirmed the hypothesis that the site consisted of a confined aquifer formed by ~12 m of diamict (confining layer) overlying a complex interbedded sequence of water-bearing very fine to fine sand, silt and pebbly silt. Moreover, this increasing understanding of the site begins to show a highly heterogeneous environment that exhibits little lateral continuity. Once monitoring wells were installed, initial water samples were taken and analyzed for physical chemistry, major and minor cations, as well as dissolved gases. Results from these initial groundwater sample tests are provided in Tables 2 and 3. Water levels were also measured and pressure transducers installed to track changes in water levels and calculate flow direction and magnitudes (Figure 5b, c). Additionally, extensive surface-based electrical resistivity surveys were also conducted through the project's key collaborator at the University of Calgary, R. Lauer, results from which are currently being interpreted and will increase understanding on heterogeneity (results not shown here but available on request). During this period other site infrastructure, such as an experimental control building and electric fencing system to keep animals out of the primary investigation area, were installed. An aerial drone photograph of the SZ FRS is

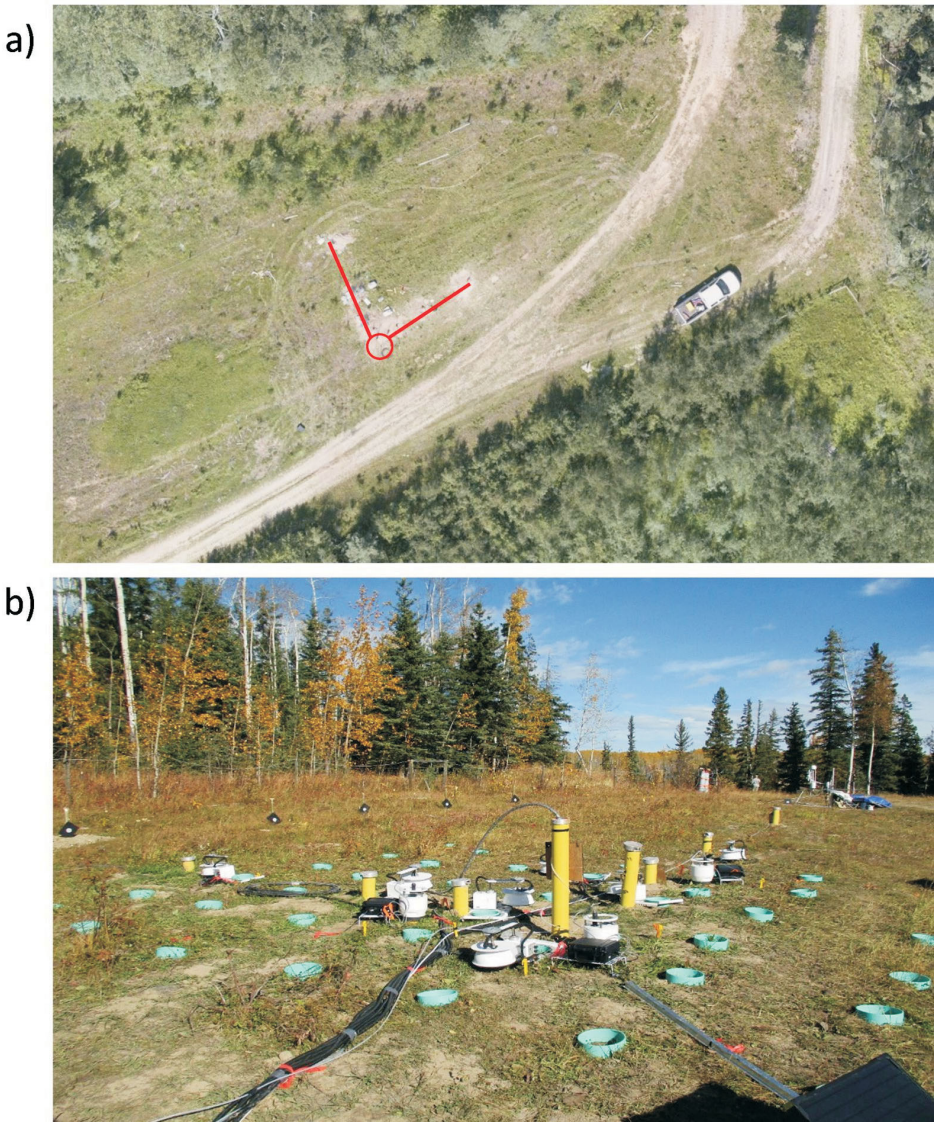

Figure 4. a) Aerial drone photograph of unsaturated zone field research site, during infrastructure installation/site investigations, showing injection zone (gas injected at 12 m depth) as red circle and red lines delineating transect profiles of multilevel soil gas monitoring wells. **b)** Site fully instrumented prior to injection of 29 m^3 of natural gas at a constant rate over five days, initiated on September 25, 2017. Monitoring is still ongoing as of November 2017 with initial results being processed.

shown in Figure 6. Less than 400 m from the site is an orphaned gas well (Figure 6; coalbed methane well drilled in 1994), which is defined as infrastructure that does not have any legally responsible or financially able party to deal with its abandonment and reclamation. Proximity to an orphaned well demonstrates the relevance of the setting in which these controlled release investigations are being undertaken.

Ongoing Work

Two separate but closely located field sites were chosen as the locations of controlled gas releases. Consequently, UBC EERI is now poised to advance knowledge on fugitive gas, as set out in the multiple successful proposals completed. A short-term gas injection experiment has been undertaken at the USZ FRS and is currently in the final stages of monitoring. This experiment alone has already generated a huge dataset and will form an important standalone study with many insights set to be gained with respect to fugitive gas. The results from the USZ FRS study will also be used to help steer and maximize results obtained from the SZ FRS study planned to take place in 2018. This will increase the likelihood that the SZ FRS study will be successful and infers many new insights will be made as proposed. A project workshop was held on November 29, 2017, at which recently gained results and plans for ongoing work were discussed.

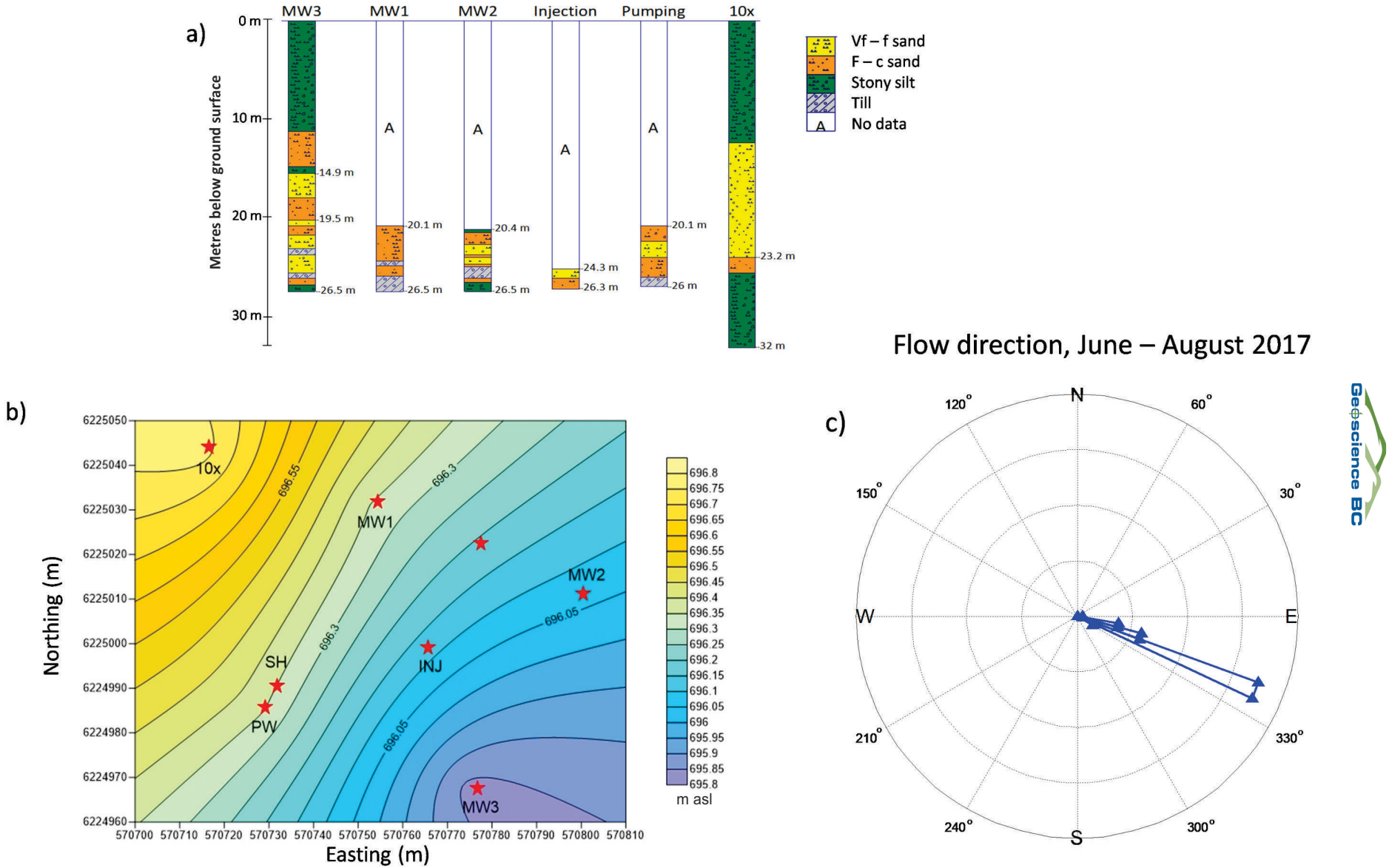

Figure 5. Saturated zone field research site: **a)** geological logs from boreholes cored during initial site investigation show a heterogeneous, confined sandy aquifer; **b)** locations of boreholes drilled in area of interest and groundwater elevation contours across the site for August 11, 2017 and **c)** groundwater flow direction rose diagram for June to August, 2017, showing flow direction is generally consistently southeast. Abbreviations: c, coarse; f, fine; vf, very fine.

Table 2. Geochemical compositions of baseline shallow groundwater samples from saturated zone field research site. Abbreviation: EC, electrical conductivity; TDS, total dissolved solids.

Property/composition	MW1	MW2	MW3	Inj	PW	10x
EC (µS/cm)	1120	955	1100	1125	1100	1131
pH	7.35	7.58	7.43	7.48	7.052	7.4
Cl (mg/L)	2.75	6.35	2.75	4.2	2.1	2.25
SO_4 (mg/L)	220.8	201.9	241.5	213.4	156.8	8.3
NO_3 (mg/L)	0.08	0.11	0	0	0.07	0
Alkalinity (mg/L)	520	500	520	520	580	180
Li (mg/L)	0.0248	0.0375	0.0267	0.0246	0.0247	0.0029
B (mg/L)	0.1080	0.1470	0.1020	0.0976	0.1170	0.0213
Na (mg/L)	73.77	100.15	62.21	53.26	61.11	7.89
Mg (mg/L)	80.24	47.28	66.53	76.11	80.06	11.44
Al (mg/L)	0.2790	0.0408	0.1150	n/a	0.4660	0.0579
Si (mg/L)	7.44	7.79	7.7	7.3	8.75	4.41
K (mg/L)	4.8	6.23	6.07	6.53	4.64	7.32
Ca (mg/L)	94.88	87.76	103.07	101.29	85.85	30.7
Mn (mg/L)	0.0444	0.3500	0.3050	0.7700	0.0666	0.0549
Fe (mg/L)	0.9930	0.3940	0.4720	0.0148	0.9150	0.5140
As (mg/L)	0.0046	0.0030	0.0021	0.0012	0.0039	0.0011
Sr (mg/L)	0.6590	0.7940	0.6100	0.6030	0.6350	0.1140
Calculated TDS (mg/L)	728	620.75	715	731.25	715	735.15

Table 3. Dissolved gas compositions of baseline shallow groundwater samples from saturated zone field research site.

Well no.	CH_4 (mg/L)	Total C2 (mg/L)	Total C3 (mg/L)	Total CO_2 (mg/L)	Total N_2 (mg/L)	Total O_2 (mg/L)
MW1	0.00814	0.00086	0.00000	29.87	36.59	0.62
MW2	0.03080	0.00371	0.00081	13.9	57.26	3.18
MW3	0.01330	0.00200	0.00041	21.09	57.2	7.32
Inj	0.00634	0.00143	0.00041	20.05	42.34	7.63
PW	0.00791	0.00160	0.00350	36.16	62.03	4.8
10x	0.00735	0.00057	0.00000	28.18	48.98	2.89

Summary of Progress

The following forms a summary of the progress made to date with respect to UBC EERI's controlled methane release investigation project:

- UBC EERI have undertaken significant leveraging activities, which have resulted in 3.4:1 additional funding above that initially provided by Geoscience BC. The total project cash budget is now in excess of $2.2 million.
- Through this additional funding, the project scope has been vastly increased and will now include a highly multidisciplinary team encompassing examination of fugitive gas from perspectives of geology, hydrogeology, soil gas and surface efflux processes, microbiology, isotope geochemistry, geophysics, eddy covariance and airborne sensing.
- Two sites (saturated and unsaturated) have been identified in the Peace region near Hudson's Hope, BC, at which natural gas has been and will be released in the subsurface and at surface in a controlled manner. These sites have been subjected to comprehensive intrusive investigations and detailed baseline site conceptual models are being developed.
- A short-term natural gas injection experiment has been initiated at the USZ FRS whereby 29 m^3 of compressed natural gas has been injected at 12 m depth and gas migration monitored in a multidisciplinary fashion. Monitoring of injected gas is ongoing.
- Setup and infrastructure installation at the SZ FRS is underway and plans are on track for a long-term injection experiment to be undertaken in 2018.

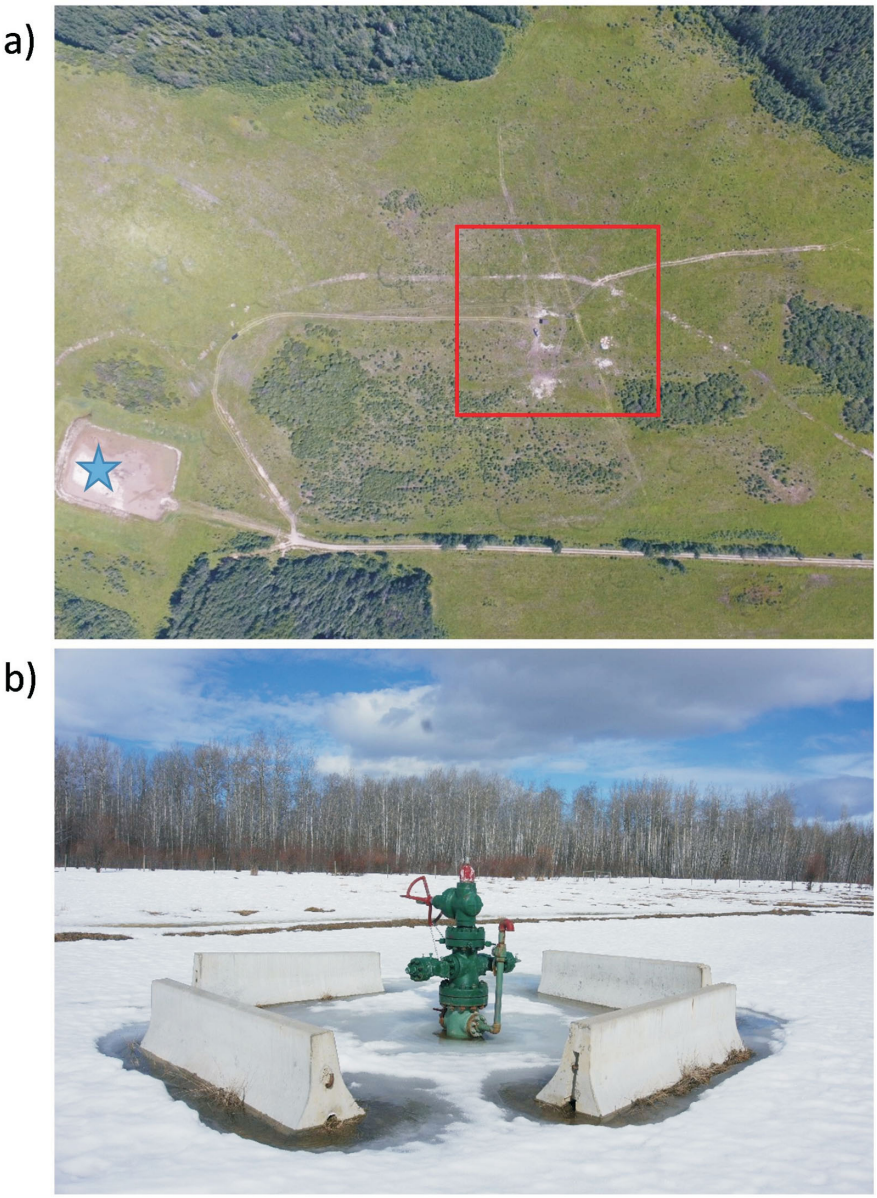

Figure 6. a) Drone aerial image of saturated zone field research site and surrounding area. The area of investigation, including the injection site, is indicated by the red square. The blue star indicates the site of an orphaned gas well (coalbed methane well drilled in 1994 but never produced). **b)** The orphaned gas well during winter drilling. Proximity to an orphaned well demonstrates relevance of setting in which the controlled releases investigations are being undertaken.

Acknowledgments

This paper was peer reviewed by L. Smith.

References

Aarhus Geophysics ApS (2016): Processing and inversion of SkyTEM data, Peace River main area–phase 1; Geoscience BC, Report 2016-09, 31 p. plus PDF, GDB, MAP and PNG files, URL <http://www.geosciencebc.com/s/Report2016-09.asp> [December 2017].

Amos, R.T., Bekins, B.A., Cozzarelli, I.M., Voytek, M.A., Kirshstein, J.D., Jones, E.J. and Blowes, D.W. (2012): Evidence for iron-mediated anaerobic methane oxidation in a crude oil-contaminated aquifer; Geobiology, v. 10, issue 6, p. 506–517, doi:10.1111/j.1472-4669.2012.00341.x

Bennett, B. and Dudas, M.J. (2003): Release of arsenic and molybdenum by reductive dissolution of iron oxides in a soil with enriched levels of native arsenic; Journal of Environmental Engineering and Science, v. 2, issue 4, p. 265–272, doi:10.1139/s03-028

Brantley, S.L., Yoxtheimer, D., Arjmand, S., Grieve, P., Vidic, R., Pollak, J., Llewellyn, G.T., Abad, J. and Simon, C. (2014): Water resource impacts during unconventional shale gas development: the Pennsylvania experience; International Journal of Coal Geology, v. 126, p. 140–156, doi:10.1016/j.coal.2013.12.017

Brown, B., Gisselø, P. and Best, M. (2016): SkyTEM airborne electromagnetic systems for hydrogeological mapping in northeastern British Columbia; *in* Geoscience BC Summary of Activities 2015, Geoscience BC, Report 2016-1, p. 43–48.

Cahill, A.G., Steelman, C.M., Forde, O., Kuloyo, O., Ruff, S.E., Mayer, B., Mayer, K.U., Strous, M., Ryan, M.C., Cherry, J.A. and Parker, B.L. (2017): Mobility and persistence of methane in groundwater in a controlled-release field experiment; Nature Geoscience, v. 10, p. 289–294, doi:10.1038/ngeo2919

Caulton, D.R., Shepson, P.B., Santoro, R.L., Sparks, J.P., Howarth, R.W., Ingraffea, A.R., Cambaliza, M.O.L., Sweeney, C., Karion, A., Davis, K.J., Stirm, B.H., Montzka, S.A. and Miller, B.R. (2014): Toward a better understanding and quantification of methane emissions from shale gas development; Proceedings of the National Academy of Sciences of the United States of America, v. 111, no. 17, p. 6237–6242, doi:10.1073/pnas.1316546111

Christensen, T.H., Bjerg, P.L., Banwart, S.A., Jakobsen, R., Heron, G. and Albrechtsen, H. (2000): Characterization of redox conditions in groundwater contaminant plumes; Journal of Contaminant Hydrology, v. 45, issue 3–4, p. 165–241, doi:10.1016/S0169-7722(00)00109-1

Dusseault, M.B., Gray, M.N. and Nawrocki, P.A. (2000): Why oilwells leak: cement behavior and long-term consequences; Society of Petroleum Engineers, International Oil and Gas Conference and Exhibition in China, Beijing, China, November 7–10, 2000, Paper SPE-64733-MS, 8 p.

Fontenot, B.E., Hunt, L.R., Hildenbrand, Z.L., Carlton, D.D., Jr., Oka, H., Walton, J.L., Hopkins, D., Osorio, A., Bjorndal, B., Hu, Q.H. and Schug, K.A. (2013): An evaluation of water quality in private drinking water wells near natural gas extraction sites in the Barnett Shale Formation; Environmental Science & Technology, v. 47, issue 17, p. 10032–10040, doi:10.1021/es4011724

Hammond, P.A. (2015): The relationship between methane migration and shale-gas well operations near Dimock, Pennsylvania, USA; Hydrogeology Journal, v. 24, issue 2, p. 503–519.

Jackson, R.B., Vengosh, A., Darrah, T.H., Warner, N.R., Down, A., Poreda, R.J., Osborn, S.G., Zhao, K. and Karr, J.D. (2013): Increased stray gas abundance in a subset of drinking water wells near Marcellus shale gas extraction; Proceedings of the National Academy of Sciences of the United States of America, v. 110, no. 28, p. 11250–11255.

Kang, M., Kanno, C.M., Reid, M.C., Zhang, X., Mauzerall, D.L., Cella, M.A., Chen, Y. and Onstott, T.C. (2014): Direct measurements of methane emissions from abandoned oil and gas wells in Pennsylvania; Proceedings of the National Academy of Sciences of the United States of America, v. 111, no. 51, p. 18173–18177, doi:10.1073/pnas.1408315111

Kerr, R.A. (2010): Natural gas from shale bursts onto the scene; Science, v. 328, issue 5986, p. 1624–1626.

LeBreton, E. (2009): Confined space; Transport Canada, URL <https://www.tc.gc.ca/eng/canutec/articles-confined-456.htm> [December 2017].

Le Mer, J. and Roger, P. (2001): Production, oxidation, emission and consumption of methane by soils: a review; European Journal of Soil Biology, v. 37, issue 1, p. 25–50.

Ng, G.H.C., Bekins, B.A., Cozzarelli, I.M., Baedecker, M.J., Bennett, P.C., Amos, R.T. and Herkelrath, W.N. (2015): Reactive transport modeling of geochemical controls on secondary water quality impacts at a crude oil spill site near Bemidji, MN; Water Resources Research, v. 51, issue 6, p. 4156–4183, doi:10.1002/2015WR016964

Osborn, S.G., Vengosh, A., Warner, N.R. and Jackson, R.B. (2011): Methane contamination of drinking water accompanying gas-well drilling and hydraulic fracturing; Proceedings of the National Academy of Sciences of the United States of America, v. 108, no. 20, p. 8172–8176.

Robertson, J.O., Chilingar, G.V., Khilyuk, L.F. and Endres, B. (2012): Migration of gas from oil/gas fields; Energy Sources, Part A: Recovery, Utilization, and Environmental Effects, v. 34, issue 15, p. 1436–1447.

Shindell, D.T., Faluvegi, G., Koch, D.M., Schmidt, G.A., Unger, N. and Bauer, S.E. (2009): Improved attribution of climate forcing to emissions; Science, v. 326, issue 5953, p. 716–718, doi:10.1126/science.1174760

Stocker, T.F., Qin, D., Plattner, G.-K., Tignor, M., Allen, S.K., Boschung, J., Nauels, A., Xia, Y., Bex, V. and Midgley, P.M., editors (2013): Climate Change 2013: The Physical Science Basis, Working Group I Contribution to the Fifth Assessment Report of the Intergovernmental Panel on Climate Change, Cambridge University Press, Cambridge, United Kingdom and New York, New York, 1535 p.

United States Environmental Protection Agency (2010): Methane and nitrous oxide emissions from natural sources; United States Environmental Protection Agency, EPA-430-R-10-001, 194 p.

Van Stempvoort, D., Maathuis, H., Jaworski, E., Mayer, B. and Rich, K. (2005): Oxidation of fugitive methane in ground water linked to bacterial sulfate reduction; Groundwater, v. 43, issue 2, p. 187–199.

Van Stempvoort, D.R., Armstrong, J. and Mayer, B. (2007): Microbial reduction of sulfate injected to gas condensate plumes in cold groundwater; Journal of Contaminant Hydrology, v. 92, issue 3–4, p. 184–207, doi:10.1016/j.jconhyd.2007.01.006

Vengosh, A., Warner, N., Jackson, R. and Darrah, T. (2013): The effects of shale gas exploration and hydraulic fracturing on the quality of water resources in the United States; Proceedings of the Fourteenth International Symposium on Water-Rock Interaction (WRI 14), Procedia Earth and Planetary Science, v. 7, Avignon, France, June 9–14, 2013, p. 863–866.

Vengosh, A., Jackson, R.B., Warner, N., Darrah, T.H. and Kondash, A. (2014): A critical review of the risks to water resources from unconventional shale gas development and hydraulic fracturing in the United States; Environmental Science & Technology, v. 48, issue 15, p. 8334–8348.

Vidic, R.D., Brantley, S.L., Vandenbossche, J.M., Yoxtheimer, D. and Abad, J.D. (2013): Impact of shale gas development on regional water quality; Science, v. 340, issue 6134, 9 p., doi:10.1126/science.1235009

Toward Understanding the Trajectory of Hydrological Change in the Southern Taiga Plains, Northeastern British Columbia and Southwestern Northwest Territories

W.L. Quinton, Cold Regions Research Centre, Wilfrid Laurier University, Waterloo, ON, wquinton@wlu.ca

A.A. Berg, Department of Geography, University of Guelph, ON

O. Carpino, Department of Geography, University of Guelph, ON

R.F. Connon, Cold Regions Research Centre, Wilfrid Laurier University, Waterloo, ON

J.R. Craig, Department of Civil and Environmental Engineering, University of Waterloo, Waterloo, ON

E. Devoie, Department of Civil and Environmental Engineering, University of Waterloo, Waterloo, ON

E. Johnson, Northeast Water Strategy, Government of British Columbia, Victoria, BC

Quinton, W.L., Berg, A.A., Carpino, O., Connon, R.F., Craig, J.R., Devoie, E. and Johnson, E. (2018):Toward understanding the trajectory of hydrological change in the southern Taiga Plains, northeastern British Columbia and southwestern Northwest Territories; *in* Geoscience BC Summary of Activities 2017: Energy, Geoscience BC, Report 2018-4, p. 77–86.

Introduction

Climate warming–induced permafrost thaw is particularly pronounced in the southern Taiga Plains ecoregion, where permafrost is thermally insulated by an organic cover of dry peat, allowing it to persist in areas where the mean annual air temperature is positive (Smith and Riseborough, 2002). The permafrost of this region has already warmed to the melting point temperature, and its discontinuous nature enables energy to enter individual permafrost bodies not only vertically from the ground surface, but also laterally from adjacent permafrost-free terrain. Because such bodies are relatively thin (<10 m), permafrost thaw in this region often results in a local disappearance of permafrost (Beilman and Robinson, 2003). Although the southern Taiga Plains region contains mineral uplands that support forest covers, this region is dominated by peatlands in the form of peat plateaus, channel fens, isolated bogs (often called collapse scars) and expansive bogs (often called poor fens). Unlike the expansive bogs, the isolated bogs are surrounded by raised permafrost and as such are hydrologically isolated from the channel fens with respect to surface or near-surface flows. The plateaus function primarily as runoff generators, given their relatively high topographic position and limited capacity to store water. Unlike the peat plateaus, which are underlain by permafrost and support a forest cover, the bogs and fens are without trees and are permafrost-free. The isolated bogs, being internally drained, are predominantly areas of water storage. The expansive bogs exchange surface and near-surface flows with channel fens during periods of high moisture supply, but otherwise predominantly store the water they receive. Water draining into channel fens from the surrounding plateaus and expansive bogs (during periods of hydrological connection) is conveyed laterally along their broad (~50–100 m), hydraulically rough channels to streams and rivers (Quinton et al., 2003).

Permafrost thaw leads to ground surface subsidence, which transforms landscapes and ecosystems and ultimately affects the distribution and routing of water. As such, permafrost thaw is confounding the prediction of hydrological responses. Streamflow has increased throughout this region since the mid-1990s despite there being no significant change in precipitation (St. Jacques and Sauchyn, 2009). Connon et al. (2015) offered a plausible explanation of how permafrost-thaw–induced land-cover change in this region can increase streamflow by increasing the proportion of the land cover contributing runoff to the stream. However, there is little consensus on the trajectory of the thaw-induced land-cover change in the southern Taiga Plains, and as a result, the water futures of this region are unclear. To properly manage the water resources of this region, decision makers require an understanding of how permafrost thaw is changing the relative proportions of the major land covers. This will allow new insights into the trajectory of land-cover change and its implications on regional water resources.

The Consortium for Permafrost Ecosystems in Transition (CPET) was formed in 2015 among academic researchers, industry partners, and community and government groups to address the aforementioned issues being faced by the northeastern British Columbia–southwestern Northwest

This publication is also available, free of charge, as colour digital files in Adobe Acrobat® PDF format from the Geoscience BC website: http://www.geosciencebc.com/s/SummaryofActivities.asp.

Territories (NBC–NWT) border region (Figure 1a). The long-term goal of CPET is to produce key insights into the trajectory of land-cover change in the southern Taiga Plains, and how this may affect water resources. This paper provides a synthesis of CPET progress to date based on a combination of published and unpublished materials.

Study Sites

The CPET is focused on a ~200 km north-south transect traversing the southern margin of thawing discontinuous to sporadic permafrost in the southern Taiga Plains (Figure 1b). Field studies are concentrated at the northern (Scotty Creek, NWT) and southern (Suhm Creek, BC) end members of this transect. Between the end-member sites, twelve areas of interest (AOI), each with a footprint of 36 km^2 (432 km^2 total area), were established to examine the temporal (1970 to present) and spatial (within and between AOIs) variations of permafrost-thaw–induced land-cover change (Quinton et al., 2017). The focus of this report, however, is on the Scotty Creek basin (61°17'N, 121°17'W), which drains a 152 km^2 area dominated by peat plateau–bog complexes and channel fens (Figure 1b). Scotty Creek basin is underlain by discontinuous permafrost (Hegginbottom and Radburn, 1992) and is covered by peatland complexes typical of the 'continental high boreal' wetland region (National Wetlands Working Group, 1988). The peat thickness at Scotty Creek basin ranges between 2 and 8 m (McClymont et al., 2013), below which lies a thick clay/silt-clay glacial till deposit of low permeability (Aylesworth and Kettles, 2000). Most of the Scotty Creek basin is a heterogeneous mosaic of forested peat plateaus underlain by permafrost, and treeless permafrost-free wetlands (Figure 1c), typical of the southern fringe of discontinuous permafrost (Helbig et al., 2016). The 1981–2010 climate normals indicate that Fort Simpson, to the north, has a dry continental climate with short dry summers and long cold winters. Fort Simpson has an average annual air temperature of –2.8°C and receives 388 mm of precipitation annually, of which 38% is snow (Environment Canada, 2017). Snowmelt usually commences in early to mid-April and continues throughout most of the month, so that by May, only small amounts of snow remain (Hamlin et al., 1998).

Results

Figure 1c shows a classified Ikonos image, acquired in 2000, of a 22 km^2 subarea within the Scotty Creek basin in which permafrost plateaus occupy the greatest (43%) area, followed by expansive bogs that are hydrologically connected to channel fens (23%), channel fens (21%), lakes (9%) and isolated flat bogs (4%). Since permafrost thaw increases the cover of the bogs and fens at the expense of the forested peat plateaus, tree cover can be used as a proxy for the presence of permafrost. The area underlain by permafrost at Scotty Creek basin decreased from 70% in 1947 to 43% in 2008 (Quinton et al., 2011), with degradation rates increasing in recent decades (Baltzer et al., 2014). This rate is consistent with estimates for the larger southern Taiga Plains region, where 30–65% of the permafrost has degraded over the last 100–150 years (Beilman and Robinson, 2003).

Recent hydrological field studies at Scotty Creek basin (Connon et al., 2014) provide valuable insights into how the land cover is changing and how such changes affect water flux and storage of water. It was shown that permafrost thaw had formed ephemeral flow connections between bogs that were assumed to be hydrologically isolated. Specifically, during periods of high moisture supply, water was found to cascade from bog to bog before reaching channel fens. It was also found that the ephemeral channels connecting the bogs were areas of preferential permafrost thaw. Two bog cascades, one draining the West sub-basin and the other draining the East sub-basin, are identified in Figure 1d. The hydrographs of the two sub-basins show the amount of water that would otherwise have remained on the plateau in the absence of the bog-to-bog drainage process (Figure 2). The annual drainage from the slightly smaller East sub-basin is substantially larger since its bogs are smaller and therefore more readily filled (Connon et al., 2015), a condition that must be reached before bog-to-bog flow can commence.

Connon et al. (2015) compared historical images of the Scotty Creek catchment, and showed that numerous bogs that were once hydrologically isolated from channel fens (e.g., Figure 3a) had over a period of a few decades become hydrologically connected to them (e.g., Figure 3b). This 'bog capture' process increases the runoff contributing area and therefore the amount of runoff produced by the basin (Connon et al., 2014). Permafrost thaw transforms hydrologically isolated bogs into 'open' bogs by removing the permafrost that once separated such a bog from the basin drainage network of channel fens. This land-cover transformation is important hydrologically because it adds two forms of runoff to the basin drainage network: 1) runoff arising from direct precipitation falling onto the captured bog (i.e., bog drainage), and 2) runoff from the captured bog's watershed (i.e., slope drainage). As captured bogs expand due to permafrost thaw at their margins, they coalesce with other bogs, a process that increases both the bog and slope drainage contributions to the basin drainage network.

Figure 4a shows an example of bog capture between 2006 and 2015 at Scotty Creek basin, as recorded by detailed ground surface elevation and permafrost table depth surveys. As the permafrost table lowered between 2006 and 2015, the plateau ground surface lowered and was flooded, a process resulting in the simultaneous loss of forest and expansion of wetlands. By 2015, the permafrost table was below the elevation of the water tables of the adjacent

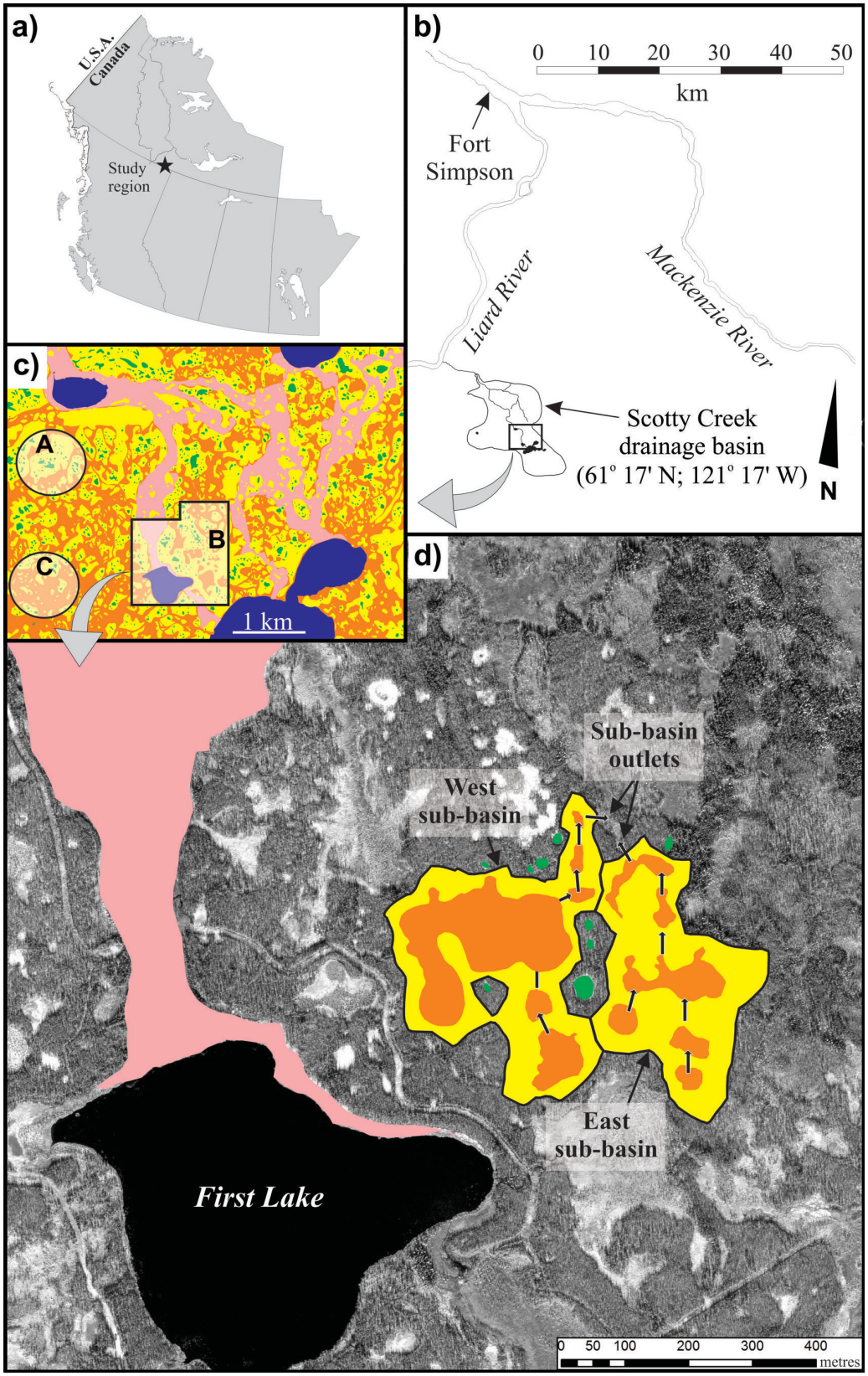

Figure 1. Location of **a)** study region and **b)** Scotty Creek drainage basin. Ikonos image (©DigitalGlobe, Inc.) of **c)** peat plateaus (yellow), isolated bogs (green), connected bogs (orange) and channel fens (pink) in the part of Scotty Creek drainage basin outlined in b); and **d)** enlarged area B, outlined in c), showing cascade bogs. Areas identified by A, B and C are defined in the 'Results' section. Small arrows in East sub-basin and West sub-basin indicate flow direction.

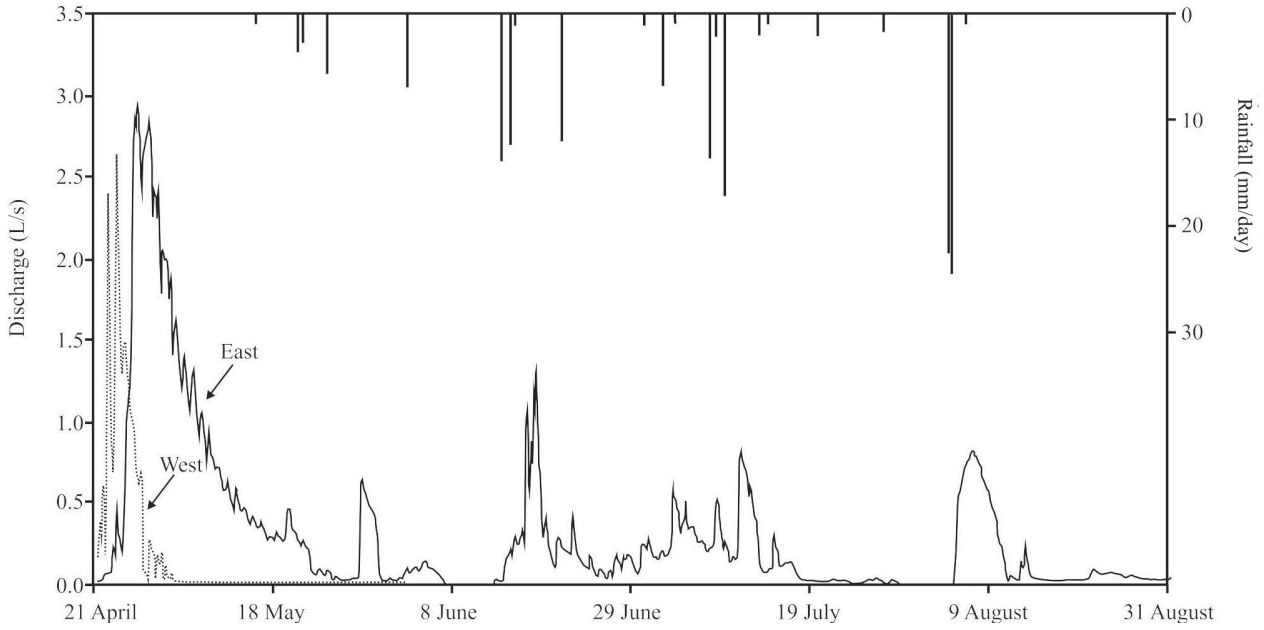

Figure 2. Runoff hydrographs measured at outlets of East sub-basin and West sub-basin bog cascades for 2014.

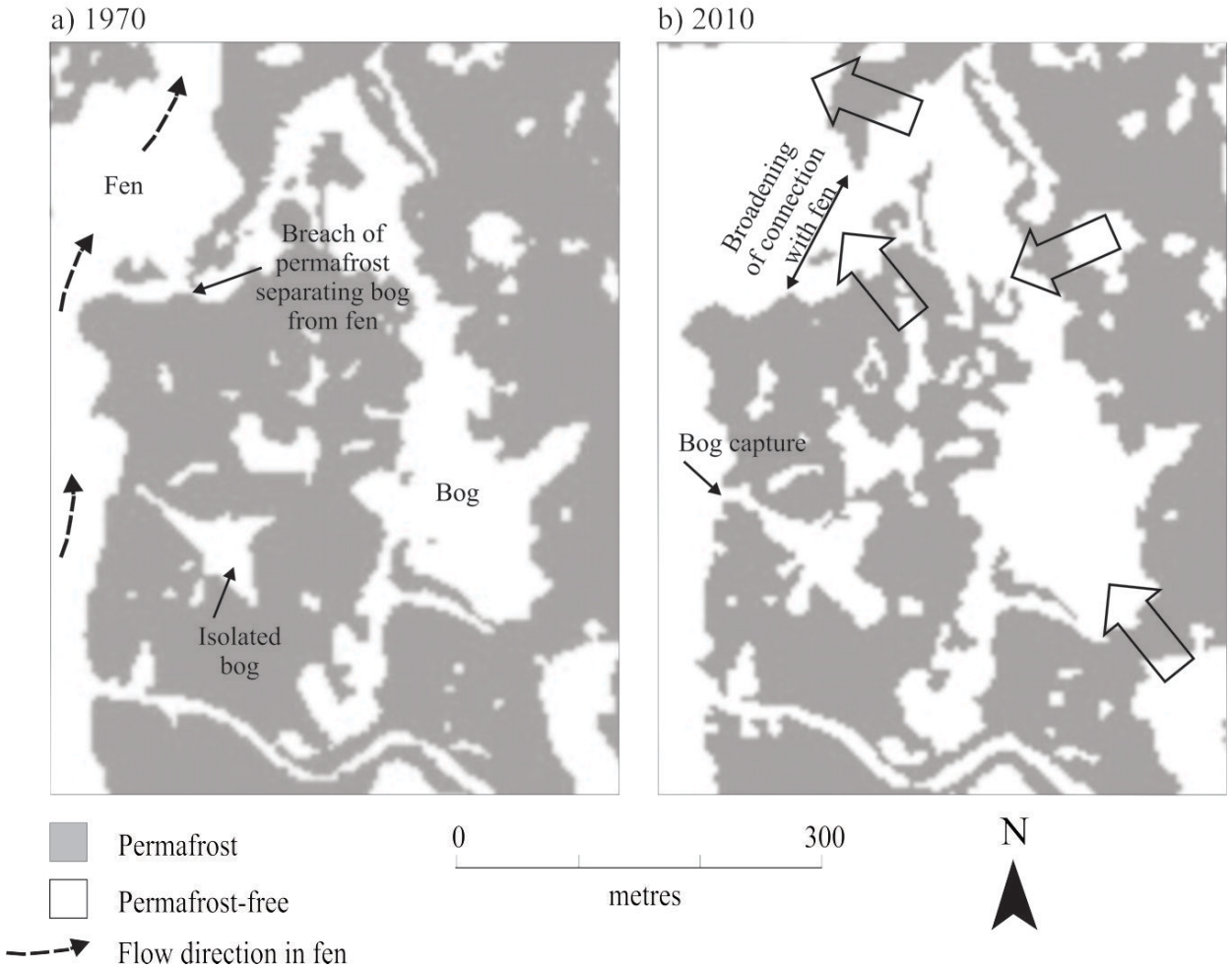

Figure 3. Classified images for a 1 km^2 area in the Scotty Creek catchment showing the change in permafrost coverage (grey) between **a)** 1970 and **b)** 2010. The large arrows in b) signify subsurface flow through taliks to the basin drainage network of channel fens. Centre of images is approximately latitude 61°18'39"N, longitude 121°18'18"W.

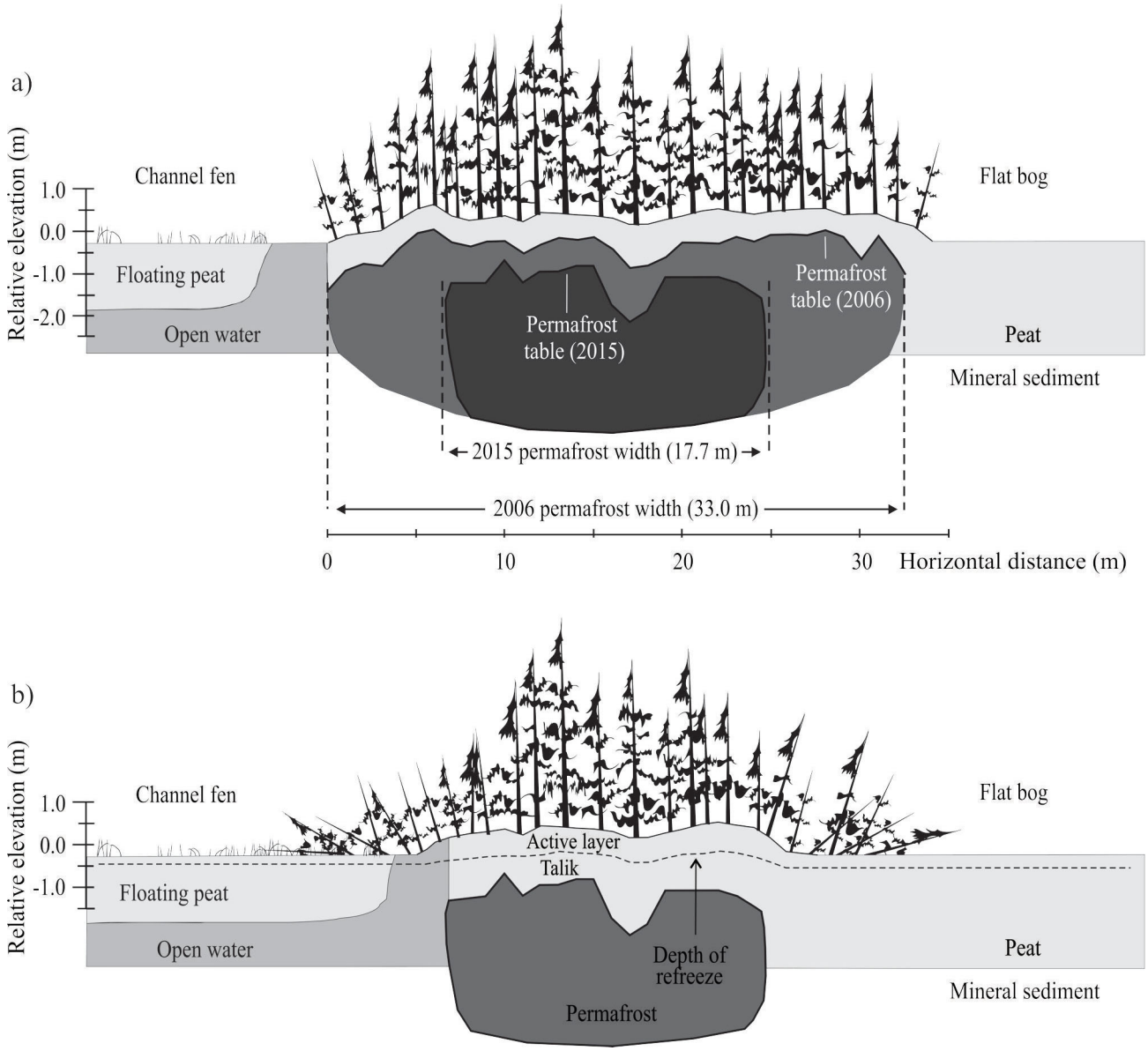

Figure 4. Cross-section of a peat plateau at Scotty Creek basin based on measurements of supra-permafrost thickness and ground surface elevation at 1 m intervals showing the difference in depth and lateral extent of the permafrost table between **a)** 2006 and 2015 and **b)** the development of a talik in 2015.

wetlands, and as a result, the permafrost body no longer prevented subsurface flow from one side of the plateau to the other (Figure 4b). By 2015, a talik (i.e., perennially unfrozen layer) had formed and enabled the plateau to conduct subsurface flow throughout the year from the bog to the fen. Subsurface flow through the talik (Figure 3b) augments the surface and near-surface flows into channel fens from the expansive bogs.

The total annual runoff from Scotty Creek and the other gauged rivers of the lower Liard River valley has steadily risen since the mid-1990s (Connon et al., 2014). The present understanding of water flow and storage processes in the southern Taiga Plains, and how climate warming and the resulting ecological changes affect these processes, cannot account for this rise, nor can it be used to predict future flows with confidence. The very low hydraulic conductivity of the glacial sediments below the peat precludes reactivation of groundwater systems as a cause of the rising flows from subarctic rivers. A more plausible explanation is the permafrost-thaw–induced expansion of runoff source areas as described by Connon et al. (2015). Field observations and image analyses (Baltzer et al., 2014) suggest that plateaus contain primary and secondary runoff source areas separated by a break in slope approximately 10 m inland from the fen-plateau edge (Figure 5).

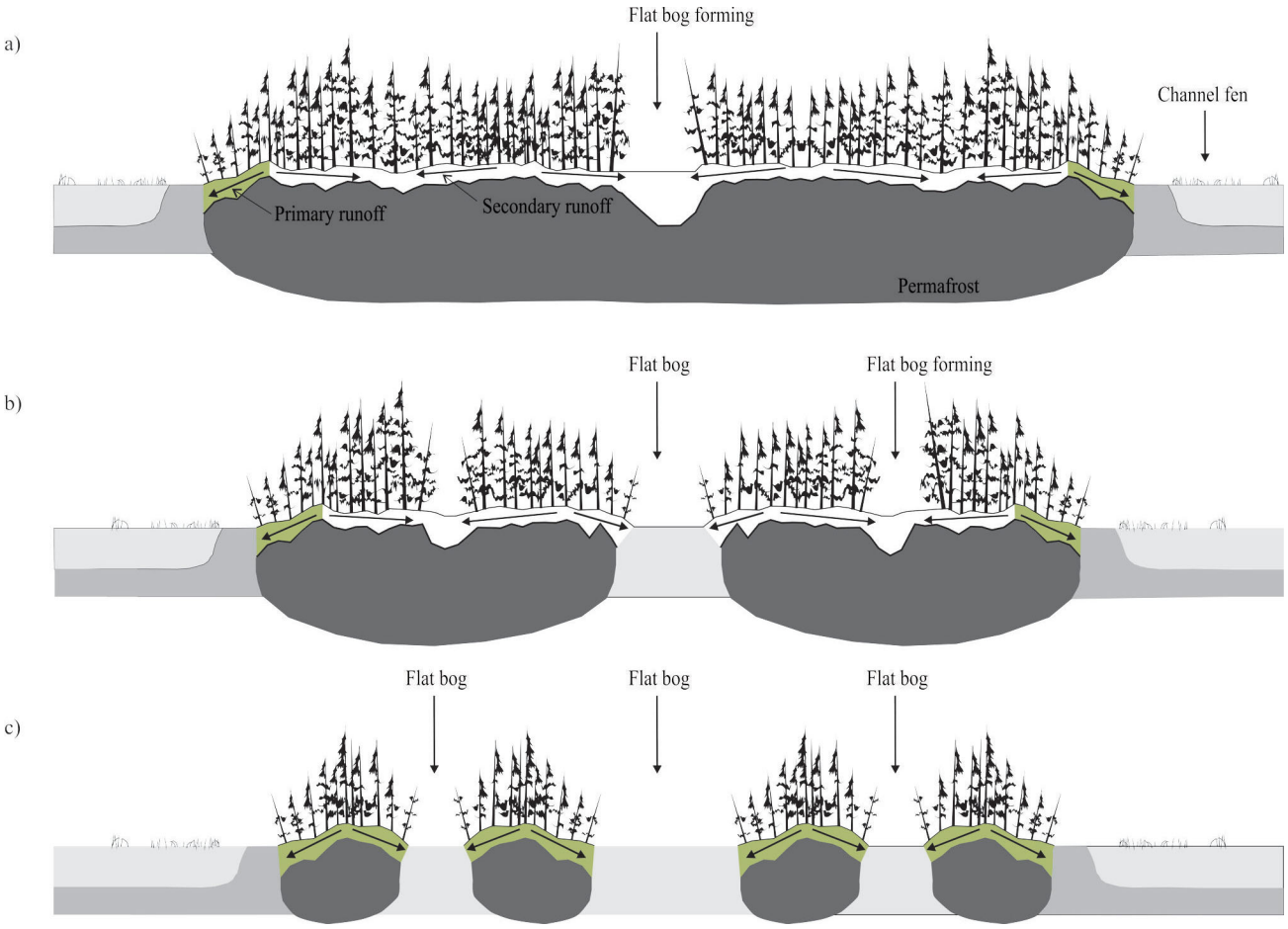

Figure 5. Conceptualization of permafrost-thaw–induced land-cover transformation in the wetland-dominated zone of discontinuous permafrost typical of the southern Taiga Plains: **a)** early stage (isolated bogs), **b)** transitional stage (isolated bogs or bog cascades) and **c)** advanced stage (plateau islands). Green areas represent the areas producing primary runoff. Examples of the early, transitional and advanced stages are identified by A, B and C in Figure 1c.

Primary runoff drains from the sloped edges of plateaus directly into the basin drainage network. Field measurements indicate that the entire primary runoff area supplies runoff to the fen throughout the thaw season. Secondary runoff drains into the interior of the plateau toward the topographic low, which is often occupied by bog within the plateau. If such a bog is hydrologically isolated, the runoff it received will remain in storage, evaporate or recharge the underlying aquifer. However, if it is part of a cascade, and if its storage capacity is exceeded, then the secondary runoff it receives will be conveyed toward the channel fen via the downslope bog or bogs. Secondary runoff is therefore, neither direct nor continuous. Its rate is greatest during periods of high moisture supply and minimal ground thaw, when the hydrological connection among the bogs of a cascade, and between individual bogs and their contributing 'bogsheds' is maximized. As the active layer thaws and drains, the contributing area for secondary runoff diminishes in size and secondary runoff therefore decreases or stops, leaving primary runoff as the predominant runoff process. However, secondary runoff can resume in response to large rain events.

Over decades of permafrost thaw, a plateau transforms through three general stages (Figure 5). Examples of each can be observed at Scotty Creek basin. For example, land cover 'A' represents an early stage of permafrost thaw where bogs are mostly hydrologically isolated, and as such, drainage into the fen is supplied only by primary runoff from the margins of the plateaus (Figure 5a). Land cover 'B' indicates a transitional stage of permafrost thaw where primary runoff is augmented by secondary runoff from bog cascades (Figures 1d, 5b). The activation of secondary runoff arises from the greater hydrological connectivity of land cover B than A. As a result, a greater proportion of the snowmelt and rainfall arriving on land cover B is converted to runoff than in land cover A (Figure 6). Land cover 'C' represents an advanced stage, where the shrinking peat plateaus occur as islands within an expansive bog (Figure 5c). By this stage, plateau diameters are on the order of a few

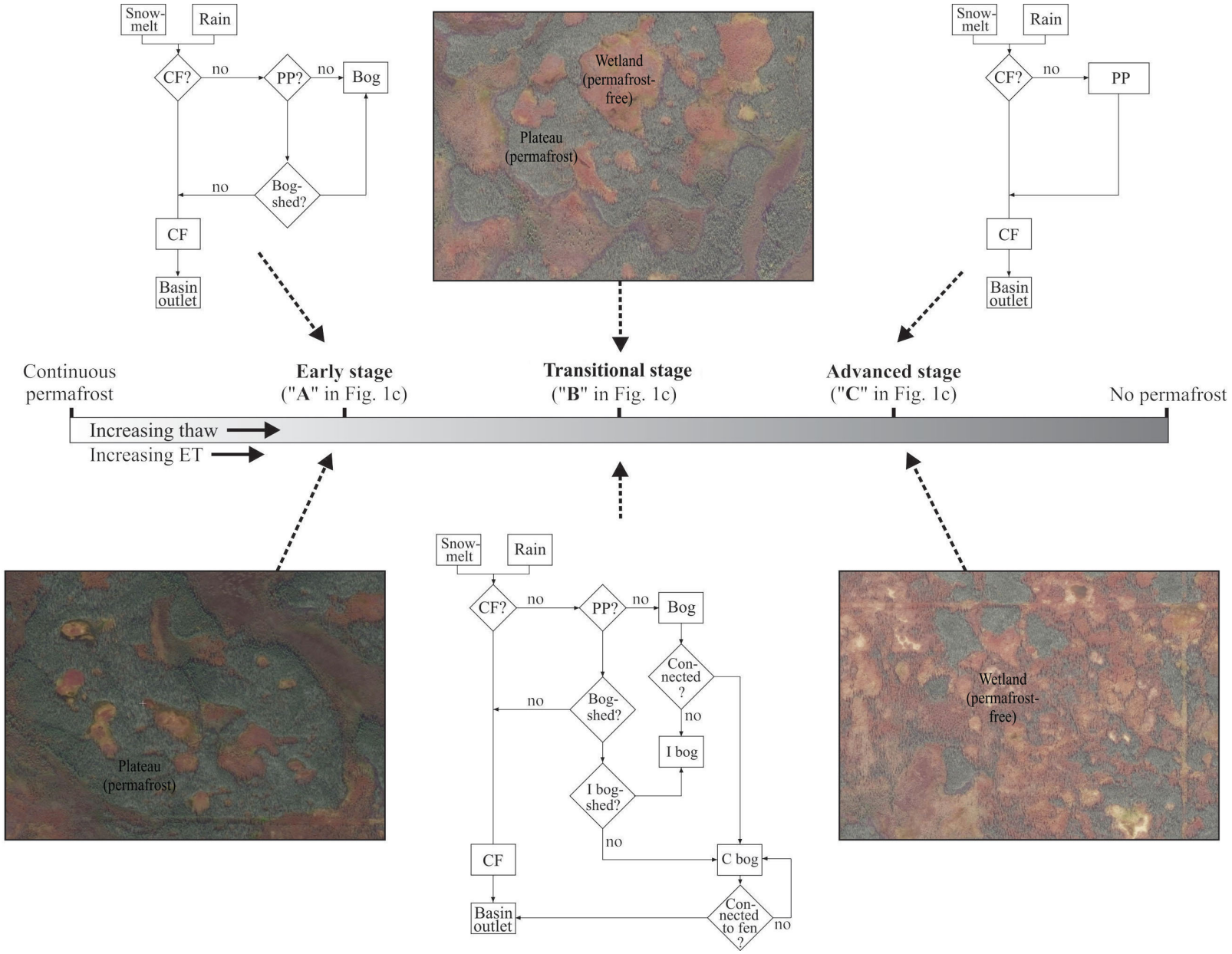

Figure 6. The transformation of runoff generation processes in peat plateaus with increasing thaw (and evapotranspiration) from left to right (image source NASA, 2017). Abbreviations: C, connected; CF, channel fen; ET, evapotranspiration; I, isolated; PP, peat plateau.

tens of metres and as such contain no secondary runoff and no interior bogs. Because land cover B is transitional between A and C, some bogs are hydrologically connected, whereas others remain hydrologically isolated.

As the land-cover transitions through the three stages, the way that peat plateaus generate runoff changes dramatically, with direct consequences on their runoff pattern and rate (Figure 6). Water arriving at the channel fen in each stage, is conveyed to the basin outlet. Water arriving in a primary-runoff–producing area of a plateau is routed directly to the adjacent fen. Water arriving directly into bogs or their bogsheds is prevented from reaching channel fens in the early stage, but can reach the fen in the transitional stage, if the bog is part of a cascade and is hydrologically connected to the downstream bog or bogs. Activation of secondary runoff therefore increases the amount of runoff between the early and transitional stages. Primary runoff may also increase between these two stages since the fragmentation of plateaus can increase the length of the overall plateau-fen edge. Water arriving onto plateaus in the advanced stage is neither stored nor routed as secondary runoff through bog cascades. As such, the advanced stage produces the greatest runoff per unit area of plateau surface, but given the relatively small total surface area of the remaining plateaus, the total plateau runoff is lowest in this stage.

Synthesis

By substituting space for time, the land-cover characteristics near the southern end of the north-south transect suggest that the trajectory of land cover change at Scotty Creek basin is toward increasing fragmentation and eventual disappearance of peat plateaus. Less clear is the trajectory of the intervening wetlands. The transect studies suggest that a concomitant expansion of the wetland area with the shrinkage and loss of peat plateaus would initially produce a wetter land cover characterized by expansive wetland with little forest cover. Although the hydrological connectivity of this stage would be high, the reduction of the plateau area reduces the impact of their relatively rapid flowpaths, and as a result, such a land cover may produce less runoff than presently observed at Scotty Creek basin. However, recent studies in the Scotty Creek region (e.g., Helbig et al., 2016) indicate increased average basin evapotranspiration as the relative coverage of wetland terrain increases (Figure 6). The transect studies also suggest that this initial wet stage is superseded by a drier land cover of the type presently observed near the NWT–BC border. In that region, the permafrost-free terrain is sufficiently dry to enable the regrowth of forest covers, which include black spruce (without permafrost) and a greater proportion of deciduous species. Although this synthesis provides some insights into the trajectory of land-cover and hydrological change in the southern Taiga Plains, there remain several significant unknowns. For example, the time scale over which the land-cover transitions will occur is not well understood. There is also a dearth of knowledge on how possible ecological and/or hydrological feedback mechanisms may affect trajectories of land-cover change. There is also little understanding of how such trajectories may change in response to changes in precipitation regimes, such as total annual precipitation (a proportion of which occurs in the form of snow), the number of multiday events and other precipitation distribution characteristics, and the timing of snowmelt.

Acknowledgments

Consortium for Permafrost Ecosystems in Transition is funded by a Natural Sciences and Engineering Research Council of Canada Collaborative Research and Development grant with partner contributions from Nexen, Petroleum Technology Alliance of Canada, Geoscience BC and BC Oil and Gas Research and Innovation Society. The authors gratefully acknowledge the support of Fort Nelson First Nation, Liidlii Kue First Nation, Jean Marie River First Nation, Government of the Northwest Territories and Government of British Columbia. This article benefited from a review by M. English at Wilfrid Laurier University.

References

Aylesworth, J.M. and Kettles, I.M. (2000): Distribution of fen and bog in the Mackenzie Valley, 60°N–68°N; *in* The Physical Environment of the Mackenzie Valley, Northwest Territories: a Base Line for the Assessment of Environmental Change, L.D. Dyke and G.R. Brooks (ed.), Geological Survey of Canada, Bulletin 547, Figure 4.

Baltzer, J.L., Veness, T., Chasmer, L.E., Sniderhan, A. and Quinton, W.L. (2014): Forests on thawing permafrost: fragmentation, edge effects, and net forest loss; Global Change Biology, v. 20, no. 3, p. 824–834, doi:10.1111/gcb.12349

Beilman, D.W. and Robinson, S.D. (2003): Peatland permafrost thaw and landform type along a climate gradient; *in* Proceedings of the Eighth International Conference on Permafrost, M. Phillips, S.M. Springman and L.U. Arenson (ed.), Zurich, Switzerland, July 21–25, 2003, A.A. Balkema, v. 1, p. 61–65.

Connon, R.F., Quinton, W., Craig, J., Hanisch, J. and Sonnentag, O. (2015): The hydrology of interconnected bog complexes in discontinuous permafrost terrains; Hydrological Processes, v. 29, issue 18, p. 3831–3847, doi:10.1002/hyp.10604

Connon, R.F., Quinton, W.L., Craig, J.R. and Hayashi, M. (2014): Changing hydrologic connectivity due to permafrost thaw in the lower Liard River valley, NWT, Canada; Hydrological Processes, v. 28, issue 14, p. 4163–4178, doi:10.1002/hyp.10206

Environment Canada (2017): Canadian climate normals: 1981–2010 climate normals and averages; Environment Canada, URL <http://climate.weather.gc.ca/climate_normals> [September 2017].

Hamlin, L., Pietroniro, A., Prowse, T., Soulis, R. and Kouwen, N. (1998): Application of indexed snowmelt algorithms in a

northern wetland regime; Hydrological Processes, v. 12, p. 1641–1657.

Heginbottom, J.A. and Radburn, L.K., compilers (1992): Permafrost and ground ice conditions of northwestern Canada; Geological Survey of Canada, Map 1691A, scale 1:1 000 000.

Helbig, M., Wischnewski, K., Kljun, N., Chasmer, L., Quinton, W., Detto, M. and Sonnentag, O. (2016): Regional atmospheric cooling and wetting effect of permafrost thaw-induced boreal forest loss; Global Change Biology, v. 22, issue 12, p. 4048–4066, doi:10.1111/gcb.13348

McClymont, A., Hayashi, M., Bentley, L. and Christensen, B. (2013): Geophysical imaging and thermal modeling of subsurface morphology and thaw evolution of discontinuous permafrost; Journal of Geophysical Research, Earth Surface, v. 118, issue 3, p. 1–12, doi:10.1002/jgrf.20114

NASA (2017): Moderate-resolution imaging spectroradiometer (MODIS) data; Zoom Earth, image, URL <https://zoom.earth/> [September 2017].

National Wetlands Working Group (1988): Wetlands of Canada; Environment Canada, Ecological Land Classification Series, v. 24, 452 p.

Quinton, W.L., Adams, J.R., Baltzer, J.L., Berg, A.A., Craig, J.R. and Johnson, E. (2017): Consortium for Permafrost Ecosystems in Transition: traversing the southern margin of discontinuous permafrost with hydrological, ecological and remote sensing research, northeastern British Columbia and southwestern Northwest Territories; *in* Geoscience BC Summary of Activities 2016, Geoscience BC, Report 2017-1, p. 79–86.

Quinton, W.L., Hayashi, M. and Chasmer, L.E. (2011): Permafrost-thaw-induced land-cover change in the Canadian subarctic: implications for water resources; Hydrological Processes (Scientific Briefing), v. 25, no. 1, p. 152–158, doi:10.1002/hyp.7894

Quinton, W.L., Hayashi, M. and Pietroniro, A. (2003): Connectivity and storage functions of channel fens and flat bogs in northern basins; Hydrological Processes, v. 17, no. 18, p. 3665–3684, doi:10.1002/hyp.1369

Smith, M.W. and Riseborough, D.W. (2002): Climate and the limits of permafrost: a zonal analysis; Permafrost and Periglacial Processes, v. 13, issue 1, p. 1–15.

St. Jacques, J.M. and Sauchyn, D.J. (2009): Increasing winter base flow and mean annual streamflow from possible permafrost thawing in the Northwest Territories, Canada; Geophysical Research Letters, v. 36, no. L01401, doi:10.1029/2008GL035822

Modelling the Disposal of Highly Saline Wastewater in the Paddy and Cadotte Members, Northeastern British Columbia (NTS 093P)

M.S. Simons, Simon Fraser University, Burnaby, BC, msimons@sfu.ca

D.M. Allen, Simon Fraser University, Burnaby, BC

D. Kirste, Simon Fraser University, Burnaby, BC

L.A. Welch, British Columbia Oil and Gas Commission, Kelowna, BC

Simons, M.S., Allen, D.M., Kirste, D. and Welch, L.A. (2018): Modelling the disposal of highly saline wastewater in the Paddy and Cadotte members, northeastern British Columbia (NTS 093P); *in* Geoscience BC Summary of Activities 2017: Energy, Geoscience BC, Report 2018-4, p. 87–96.

Introduction

The drilling and hydraulic fracturing of wells and subsequent hydrocarbon production often generates highly saline wastewater (Goss et al., 2015), with total dissolved solids (TDS) in excess of the typical value for seawater of 35 000 mg/L. The cumulative amount of wastewater produced from hydraulic fracturing is increasing rapidly with the steady appearance of new wells and a trend toward more water use per well (Alessi et al., 2017). In northeastern British Columbia (NEBC), an average of 75 m^3 of wastewater is generated for every million cubic metres of gas produced from the Montney play (IHS Energy, 2016), the most productive gas play in the province (BC Oil and Gas Commission, 2015). Although reuse and recycling is employed where practicable, ultimately large quantities of wastewater must be disposed of and the most viable method of disposal is injection into deep, permeable geological formations.

Disposal well operations in BC are regulated by the BC Oil and Gas Commission (BCOGC). Formations considered appropriate for hosting wastewater disposal are of high permeability (most commonly deep saline units or depleted hydrocarbon reservoirs) relative to confining layers (typically shale units) above and below them (BC Oil and Gas Commission, 2016). These confining layers have been demonstrated to be effective at limiting the vertical migration of groundwater (Hendry et al., 2013), and serve to restrict wastewater to the targeted disposal formation. Companies seeking approval for a disposal well must demonstrate that the confining layers are free of any preferential pathways (faults, fractures, abandoned and/or improperly cemented boreholes) by which wastewater could travel upward and contaminate shallower, potentially potable, groundwater. Additionally, the BCOGC restricts disposal formations to units that contain "deep groundwater" as defined in the BC *Water Sustainability Act* (Government of British Columbia, 2017), which begins 300–600 m below ground surface depending on local geology.

Throughout the life of a disposal well, certain pressure conditions must be met (BC Oil and Gas Commission, 2016). Firstly, the injection pressure at the wellhead should not exceed 90% of the formation fracture pressure, in order to avoid unintentionally fracturing the formation. Secondly, disposal well operations cannot increase the formation pressure beyond 120% of the initial virgin reservoir pressure (IVRP), that is, the pressure in the formation prior to any production or disposal. These pressure requirements increase confidence that wastewater is contained within the disposal formation, but also limit both the amount of wastewater that can be stored in a formation and the rate at which it can be injected.

This paper presents a numerical modelling study that investigates modifications to the formation/reservoir pressure at a disposal well in a deep formation as a result of wastewater disposal. This model will provide insights into factors that influence the potential for disposal well operations to exceed the required limit of 120% of IVRP in the Paddy and Cadotte members, NEBC. This study does not consider the fracture pressure requirement or aspects of potential well interference. Model parameterization is based on the Paddy and Cadotte members (see below), which have only recently (within the last five years) become a target for wastewater disposal. Previous work (Simons et al., 2017) used the same model to investigate the structure and extent of wastewater plumes created via disposal, but this paper focuses solely on disposal pressures and formation and fluid characteristics that have the potential to influence a wastewater plume. Simulated modelled pressures are compared to the IVRP to understand what factors can lead to formation pressures surpassing the 120% of IVRP limit imposed by the BCOGC. The models are not calibrated against pressure data, and thus cannot be used to make site-

This publication is also available, free of charge, as colour digital files in Adobe Acrobat® PDF format from the Geoscience BC website: http://www.geosciencebc.com/s/SummaryofActivities.asp.

specific predictions. Instead, they provide insight as to the relative pressure changes in a formation as a response to varying formation and disposal characteristics. This is accomplished through a sensitivity analysis performed on a defined base case model to assess the influence of disposal rate, wastewater salinity, and formation permeability and thickness on reservoir pressures. The results are unconstrained due to the uncertainty in the outflow boundary condition. As such, an additional sensitivity analysis was conducted to evaluate the effect of different outflow boundary conditions on reservoir pressure buildup.

Disposal and Water Source Well Operations in the Paddy and Cadotte Members

To frame the relevance of this study, an overview is given of disposal and water source well operations targeting the Paddy and Cadotte members in NEBC. At present, disposal wells and water extraction/source wells in the Paddy and Cadotte members are focused within an approximate 120 km^2 area located approximately 20 km west of the City of Dawson Creek (Figure 1). Disposal wells and water source wells in this area began operating within the past five years, which, in combination with the relatively small number of wells targeting the formation, means that the Paddy and Cadotte members in this area have a much simpler disposal history than other disposal formations that may have been used for decades. The five disposal wells are vertical at this location and operate at 100–200 m^3/day (d), though one well (well authorization number 10677 [BC Oil and Gas Commission, 2017b] in Figure 1) operates at approximately 1000 m^3/d (IHS Energy, 2016). The six water source wells (which are all horizontal wells) operate at a rate of approximately 200 m^3/d. These source wells are not included in the model, but are described nonetheless as they will eventually be incorporated into a regional model of the area.

The injected wastewater is sourced primarily from the Montney Formation. This wastewater is a combination of flowback—water used for hydraulic fracturing that returns to the surface— and produced water—saline water that is extracted along with gas from shale formations. Except to define the regulatory category for disposal at the application stage (e.g., 'saline water' versus 'non-hazardous waste'), disposal well operators are not required to report chemistry of disposed wastewater in BC (Alessi et al., 2017). Salinity and chemistry may be variable and dependent on a number of factors, including variability in the produced water itself and any prior water recycling activities.

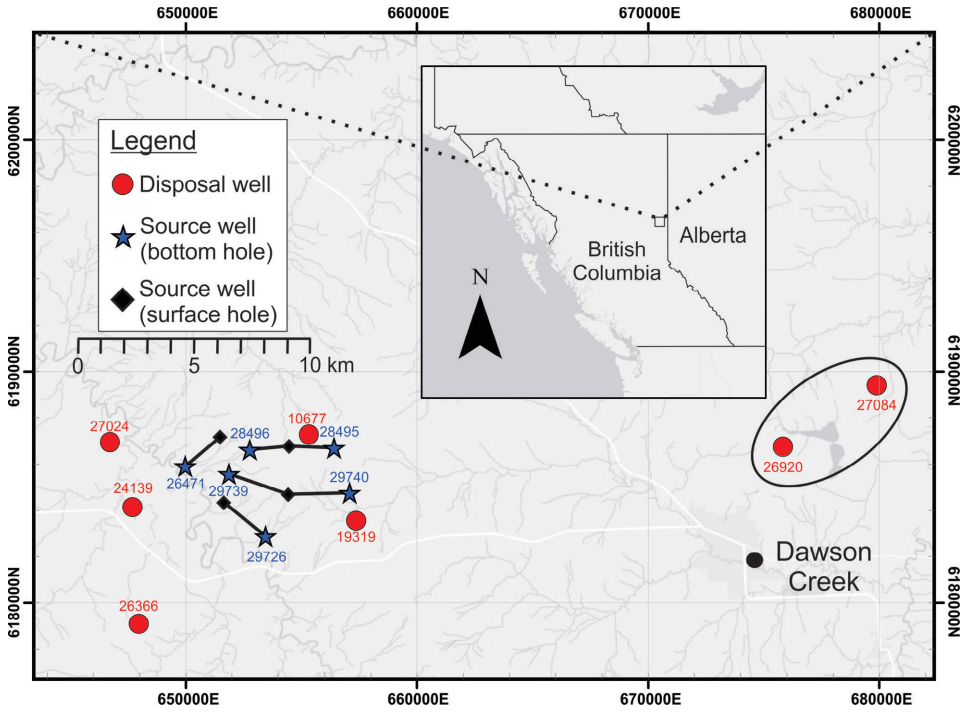

Figure 1. Map showing the locations of disposal wells (red dots), water source well bottom locations (blue stars) and water source well surface locations (black diamonds) targeting the Paddy and Cadotte members. Because the water source wells are horizontal, the location of both the surface hole and bottom hole locations are marked, with the surface hole being the location where drilling was initiated and bottom hole being the toe of the horizontal leg of the well. Wells are labelled according to their BC Oil and Gas Activities Act (OGAA) well authorization numbers (BC Oil and Gas Commission, 2017b). Note that some water source wells have proximal surface hole locations. Disposal wells 26920 and 27084 (circled to the east) are active disposal wells targeting the Paddy and Cadotte members but are not considered in this study due to their distance from the well field of interest. All co-ordinates are in UTM Zone 10.

As an indicator of potential chemistry of disposal water, available Montney Formation water analyses were compiled and found to be dominantly NaCl type, with TDS ranging from 50 to 300 g/L (BC Oil and Gas Commission, 2017a). The TDS concentration is used in the model to represent salinity (assumed to be entirely NaCl), making TDS and salinity equivalent in the context of this research. Both terms are used interchangeably.

Geology

The Paddy and Cadotte are members of the Peace River Formation (Figure 2), which was deposited during the middle to upper Albian at the southern end of the Hulcross Sea. Both members are interpreted to represent part of a major transgressive-regressive cycle (Buckley and Plint, 2013). The Paddy and Cadotte members are clastic units composed dominantly of quartz-rich sandstone sourced from the Rocky Mountain Cordillera to the west (Buckley and Plint, 2013). These units are bounded below by the Harmon Member shale and above by the Shaftesbury Formation shale, and are separated by a depositional hiatus, during which time the Cadotte Member was incised and the Paddy Member was deposited unconformably atop it (Leckie et al., 1990). The disposal wells indicated on Figure 1 target the Paddy and Cadotte members at depths of approximately 1 km below ground surface.

The Paddy Member is interpreted to have been deposited in a tidally influenced estuarine environment (Leckie et al., 1990), and is 25–40 m thick in the area of the five disposal wells shown on Figure 1. The Cadotte Member is a clastic shoreface deposit which coarsens upward into a pebbly conglomerate (Leckie et al., 1990). The Cadotte Member is 40–50 m thick, with the upper 15–25 m being of higher permeability relative to the rest of the Cadotte and Paddy members. This upper zone is the target horizon for wastewater disposal (Encana Corporation, 2014).

Hydrogeology

Available equivalent freshwater hydraulic head data in the Cadotte Member (Figure 3) and Paddy Member are similar, with a high of 600 metres above sea level (m asl) to the southwest and a low of 300 m asl to the northeast (Petrel Robertson Consulting Ltd. and Canadian Discovery Ltd., 2011). The interpreted groundwater flow direction in the area of the disposal wells, using the equivalent freshwater hydraulic head data, is to the east-northeast. The main productive horizon near the top of the Cadotte Member has porosity values of 20–30%, a thickness of 4–22 m, and perme-

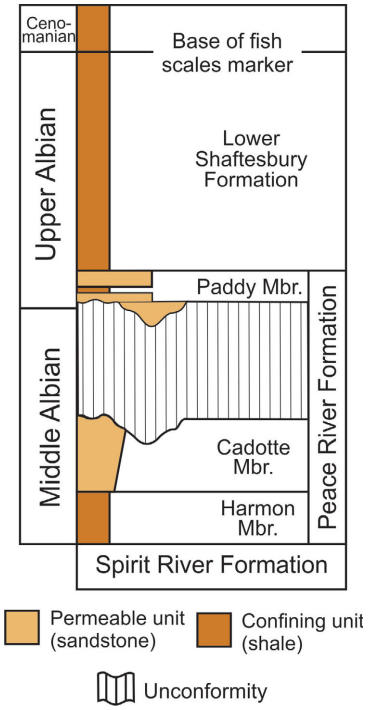

Figure 2. Stratigraphy of the middle to upper Albian in the plains area of northeastern British Columbia showing the positions and lithologies of the Harmon, Cadotte and Paddy members and Shaftesbury Formation. Modified from Leckie and Reinson (1993).

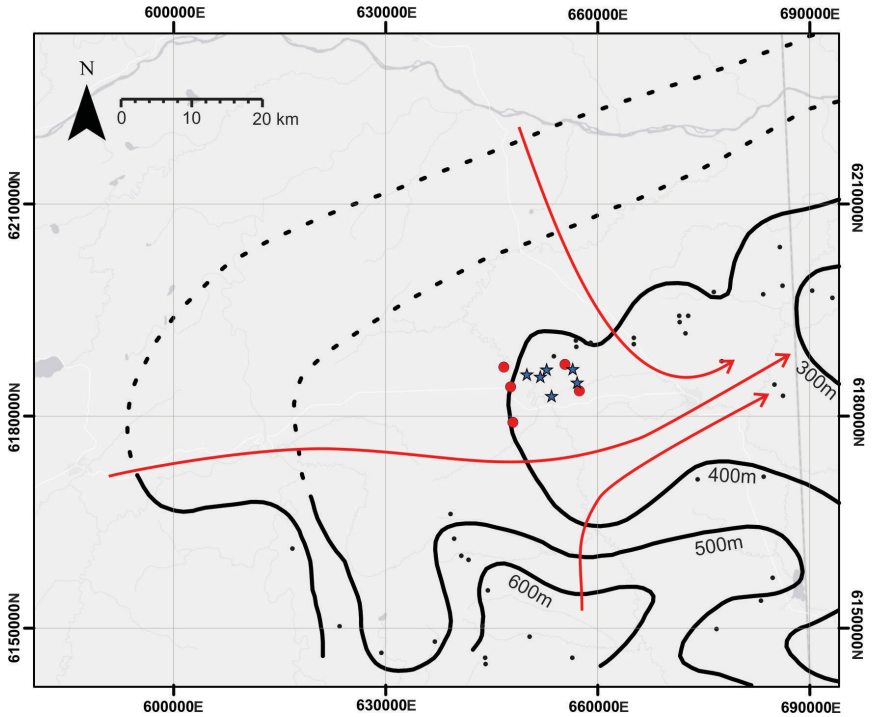

Figure 3. Equivalent freshwater hydraulic head contour map for the Cadotte Member (in metres above sea level). Red circles represent disposal wells, blue stars represent water source well bottom hole locations, black dots represent pressure measurement locations, which provided data that were converted to equivalent freshwater hydraulic head, and red arrows show representative interpreted groundwater flow directions. Contour interval is 100 m and dashed portions of contours represent poorly constrained head due to lack of data. Modified from Petrel Robertson Consulting Ltd. and Canadian Discovery Ltd. (2011). All co-ordinates are in UTM Zone 10.

ability in the range of 200–500 millidarcies (mD), whereas the Paddy Member and remaining lower section of the Cadotte Member have permeabilities that are approximately one order of magnitude lower (Petrel Robertson Consulting Ltd. and Canadian Discovery Ltd., 2011; IHS Energy, 2016). Formation water in the Paddy and Cadotte members is dominantly NaCl type and has a TDS of approximately 5–30 g/L in the study area (IHS Energy, 2016).

Methodology

Numerical modelling was completed using the groundwater modelling code FEFLOW (Diersch, 2014) to investigate the pressure increases caused by wastewater disposal. This code was chosen for its ability to simulate coupled density-dependent groundwater flow, and heat and mass transport, all of which have the potential to influence the distribution of formation pressure. The model domain is represented by a simple box model representing a cross-section through the Paddy and Cadotte members. An axisymmetric projection (Figure 4) was chosen as it has been shown to greatly reduce the computation time relative to an equivalent, full 3-D model (Langevin, 2008). A limitation of this projection type is that conditions must be assumed to be radially symmetric around the disposal well, meaning that a hydraulic gradient, variations in permeability and sloping topography cannot be simulated. These factors will be investigated in future models.

The construction of the base case model is presented here. The model domain was constructed to represent disposal into the Paddy and Cadotte members, and consists of a vertical cross-section 500 m long and 50 m high, with a vertical disposal well located along the length of the left-hand side (Figure 4). The length of the box model was selected so as to accommodate the anticipated plume size for the disposal time period chosen. The thickness of the model layer (50 m) was selected as it is approximately twice that of the horizon in the Paddy and Cadotte members used for wastewater disposal, based on geological logs in the area of the disposal wells. The domain was discretized using the triangle setting in FEFLOW's mesh generator. Higher discretization was used near the disposal well, for a total of 159 809 elements in the domain.

The top and base of the model represent the low permeability Shaftesbury Formation and Harmon Member shales, respectively, and were represented as no-flow boundaries. The left-hand side of the model represents the disposal well and was assigned flow, mass and heat boundary conditions. For flow, a well boundary condition with a conservative disposal rate of 100 m^3/d was chosen. This value was distributed along the 259 nodes defining the disposal well and then divided by 2π to account for the axisymmetric projection, resulting in a final disposal rate of 6.145×10^{-2} m^3/d per node. A constant mass boundary condition of 200 g/L and

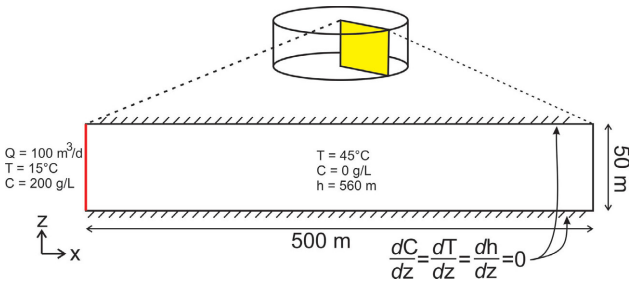

Figure 4. Axisymmetric projection showing a zoomed view of the model domain (yellow slice). The disposal well is simulated on the left boundary of the domain (red vertical line). Dots represent locations of modelled observation points. Vertical exaggeration is 1.7 times. Abbreviations: C, salinity concentration; d, day; *d*, derivative; h, hydraulic head; Q, disposal rate; T, temperature.

constant temperature boundary condition of 15°C were applied to each of these nodes as well, in order to give the injected water characteristics that are typical of wastewater that is disposed of in the Paddy and Cadotte members. This temperature was recommended by the Encana Corporation (pers. comm., 2017), as wastewater is commonly stored in tanks on the surface prior to disposal and has time to equilibrate to surface temperature. The right side of the model was set as a fluid-transfer boundary condition (similar to a general head boundary in MODFLOW; Langevin et al., 2017) with a reference head of 560 m, and the elements bordering this boundary were assigned an out-transfer rate of 9.867×10^{-10} s^{-1}. This out-transfer rate was determined by dividing the model hydraulic conductivity (see below) by the distance from the boundary at which the reference head is specified. In the base case, the reference head was assumed to be 1.5 km from the boundary, giving an effective domain length of 2 km, which was expected to be far enough from the injection well so as not to influence the results. It is important to note that no data could be used to constrain this boundary condition in the box models. Therefore, a sensitivity analysis was carried out to explore the influence of the boundary. Accordingly, the reference head was moved to 3 km from the edge, 100 km from the edge, and then changed to a no-flow boundary (no water can escape the model).

Additional parameter values selected for the model are shown in Table 1. Due to the axisymmetric nature of the model, an initial, uniform head distribution was required. Pressures measured in the Paddy and Cadotte members are roughly 5000 kilopascals (kPa), which, in the co-ordinate system selected for the model, translate to an equivalent freshwater hydraulic head value of approximately 560 m. This value was assigned as an initial condition to all elements in the domain.

A homogeneous permeability of 200 mD was selected for the model based on core permeability measurements for the disposal horizon in the Paddy and Cadotte members (IHS

Energy, 2016), which, in combination with the density and viscosity of FEFLOW's default reference water (freshwater at 10°C), is equivalent to a hydraulic conductivity of 1.48×10^{-6} m/s. Throughout the simulation, the code adjusts the hydraulic conductivity in each element based on the density and viscosity of the water in the element, which are dependent on temperature, pressure and solute concentration.

For this base case model, the initial solute concentration of the formation water was specified as 0 g/L and was not changed in the sensitivity analysis. Disposed wastewater salinity was specified at 200 g/L, based on available data for Montney Formation water chemistry. Water density values for the 0 g/L formation water and 200 g/L wastewater are 999.74 and 1126.1 kg/m^3, respectively, based on the pressure, temperature and salinity conditions (Driesner and Heinrich, 2007). This results in a density difference factor of 0.126.

Thermal parameter values of the solids were based on literature values for sandstone (Eppelbaum et al., 2014). Temperatures in the Paddy and Cadotte members are roughly 45°C (Encana Corporation, pers. comm., 2017), and so this temperature was assigned as an initial condition to the entirety of the model domain.

Disposal was simulated for 10 years of active injection, and the pressure values for each node along the disposal well, where increases are the greatest, were exported for analysis. For the base case model only, pressures were also exported for observation points located in the middle of the formation (z = 25 m) at increasing distances from the disposal well in order to assess the influence of disposal on pressures more distal to the well.

The base case model was then subjected to a sensitivity analysis in which disposal rate, permeability and wastewater salinity were varied within a reasonable range (reflecting conditions that could be encountered during disposal in the Paddy and Cadotte members) in order to understand their effect on disposal pressures in comparison to the base case. The values selected for these additional runs are presented in Table 2. An additional simulation was carried out for the base case model where the model height was reduced by 50% (50 to 25 m), so as to more accurately reflect the horizon targeted for disposal.

Results

The pressures simulated along the disposal well increase with depth, as is typical due to the hydrostatic gradient, though the shift in pressure throughout a model run is uniform at all depths. In order to obtain a metric that quantitatively represents a single pressure measurement at the well (allowing the comparison of the results of the sensitivity analysis and the investigation of influences on pressure values at the well relative to IVRP), a mean pressure value was calculated for each model node along the well at every time step for each simulation. This value was then normalized to the mean IVRP (calculated to be 5247 kPa for all models except the 25 m thick case, which had a mean pressure of 5370 kPa) in order to express changes in pressure as a percentage relative to this initial pressure in the model and evaluate it in relation to the regulatory requirement of remaining under 120% of IVRP. These values were plotted for each parameter investigated in the sensitivity analysis and are shown in Figure 5.

Table 1. Parameter values used in base case model. Abbreviations: K, Kelvin; K_x, hydraulic conductivity in x-direction; K_y, hydraulic conductivity in y-direction; J, joule; MJ, megajoule.

Parameter	Value
Fluid flow	
Hydraulic conductivity (m/s)	1.48×10^{-6}
Anisotropy of conductivity (K_y/K_x)	0.1
Density ratio	0.126
Specific storage (1/m)	0.00001
Mass transport	
Porosity	0.25
Molecular diffusion (m^2/s)	1.99×10^{-9}
Longitudinal dispersivity (m)	5
Transverse dispersivity (m)	0.5
Heat transport	
Porosity	0.25
Fluid heat capacity (MJ/m^3/K)	4.2
Solid heat capacity (MJ/m^3/K)	2.46
Fluid thermal conductivity (J/m/s/K)	0.65
Solid thermal conductivity (J/m/s/K)	1.79
Longitudinal dispersivity (m)	5
Transverse dispersivity (m)	0.5
Fluid properties	
Wastewater salinity (g/L)	200
Formation water salinity (g/L)	0
Wastewater density (kg/m^3)	1126.1
Formation water density (kg/m^3)	999.74
Formation water temperature (ºC)	45

Table 2. Parameters and their associated range of values investigated in the sensitivity analysis. Abbreviations: d, day; mD, millidarcies.

Parameter	Range	Base case value
Permeability (mD)	20–500	200
Disposal rate (m^3/d)	100–1000	100
Wastewater salinity (g/L)	50–300	200
Formation thickness (m)	25–50	50

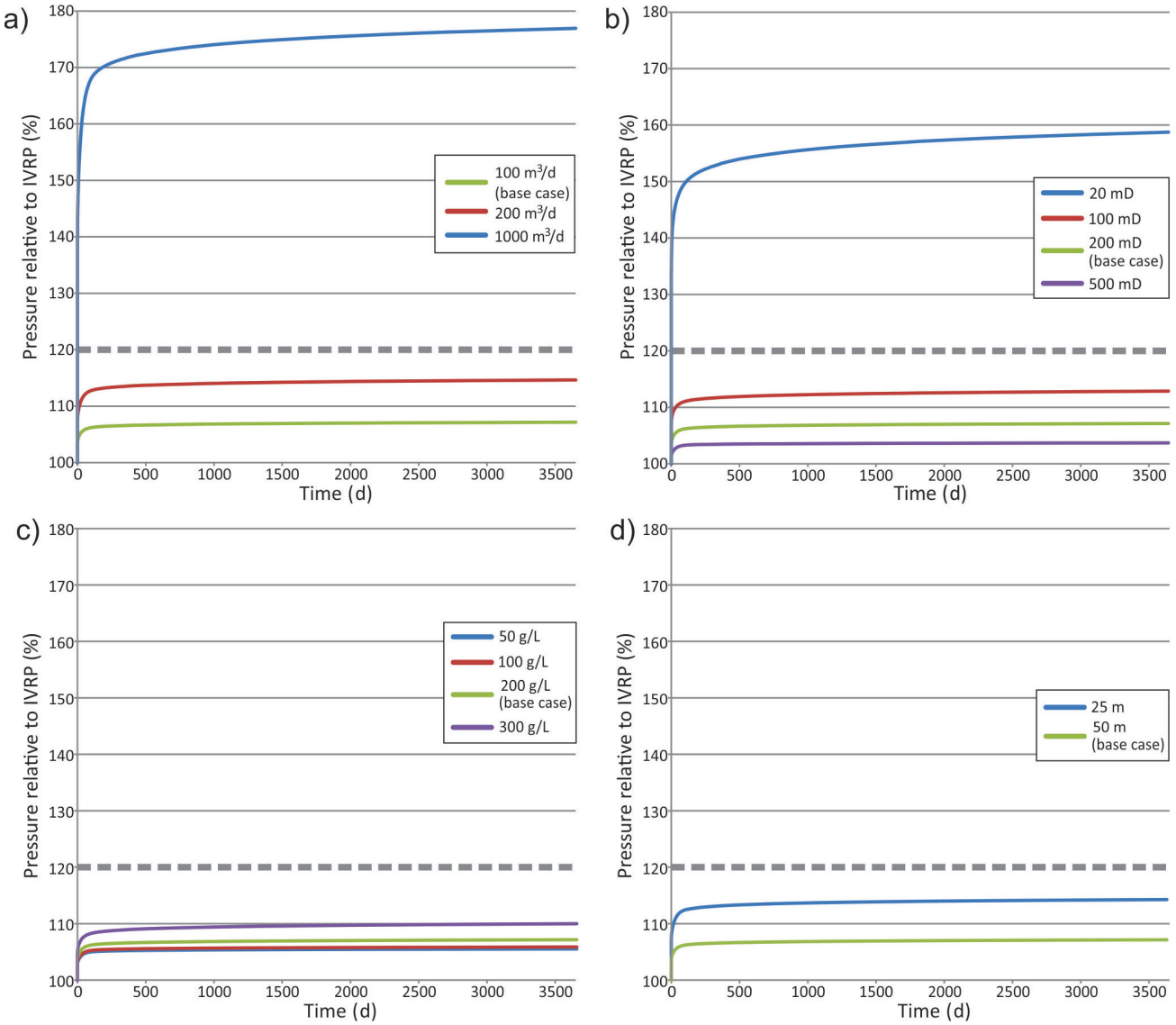

Figure 5. Mean percent change in pressure along the disposal well relative to the initial virgin reservoir pressure (IVRP) for different cases of **a)** disposal rate, **b)** formation permeability, **c)** injected wastewater salinity, and **d)** formation thickness. All base case results are shown in green. The 120% of IVRP value is marked by the thick dashed line. Abbreviations: d, day; mD, millidarcies.

Considering just the base case result, pressures increase most rapidly in the first 100 days after disposal begins. As injected wastewater begins to spread farther from the well, the pressure increase slows to a near steady rate, though this is difficult to discern in Figure 5. After 10 years of injection, pressures reach roughly 107% of IVRP, suggesting that, under the conditions chosen for the base case, the 120% of IVRP limit is not reached. Pressures were exported in the middle of the formation at increasing distance from the well, and it was found that just 5 m from the well pressures were reduced to 103.5% of IVRP. At 500 m from the disposal wells, pressures reached 101.4% of IVRP.

Disposal rates of 100 and 200 m^3/d are shown to produce pressure increases that are safely within the BCOGC's regulatory limit, reaching peak values of 115% of IVRP (Figure 5a). The 1000 m^3/d case surpasses this limit very early in the simulation, approaching 180% of IVRP after 10 years. This value was selected as a part of the analysis because one well targeting the Paddy and Cadotte members operates at this rate.

Formation permeability strongly influences disposal pressures (Figure 5b). Relative to the base case of 200 mD, the higher permeability (500 mD) results in a pressure that remains well below 120% of IVRP limit (103%). For a lower permeability of 100 mD, the pressure is 113% of IVRP, and for 20 mD, the pressure increases rapidly and reaches nearly 160% after 10 years.

Pressure was found to increase as the salinity was raised (Figure 5c). This occurs because, as salinity rises, so does

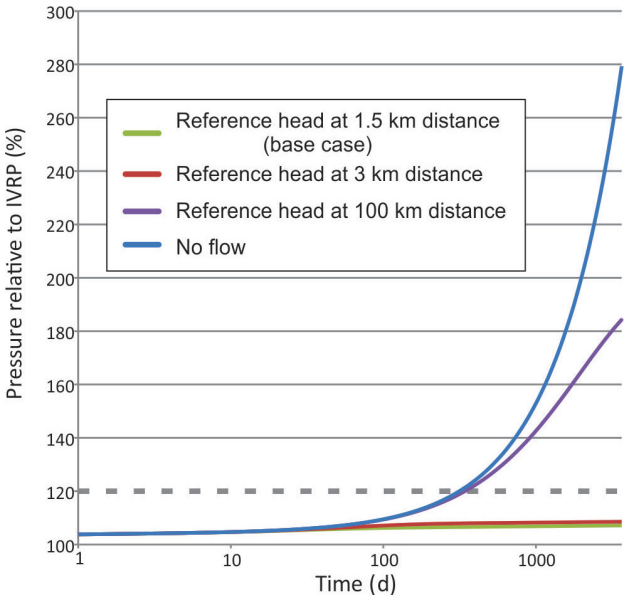

Figure 6. Mean percent change in pressure along the disposal well relative to the initial virgin reservoir pressure (IVRP) with modifications to the outflow boundary edge. The 120% of IVRP value is marked by the thick, dashed line. The x-axis is on a log scale.

the fluid density and viscosity, reducing the ease with which fluid travels through the disposal formation, leading to greater pressures. Wastewater salinity does not appear to have as significant an effect on the pressure increase relative to the IVRP as disposal rate or formation permeability does. There is a 3% difference in final reservoir pressure between the 200 and 300 g/L cases, and only a 1% difference between the 100 and 200 g/L cases. The 300 g/L salinity value represents an extreme case, and most of the water analyses compiled for this study fall in the 100–200 g/L range, indicating that only minor variation in formation pressures should be expected as a result of wastewater concentration.

Finally, the effect of reducing the model layer thickness to half that of the base case model (i.e., 25 m) was to increase the pressure to 114% of IVRP, whereas the 50 m thick model was 107% of IVRP (Figure 5d).

The results of modifying the outflow boundary of the model are shown in Figure 6. It is evident that this boundary exerts a strong control over simulated pressures. When the boundary reference head is closer to the model edge, as in the 1.5 and 3 km cases, pressures remain low. This boundary acts as a sink for pressure, preventing it from rising too high within the domain. In the extreme case, where the outflow boundary is replaced with a no-flow boundary, pressures rise indefinitely, never reaching a plateau as seen in Figure 5. Using a no-flow boundary within 500 m of the well simulates the pressure buildup in a closed system, which is likely not realistic. The intermediate case, with the reference head positioned 100 km from the model edge, simulates pressures that approach those seen in the no-flow boundary case. This suggests that, as the reference head is moved farther from the model edge, pressures more closely approximate those of the no-flow boundary case.

Discussion

The results of this model sensitivity analysis suggest that disposal rate, formation permeability and formation thickness are important factors to consider with respect to maximizing disposal potential at a well location while meeting the 120% threshold for increased pressure. The results further suggest that of the parameters varied, disposal well pressures are most sensitive to disposal rate and formation permeability, with lesser but some sensitivity to formation thickness. Formation pressure at the well was least sensitive to variability in disposal water density (salinity). The relatively strong dependency of formation pressure on permeability suggests that characterization of permeability and permeability variability (vertically and horizontally) is useful with respect to predicting disposal well performance in the short term and long term. The results also suggest that near-well formation pressures can be managed through adjustments to the disposal rate. For the base case (200 mD permeability, 50 m layer thickness), disposal rates greater than approximately 200 m^3/d caused increases in formation pressure approaching 120% of the specified IVRP. At this rate, the sensitivity analysis indicated that a reduction in permeability by more than 100 mD or a reduction in the layer thickness by one half caused the simulated pressures to approach this injection pressure threshold. The combination of factors (permeability, thickness) would result in a unique resulting pressure at the well, affecting the potential for the pressure threshold to be exceeded. This is particularly the case for areas near the disposal well, where the effects of pressure are most strongly manifested soon after disposal and where they are measured for compliance monitoring. Although this study did not consider the complexities of geological heterogeneities, the results suggest that small changes in permeability or layer thickness, which can reasonably be expected over a few hundred metres, could affect injection potential. For example, the model simulation using a disposal rate of 1000 m^3/d, resulted in very high simulated pressures, yet well 10677 actually operates at this rate, meeting BCOGC operational requirements with respect to pressure requirements. Thus, it is likely that the actual permeability near this particular well is higher than that used in the model. This supports the interpretation that the Paddy and Cadotte members are heterogeneous at the near-well scale.

This study was developed to provide a preliminary examination of potential factors affecting reservoir pressures near disposal wells in the Paddy and Cadotte members study area of NEBC, and the results provide preliminary insights in regard to potential factors influencing disposal well performance. The results do not imply conditions un-

der which the pressure threshold could be exceeded in reference to any particular well. The results of modifying the outflow boundary condition demonstrate this, as pressures within the model were strongly influenced by moving the boundary farther from the disposal edge. Instead, this study provides insights into the sensitivity of disposal pressures to the different parameters tested. It is the relative change in pressure in response to modifying formation or disposal parameters that is important. Moreover, the modelled final well pressure does not accurately represent a measurement that is consistent with standardized methods for obtaining stabilized pressure measurements at a well for the purposes of establishing regulatory compliance.

Finally, this study did not consider layered heterogeneity, which can be expected due to differences in bed- to bedset-scale heterogeneity, or lateral changes in permeability (extending beyond the well field). Also, this study did not test the sensitivity to changes in specific storage, which also directly affects the pressure response to injection. The same value was used for all simulations, but, if the specific storage is reduced, the same volume of injected wastewater will lead to even higher pressures.

Conclusions

In this study, axisymmetric box models approximating the Paddy and Cadotte members of NEBC were used to simulate pressure changes as a result of wastewater disposal. Various parameters, including disposal rate, formation permeability, formation thickness and wastewater salinity (and resulting density), were varied in order to assess their control on formation pressure at a disposal well. The results were evaluated relative to the 120% of IVRP threshold imposed by the BCOGC. It was determined that in order to optimize disposal, operators must achieve a delicate balance between disposal rates and unit permeability and thickness. This result is not surprising as it is founded on well and reservoir hydraulic theory. What this sensitivity analysis demonstrates is that disposal well operation is quite sensitive to these parameters. A reduction in permeability by 100 mD or a two-fold reduction in thickness of the disposal unit resulted in injection pressures very close to the IVRP limit for the modelled scenario. Although this study did not model local or regional geological heterogeneities on disposal well performance, given the sensitivity of pressures at the well to reservoir permeability, pressure sensitivity to local or regional geological heterogeneities is inferred. As some uncertainty in local and regional geological heterogeneities is a reality for deep geological formations, the results emphasize the importance of pressure monitoring for maximizing disposal well efficiency and performance and ensuring compliance with pressure requirements.

In future work, a regional model of the Paddy and Cadotte members incorporating all wells shown in Figure 1 will be constructed. The aim of this model is to assess the influence of a regional hydraulic gradient, formation slope and proximal source water extraction on the overall distribution of disposed wastewater in the subsurface.

Acknowledgments

In addition to Geoscience BC, this research is supported by the Pacific Institute for Climate Solutions (PICS) and the Society of Contaminated Sites Approved Professionals of British Columbia (CSAP). Thanks are extended to the BC Oil and Gas Commission Reservoir Engineering Department staff and Encana Corporation for their help with the project, as well as to S. Van Pelt for providing a review of this manuscript.

References

Alessi, D.S., Zolfaghari, A., Kletke, S., Gehman, J., Allen, D.M. and Goss, G.G. (2017): Comparative analysis of hydraulic fracturing wastewater practices in unconventional shale development: water sourcing, treatment and disposal practices; Canadian Water Resources Journal/Revue canadienne des ressources hydriques, v. 42, issue 2, p. 105–121.

BC Oil and Gas Commission (2015): British Columbia's oil and gas reserves and production report; BC Oil and Gas Commission, URL <http://www.bcogc.ca/node/13607/download> [October 2017].

BC Oil and Gas Commission (2016): Water service wells summary information; BC Oil and Gas Commission, URL <http://www.bcogc.ca/node/5997/download> [May 2017].

BC Oil and Gas Commission (2017a): Data downloads; BC Oil and Gas Commission, web application, URL <http://www.bcogc.ca/online-services> [July 2017].

BC Oil and Gas Commission (2017b): Well lookup and reports; BC Oil and Gas Commission, web application, URL <http://www.bcogc.ca/online-services> [October 2017].

Buckley, R.A. and Plint, A.G. (2013): Allostratigraphy of the Peace River Formation (Albian) in north-western Alberta and adjacent British Columbia; Bulletin of Canadian Petroleum Geology, v. 61, no. 4, p. 295–330.

Diersch, H.J.G. (2014): FEFLOW: Finite Element Modeling of Flow, Mass and Heat Transport in Porous and Fractured Media; Springer Science+Business Media LLC, Berlin, Germany, 996 p., doi:10.1007/978-3-642-38739-5

Driesner, T. and Heinrich, C.A. (2007): The system H_2O-NaCl. Part I, correlation formulae for phase relations in temperature-pressure-composition space from 0 to 1000°C, 0 to 5000 bar, and 0 to 1 X_{NaCl}; Geochimica et Cosmochimica Acta, v. 71, issue 20, p. 4880–4901.

Encana Corporation (2014): Application for dual water source and water disposal wells: ECA CRP Sunrise 14-35-78-17W6 (10677), ECA CRP Hz Sunrise A13-33-78-17W6 (26471), ECA CRP Hz Sunrise 09-34-78-17W6 (28495), ECA CRP Hz Sunrise A09-34-78-17W6 (28496), Sunrise area; submitted to BC Oil and Gas Commission, Kelowna, BC, 50 p.

Eppelbaum, L., Kutasov, I. and Pilchin, A. (2014): Thermal properties of rocks and density of fluids; *in* Applied Geothermics, Springer-Verlag, Berlin, Heidelberg, p. 99–149.

Goss, G.G., Alessi, D., Allen, D., Gehman, J., Brisbois, J., Kletke, S., Sharak, A.Z., Notte, C., Thompson, D.Y., Hong, K.,

Junes, V.R.C., Neto, W.B.G.A. and Prosser, C. (2015): Unconventional wastewater management: a comparative review and analysis of hydraulic fracturing wastewater management practices across four North American basins; report prepared for Canadian Water Network, Waterloo, Ontario, 168 p.

Government of British Columbia (2017): Water Sustainability Act, Water Sustainability Regulation; Statutes of British Columbia 2014, chap. 15, URL <http://www.bclaws.ca/civix/document/id/complete/statreg/36_2016> [May 2017].

Hendry, M.J., Barbour, S.L., Novakowski, K. and Wassenaar, L.I. (2013): Paleohydrogeology of the Cretaceous sediments of the Williston Basin using stable isotopes of water; Water Resources Research, v. 49, issue 8, p. 4580–4592.

IHS Energy (2016): IHS AccuMap®, version 26.06; IHS Energy, mapping, data management and analysis software, URL <https://www.ihs.com/products/oil-gas-tools-accumap.html> [January 2016].

Langevin, C.D. (2008): Modeling axisymmetric flow and transport; Groundwater, v. 46, issue 4, p. 579–590.

Langevin, C.D., Hughes, J.D., Banta, E.R., Provost, A.M., Niswonger, R.G. and Panday, S. (2017): MODFLOW 6 modular hydrologic model version 6.0.1; United States Geological Survey, software release, September 28, 2017, doi:10.5066/F76Q1VQV

Leckie, D.A. and Reinson, G.E. (1993): Effects of middle to late Albian sea level fluctuations in the Cretaceous interior seaway, western Canada; *in* Evolution of the Western Interior Basin, W.G.E. Caldwell and E.G. Kauffman (ed.), Geological Association of Canada, Special Paper 39, p. 151–176.

Leckie, D.A., Staniland, M.R. and Hayes, B.J. (1990): Regional maps of the Albian Peace River and lower Shaftesbury formations on the Peace River Arch, northwestern Alberta and northeastern British Columbia; Bulletin of Canadian Petroleum Geology, v. 38, issue 1, p. 176–189.

Petrel Robertson Consulting Ltd. and Canadian Discovery Ltd. (2011): Deep subsurface aquifer characterization in support of Montney tight gas development; Geoscience BC, Report 2011-11, 386 p.

Simons, M., Allen, D.M., Kirste, D. and Welch, L.A. (2017): Numerical modelling of highly saline wastewater disposal in northeast British Columbia; GeoOttawa 2017, 70th Canadian Geotechnical Conference and 12th Joint Canadian Geotechnical Society/Canadian National Chapter of the International Association of Hydrogeologists Groundwater Conference, October 1–4, 2017, Ottawa, Ontario, abstract, URL <http://www.geoottawa2017.ca/calendar_paper.php?id=217> [December 2017].

1101-750 West Pender Street
Vancouver,BC V6C 2T7

t: 604.662.4147
e: info@geosciencebc.com
w: www.geosciencebc.com